Università degli Studi di Padova
Facoltà di Scienze MM.FF.NN.
Dipartimento di Fisica "G. Galilei"

scuola di dottorato di ricerca in fisica

ciclo XXIII

Pairing and superconductivity in a spin-charge gauge approach to HTS cuprates

Coordinatore: Ch.mo Prof. ATTILIO STELLA

Supervisore: Ch.mo Prof. PIERALBERTO MARCHETTI

Dottorando: Dott. MICHELE GAMBACCINI

January 31, 2011

Abstract

This thesis deals with different aspects of high temperature superconductivity in hole-doped cuprates. We assume the $t-J$ model to describe the CuO_2 planes of cuprates and we use a spin-charge gauge approach with spin-charge separation to describe holes in terms of a spinless fermion carrying the charge (holon) and a neutral boson carrying spin 1/2 (spinon), coupled by a slave-particle gauge field.

In this framework we consider the effects of the presence of a finite density of incoherent holon pairs in the normal state as a precursor of superconductivity. We show that it is possible to take such pairs into account through a strongly direction dependent spectral weight for holons, which suppresses quasi-particles starting from the anti-nodal directions, and a wave function renormalization for the slave particle gauge field. In this way we prove that, when temperature is reduced, the formation of holon pairs causes both the deviation from linearity of the resistivity and the deviation from the constant value of the Knight shift. Moreover we point out the need for a negative next-nearest-neighbor hopping term ($t-t'-J$ model) to get a good continuum limit and to evaluate the Knight shift. These results are obtained through a Green's function, which follows naturally from the formalism and analytically interpolates between a Fermi liquid-like behavior and a d-wave superconductor when the coherence length of the holon pair order parameter is increased. The system preserves a finite Fermi surface until the superconducting transition, where it reduces to four nodes.

Finally when, at lower temperatures, both the holon pairs and the RVB spinon pairs condense we enter the superconducting phase. In this phase we study the magnetic excitations showing how to extend to spin waves the hourglass-shape dispersion, found for spinons near the antiferromagnetic vector, if a suitable local mechanism of attraction between spinon and anti-spinon is assumed. The resulting spin wave Green's function, whose imaginary part is directly comparable with experiments, generates the hourglass with a finite gap between the two branches. Since the $U(1)$ slave-particle gauge field gains mass in the superconducting phase via Anderson-Higgs mechanism, we propose the necessary mechanism of attraction comes from the unbroken Z_2 subgroup of the $U(1)$ gauge group.

Questa tesi riguarda diversi aspetti della superconduttivit nei cuprati drogati con lacune trattati con una variante del formalismo di "slave-particle", lo "spin charge gauge approach". Si assume il modello $t - J$ in due dimensioni per descrivere i piani CuO_2 e si utilizza l'approccio di gauge "slave particle" con separazione di spin e carica, riscrivendo le lacune in termini di una eccitazione fermionica carica ma priva di spin (l'holone) ed una neutra con spin 1/2 (lo spinone) accoppiate dal campo di gauge.

In tale ambito si studia l'effetto della formazione di coppie incoerenti di holoni nella fase normale. Si mostra come si possa tenere conto dell'effetto di quaste coppie tramite un peso spettrale per gli holoni fortemente dipendente dalla direzione che sopprime i modi a partire dalle direzioni antinodali. Si mostra poi come alla formazione di queste coppie sia imputabile, al decrescere della temperatura, sia la deviazione dalla linearita' della resistivita' che la deviazione dal valore costante del Knight shift (per il modello con secondi vicini $t - t' - J$). Tali risultati sono ottenuti tramite una funzione di Green che appare naturalmente nel formalismo ed interpola analiticamente tra un comportamento di tipo liquido di Fermi ed uno superconduttivo d-wave al decrescere della temperatura.

Infine si studiano le eccitazioni magnetiche nella fase superconduttiva, che compare quando, diminuendo la temperatura, sia le coppie di holoni che le coppie di singoletto (RVB) di spinoni condensano. Si mostra come, assumendo un meccanismo di attrazione locale tra spinoni, sia possibile estendere al magnone la dispersione trovata in precedenza per gli spinoni che, in prossimita' del vettore antiferromagnetico, caratterizzata da due rami, uno crescente ed uno decrescente. La dispersione per i magnoni direttamente comparabile con i dati sperimentali sulle eccitazioni magnetiche (il cosidetto "hourglass"). Si congettura che il meccanismo di attrazione tra spinoni possa essere originato dal sottogruppo Z_2 del gruppo $U(1)$ di gauge "slave-particle" che rimane non rotto nella fase superconduttiva.

Contents

Introduction

High temperature superconductivity was discovered by Bednorz and Muller in 1986 studying a class of materials called cuprates. Cuprates are complex oxides containing quasi-two dimensional copper-oxygen (CuO_2) planes considered to be the origin of their anomalous properties. Indeed it is widely believed that the physics of cuprates is that of these CuO_2 planes, which are the principal seat of superconductivity. Layers of other atoms, surrounding the copper-oxygen sheets, play the role of charge reservoirs.

Doping radically changes the properties of cuprates. Undoped samples are half filled Mott-Hubbard insulators with long range antiferromagnetic order. When, doping the samples, charge carriers (holes) are introduced into the copper-oxygen planes, they delocalize disturbing locally the spin order. As a result the system consists of moving holes surrounded by droplets of spin liquid and, depending on temperature, it behaves like a metal or it becomes a superconductor.

Apart from the high transition temperature, the properties of the superconducting compounds seem relatively normal, similar to conventional BCS superconductor. There are two main differences: the superfluid density of the superconductor is small and vanishes for low dopings (due to the proximity to the Mott insulator); the superconducting gap vanishes on four points (nodes) on the Fermi surface (pairing is d-wave) so that there are gapless quasi-particle excitations affecting the physical properties even at low temperatures. However the superconducting mechanism nowadays is not clear. On the contrary in the normal state (i.e. in absence of superconductivity) the properties of these materials are very peculiar. They do not match traditional Fermi liquid theory and a variety of physical observables deviate strongly from standard predictions.

There have been several attempts to derive a unifying and consistent low energy theory for cuprates but the debate is still open and controversial. However, there are some generally accepted basis. For example the Hubbard model and the $t - J$ model are believed to contain the relevant physics for the copper-oxygen planes of cuprates. These models take Coulomb repulsion into account making electrons strongly correlated.

The main difficulties are the lack of a small parameter in the theory and the fact that these models are not integrable in two dimensions, therefore some approximation schemes are needed. Since we are interested in energy scales much smaller than the on

site Coulomb repulsion, the constraint of no double occupied sites have to be implemented exactly. The gauge theory approach to the $t-J$ model followed in this thesis is an attempt to implement the no doubly occupation in a non-perturbative way.

Gauge theories successfully explained the Fractional Quantum Hall Effect in two dimensional systems subject to strong magnetic field. The idea is to attach a magnetic flux quanta to the real electrons and rewrite action and partition function in terms of anyons, i.e. fields composed of fermion and gauge flux obeying a different statistics because of Aharonov-Bohm effect.

The idea is to perform spin-charge separation creating a spinless fermion (holon) and a neutral boson doublet (spinon). In such a way the Pauli principle no longer "sees" spin and automatically forbids double occupation.

A useful tool to formally separate the spin and the charge degrees of freedom is Chern-Simons bosonization. The price to pay is the introduction in the theory of minimally coupled statistical gauge fields, gauging the global symmetries of the model.

Another important point is that the spin-charge separation introduces a fictitious $U(1)$ local symmetry so that holons and spinons scatter against a slave-particle (h/s) $U(1)$ gauge field. This is the main source of dissipation at low temperatures. In two dimensions, because of the h/s gauge field, the spin-charge separation is not complete.

The Chern-Simons representation of the $t-J$ model is exact but generally is more complicated than the original one. One hopes nevertheless that the new version is more suitable for a mean field approximation and contains, in a non perturbative way, some features that would have been neglected in standard mean field approaches.

In chapter 1, briefly discussing composition and structure of cuprates, we introduce the temperature-doping phase diagram of the copper-oxygen planes. Then we justify that the $t-J$ model is the appropriate model for these planes. Finally we analyze the phenomenology of cuprates which will be useful in the following, showing the most important anomalous properties.

In chapter 2 we present our spin-charge gauge approach. We introduce the rules of Chern-Sinons bosonization and apply them to the $t-J$ model to perform spin-charge separation. Then we derive the optimal spinon configuration (roughly speaking a Neel state with spin-vortices attached to holons which chirality depends on the sublattice where the holon is located) and the low energy actions for spinons, holons and gauge field in the normal state (both strange metal and pseudo-gap). We conclude summarizing the main predictions of our approach in the normal state.

In chapter 3 we extend the approach to the superconducting region starting from the pseudo-gap regime. We propose a new non-BCS mechanism for superconductivity via attraction between spin vortices and strongly based on the composite nature of the electron. We find two crossover temperatures above the superconducting transition. Below

the higher one a finite density of incoherent holon pairs appears and below the lower one incoherent RVB hole pairs forms which become coherent at the superconducting transition. Finally we analyze the spin-spin correlation in the superconducting region explaining the hourglass-shape dispersion of the magnon near the antiferromagnetic vector.

In chapter 4 we consider superconductivity arising from the strange metal region and incorporate in the theory the fluctuations of the phase of the holon pairs order parameter. We study the Fermi surface of the holons and the phase fluctuations of the holon pairs and combining them we obtain an explicit expression for the Green's function of quasi-particles that interpolates between the normal state and the superconducting state. The inverse coherence length turns out to be the relevant parameter that determines the behavior of quasi-particles. The resulting density of state turns out to be in qualitative agreement with experiments and proves the necessity of the slave particle gauge field.

In chapter 5, using the results of the previous chapter, we show that, by a suitable renormalization of some parameters (in particular using two wave function renormalization for holon field and for the h/s gauge field) it is possible to take holon pairs into account. In this way we evaluate effect of holon pairs on resistivity and Knight shift we find that both the observables deviate downward, at low temperature, accordingly to experiments. The evaluation of the Knight shift formula is performed in detail.

The approach to superconductivity performed in chapter 3 has been very recently proposed. The original contributions, in this thesis, are the final section of Chapter 3, dealing with spin-spin correlation, and the whole discussion made in Chapters 4 and 5.

Chapter 1

Basic properties of hole-doped HTS cuprates

1.1 Phase diagram of CuO_2 planes

High temperature superconducting cuprates ($HTSC$) are a class of materials, synthesized in the laboratory since eighties (Bednorz Muller 1986), with high superconducting transition temperature T_c (above the liquid-air barrier of 77 K) accompanied by high critical magnetic fields and high current densities. However the value of T_c is critically dependent on the chemical stoichiometry.

Following Leggett [1], it is possible to specify the composition of cuprates in the form

$$(CuO_2)_n A_{n-1} X \tag{1.1}$$

where n is a positive integer, A is an alkaline or rare earth (or Y) and X is an arbitrary collection of elements, in general in nonrational stochiometric proportions. Common examples include $La_{2-\delta}Ba_\delta CuO_4$ (shorthand named $LBCO$), $Bi_2Sr_2CaCu_2O_{8+\delta}$ ($BSCCO$) and $YBa_2Cu_3O_{6+\delta}$ ($YBCO$), where δ is a positive fraction.

The undoped material is called parent compound. In this case δ takes the integral value at which the valence of the formula equals the number of Cu's (e.g. La_2CuO_4, $Bi_2Sr_2CaCu_2O_8$, $YBa_2Cu_3O_7$). Superconductivity occurs close to these integral values, that is close to one hole per CuO_2 unit.

The crystal structures of cuprates are oxygen-defect modifications of the perovskite structure, with about one-third of the oxygen positions vacant. Referring to Eq. (1.1), the unit cell consists of a group of n CuO_2 planes spaced by $n-1$ layers of the spacer element A and separated from the next set of planes by the charge reservoir unit X.

Typical distance, along the c axis, between planes belonging to the same group is about 3.1 Å while the separation between groups of planes, due to charge reservoirs, depends on X and can be much greater, about 15 Å for $BSCCO$.

CuO_2 $a-b$ planes are a hallmark feature of all cuprates. It is widely believed that the physics of HTS cuprates is that of these planes, which are the principal seat of superconductivity. They are square lattice with Cu atoms at the corners and O atoms at the midpoints of the sides. Sides are approximately 3.85 Å.

It is possible to change slightly the number of holes per CuO_2 unit, from unity to $1+\delta$, changing one or more charge reservoir elements, i.e. hole-doping the parent compounds via chemical substitution.

Doping δ (ranging from 0 to about 0.4) and temperature T (ranging from 0 to few hundreds K) (also magnetic field is an important control variable) play huge role on the physical behavior of CuO_2 planes. The typical phase diagram of these planes in the variables doping and temperature (T, δ) is shown in Fig. (1.1).

At low doping and not too high temperature the system is a classic Mott-Hubbard insulator with long range anti-ferromagnetic order (AF). In this phase there is one localized hole per Cu atom with staggered spins (the magnetic unit cell is twice the crystal unit cell). Upon doping beyond a few per cent the anti-ferromagnetic order becomes zero and a second-order phase transition leads to the pseudo-gap regime (PG). Below PG regime the system shows an insulating spin-glass (SG) behavior. At slightly higher doping, $\delta \approx 0.05$, up to about $\delta \approx 0.27$ and temperature below the curve $T_c(\delta)$, the compounds become superconducting (SC). Optimal doping is the δ-value at which $T_c(\delta)$ reaches its maximum ($\delta \approx 0.16$). Underdoped and overdoped are called compounds with lower or higher doping than the optimal one. The curve $T_c(\delta)$ is depressed by magnetic field and impurities in the CuO_2 planes. Above the superconducting phase transition, a line $T^*(\delta)$ marks a crossover from PG regime to strange-metal regime (SM). Both PG and SM regimes are not described by standard Fermi liquid theory (FL) and anomalous physical properties arise. While SM display an anomalous metallic behavior, in PG the resistivity has a minimum and increases dramatically lowering temperature and doping showing an insulating behavior. A striking metal-insulator crossover (MIC) is a hallmark of the PG region. Finally, further increasing doping, the system has a crossover from SM and a phase transition from SC phase towards a normal metal behavior and FL theory provides the correct description.

We notice that the above general description omits particular features that may play some rule in the physical system behavior but depend on the specific material and are not

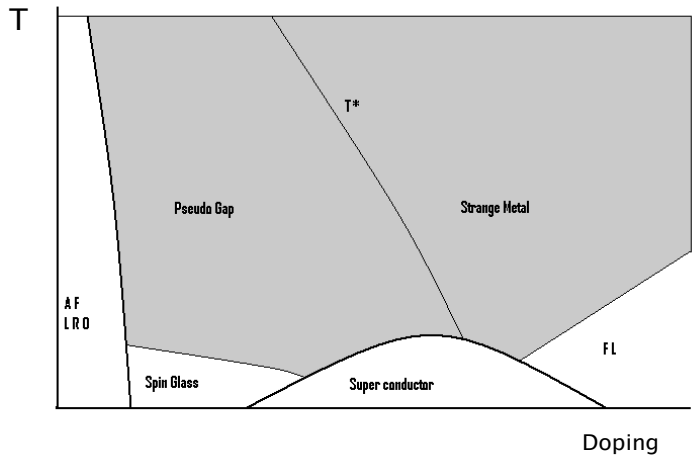

Figure 1.1: Generic (T, δ) phase diagram of hole-doped cuprates; the shaded region shows the normal state (Strange Metal and Pseudo-gap separated by T^* line); from Ref. [13].

shared by all HTC cuprates. Some examples are chains (conventionally along the b axis), anisotropy of the CuO_2 planes, buckling of the $Cu-O$ bonds, chemical and structural environment of planes.

1.2 t-J model

Now we introduce the model we assume to describe the low energy physics of the CuO_2 planes. Consider the cluster formed by one Cu and the square of four oxygens around it. In undoped materials one hole occupies the highest energy orbital $3d_{x^2-y^2}$ of the copper (Cu^{2+} copper ion) while oxygens $2p$ shells are completely filled (O^{2-} ions). Upon doping, additional holes are introduced in the layers. Each of these doping-induced holes resides primarily on a combination of the four oxygen p orbitals with the same symmetry of the central $3d_{x^2-y^2}$ Cu ion orbital. This hybridization binds a doping-induced hole to the central Cu ion and their spins form a spin singlet, the so called Zhang-Rice singlet [2]. Moreover strong Coulomb interaction prevents two holes residing on the same oxygens square. Since neighboring clusters have one oxygen is common the charged singlet can move in the anti-ferromagnetic background of copper ions. Zhang and Rice showed that the single band two dimensional $t-J$ model Hamiltonian with explicit no double occupancy constraint, describes the motion of the singlet and accordingly describes the low energy physics of the CuO_2 planes. The $t-J$ model Hamiltonian reads

$$H_{t-J} = P_G \left(-t \sum_{\langle i,j\rangle,\sigma} c^{\dagger}_{i,\sigma} c_{j,\sigma} + \mu \sum_j n_j + J \sum_{\langle i,j\rangle} \vec{S}_i \cdot \vec{S}_j \right) P_G \tag{1.2}$$

where i correspond to Cu sites, the particle number and spin operators are defined as

$$n_i = \sum_{\sigma} c^{\dagger}_{i\sigma} c_{i\sigma}, \qquad \vec{S}_i = \sum_{\alpha\beta} c^{\dagger}_{i\alpha} \frac{\vec{\sigma}_{\alpha\beta}}{2} c_{i\beta} \ . \tag{1.3}$$

In the above equations $\vec{\sigma}_{\alpha\beta}$ are the Pauli matrices, μ the chemical potential and $P_G = \prod_i (1 - n_{i\uparrow} n_{i\downarrow})$ is the Gutzwiller projection eliminating double occupation and introducing Coulomb interaction in the model. Numerical simulations yield $t \simeq 0.4eV$, $J \simeq 0.13eV$, and, using the relation $J = 4t^2/U$ (derived by the Hubbard model from which $t-J$ model follows in the strong coupling limit $U \to \infty$ [32]), we get a reasonable Coulomb repulsion $U \simeq 8eV$ justifying no double occupation constraint.

Our starting point is the euclidean action of the $t-J$ model in the path integral representation in terms of spin $\frac{1}{2}$ fermionic fields $\Psi_\alpha, \Psi^*_\alpha$ and complex Hubbard-Stratonovich gauge field $X_{<ij>}$ [3]:

$$\begin{aligned} S_{t-J}(\Psi, \Psi^*, X, X^*) \ = \ & \int_0^\beta dx^0 \left\{ \sum_{<ij>} \left(\frac{2}{J} X^*_{<ij>} X_{<ij>} + [(-t + X_{<ij>}) \Psi^*_{i\alpha} \Psi_{j\alpha} + h.c.] \right) \right. \\ & \left. + \sum_i \Psi^*_{i\alpha} (\partial_0 + \mu) \Psi_{i\alpha} + \sum_{i,j} u_{i,j} \Psi^*_{i\alpha} \Psi^*_{j\beta} \Psi_{j\beta} \Psi_{i\alpha} \right\}, \end{aligned} \tag{1.4}$$

where the two-body potential $u_{i,j}$, taking into account Gutzwiller projection, is given by

$$u_{i,j} = \begin{cases} +\infty, & \text{if} \quad i = j \\ -\frac{J}{4}, & \text{if} \quad i,j \ \ n.n. \end{cases} \tag{1.5}$$

Summation over repeated indices is understood and dependence on euclidean time x^0 is not explicitly exhibited. $T = 1/\beta$, choosing the Boltzmann constant equal to one. Eq. (1.4) is obtained by normal ordering the $t-J$ Hamiltonian in Eq. (1.2), replacing the operators with fermionic fields, adding the imaginary-time temporal addend and performing Hubbard-Stratonovich transformation [4].

1.3 Phenomenology of cuprates

In this section we analyze the anomalous T-dependence of some experimental observables of HTS cuprates useful for subsequent discussions on normal (i.e. PG and SM)

and superconducting state. Anomalous means different w.r.t. the predictions of standard FL theory. This is mainly due to the strong correlation between electrons. In FL theory resistivity is the sum of a constant term due to impurity (always present in metals) and a term proportional to T^2 due to electron-electron scattering, $\rho = a + bT^2$. Spin susceptibility χ is constant (Pauli) as well as Knignt shift K_s (being proportional to the real part of χ). Spin lattice relaxation rate follows the Korringa low $\frac{1}{T_1} = cT$ with $c \propto K_s^2$.

Notice that some observables like resistivity and spin susceptibilities are quite universal for many hole-doped cuprates.

1.3.1 In-plane resistivity

We begin considering the anomalous T-dependence of the in-plane resistivity ρ_{ab}. Denoting by $\vec{J}$ the electromagnetic current, Kubo formula leads to

$$\frac{1}{\rho_{ab}} = \sigma_{ab} = -\lim_{\omega \to 0} \frac{1}{\omega} \Im \langle \vec{J} \cdot \vec{J} \rangle^R (\vec{q} = 0, \omega) \tag{1.6}$$

where the superscript R means retarded correlation and σ_{ab} is the conductivity.

As shown in Fig. (1.2), resistivity in cuprates is linear over a wide range of temperatures, from few tens or few hundred K (depending on the material and doping) to a thousand K. It decreases with increasing doping and for optimally doped samples, the range of linearity is the widest.

At low temperatures, to a greater extent in underdoped and overdoped samples, ρ_{ab} is far from linear. A remarkable and universal feature appearing in strongly underdoped samples is the MIC, that is the resistivity shows a minimum at $T_{MIC} \approx 50 - 100K$. At lower temperatures the conductivity behavior is insulating $\frac{d\rho_{ab}}{dT} < 0$ while at higher temperature is metallic $\frac{d\rho_{ab}}{dT} > 0$. In these samples $k_F l < 0.1$ at T_{MIC} (l is the mean free path), i.e. the resistivity is well above the Mott-Regel limit ($k_F l \sim 1$). For this reason we believe that MIC is not due to disorder localization. Increasing doping T_{MIC} lowers and eventually MIC disappears.

Another quite universal characteristic feature of underdoped samples is a maximum of $\frac{d\rho_{ab}}{dT}$ at T^*, about 100-200K. At temperatures higher than T^*, the resistivity approaches from below the linear behavior. T^* disappears for higher doping. Notice that this is a criterion to draw the line $T^*(\delta)$ (separating PG from SM) from resistivity measures.

In overdoped samples the resistivity is always metallic, $\rho_{ab} \sim T^\alpha$ with $\alpha > 1$ and the high T linear behavior is reached from above.

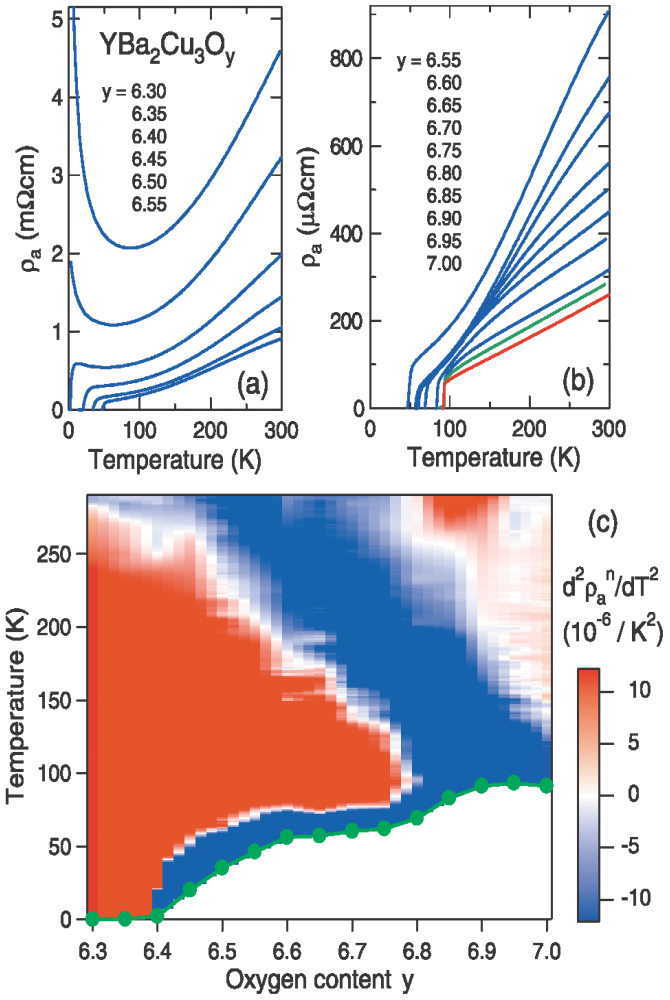

Figure 1.2: (a), (b) in-plane resistivity data of $YBCO$ for different doping y values (the relation $\delta = 0.2(y-6)$ approximately holds); underdoped (overdoped) samples are shown in blue (red) while the optimum doping is shown in green; (c) in-plane resistivity curvature mapping (second derivative of resistivity w.r.t. temperature) in the (T, y) plane; green circles show T_c; from Ref. [30].

1.3.2 Knight shift

The Knight shift of the resonant frequency of a nuclear spin in a static magnetic field is due to hyperfine interaction between the magnetic moments of the nucleus and conduction electrons. It is determined by the real part of the static magnetic susceptibility at a given nucleus

$$K_s = A\Re\chi(\omega = 0, \vec{q} = 0) \tag{1.7}$$

where A is the hyperfine constant.

We notice in Fig. (1.3) that $K_s(T)$ is depressed at low T and the deviation from the constant value at high T begins at temperatures higher that the opening of the spin gap at $T < T^*$ [51].

1.3.3 Spin lattice relaxation rate

The spin lattice relaxation rate $\frac{1}{T_1}$ measures the average spin fluctuation response at a given nucleus to a quasi-static magnetic field. It is related to the imaginary part of the magnetic susceptibility

$$\frac{1}{T_1 T} = A \lim_{\omega \to 0} \frac{1}{\omega} \int d^2 q F(\vec{q}) \Im\chi(\omega, \vec{q}) \tag{1.8}$$

where $F(\vec{q})$ is the structure factor depending on the lattice. At the Cu sites it is peaked around the anti-ferromagnetic vector Q_{AF}.

Fig. (1.3) show that for optimally or slightly overdoped samples $\frac{1}{T_1 T} \propto \frac{1}{T}$. The same temperature dependence holds for underdoped samples at relatively high temperature. Decreasing T, $\frac{1}{T_1 T}$ reach a broad maximum and then it decreases.

Notice that experimentally $\frac{1}{T_1 T}$ share the same temperature dependence as the in-plane conductivity σ_{ab} in both PG and SM regions.

1.3.4 Fermi surface

Angle resolved photoemission spectra ($ARPES$) show that optimal and overdoped cuprates have a large Fermi surface FS consistent with Luttinger theorem. As shown in Fig. (1.4), this is essentially the SM regime where the resistivity is T-linear. Underdoped samples, in the PG region, develop a small FS with four half-pockets centered at $\left(\pm\frac{\pi}{2}, \pm\frac{\pi}{2}\right)$ in the Brillouin zone. Decreasing the temperature below T^* the FS disappears

starting from the antinodal direction, eventually leaving four short and disconnected half-pockets. Finally in the SC phase these arcs shrink to four nodal points of a gap function with d-wave symmetry [50].

1.3.5 Density of states near the Fermi surface

Tunnelling and $ARPES$ experiments show that there is a suppression of the low energy single particle spectral weight in favor of two separate peaks even at temperature above T_c, as shown in Fig. (1.4). The scale of energies and the momentum dependence of this suppression are reminiscent of a d-wave superconducting gap observed in the same material well below T_c. This is suggestive of an influence on the normal state properties of some form of local superconducting pairing. We will show that indeed this is the case in our approach.

Note that there is no tendency for the gap to close as T_c is approached from below, the gap persists also in the normal state and the gap frequency seems to be quite temperature independent. On the other hand the sharp peaks of the spectrum in the SC phase reduce near T_c and become smaller in the normal state, until they vanish.

The gap, measured by the separation between the peaks, increases as the doping level is reduced.

1.3.6 Spin waves in the superconducting phase

Inelastic neutron scattering experiments [37], which measures the momentum and energy dependence of the dynamic spin susceptibility, in the superconducting state, show a resonant mode below the superconducting gap (or particle-hole continuum).

The spectrum for the magnetic excitations resembles an hourglass in energy-momentum space near the anti-ferromagnetic vector, as shown in Fig. (1.5). The dispersion comprises an upward and a downward branches merging at the wave-vector $Q_{AF} = (\pi, \pi)$ at an energy $E_{res} = 37,5\text{meV}$ for $YBa_2Cu_3O_{6.6}$. Probably there is a small gap between the high branch and the low branch.

While the high energy excitations hardly changes between SC and PG, the low energy magnetic spectral weight starts to increase in PG and below T_c the spectral rearrangement leads to the formation of the lower branch of the hourglass. Just above T_c, in the PG region, E_{res} is no more discernible and the hourglass-shape is replaced by an unusual "vertical" dispersion (dispersion means the position of the peaks of the magnetic intensity in the energy-momentum space).

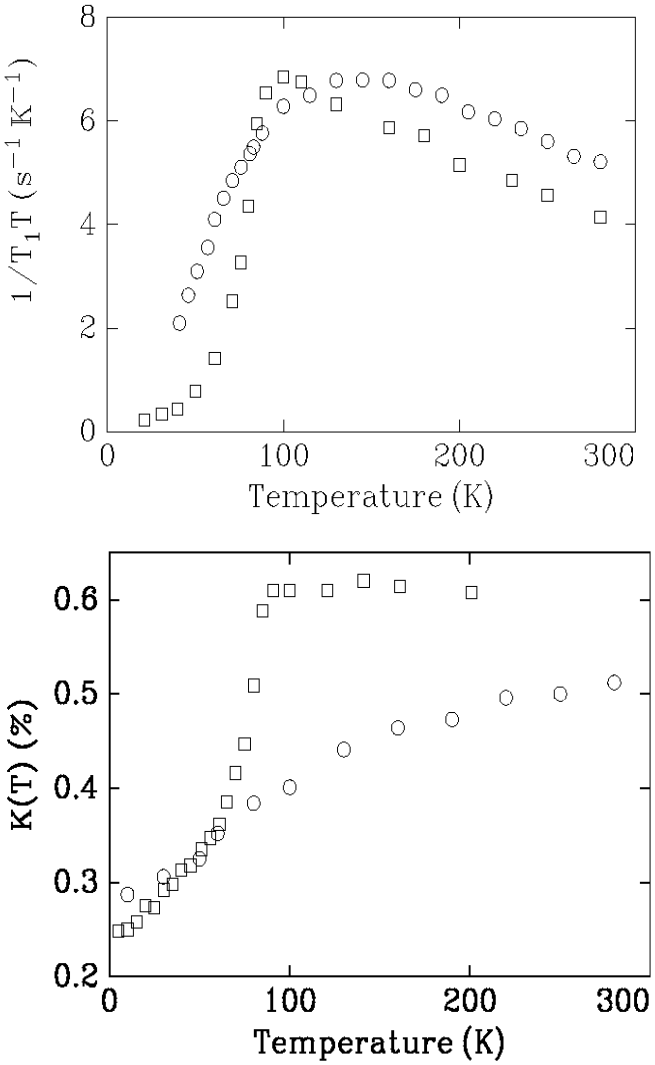

Figure 1.3: Temperature dependence of the planar ^{63}Cu relaxation rate $\frac{1}{T_1T}$ and Knight shift K in optimally doped $YBa_2Cu_3O_{6.95}$ (squares) and underdoped $YBa_2Cu_3O_{6.64}$ (circles); from Ref. [34].

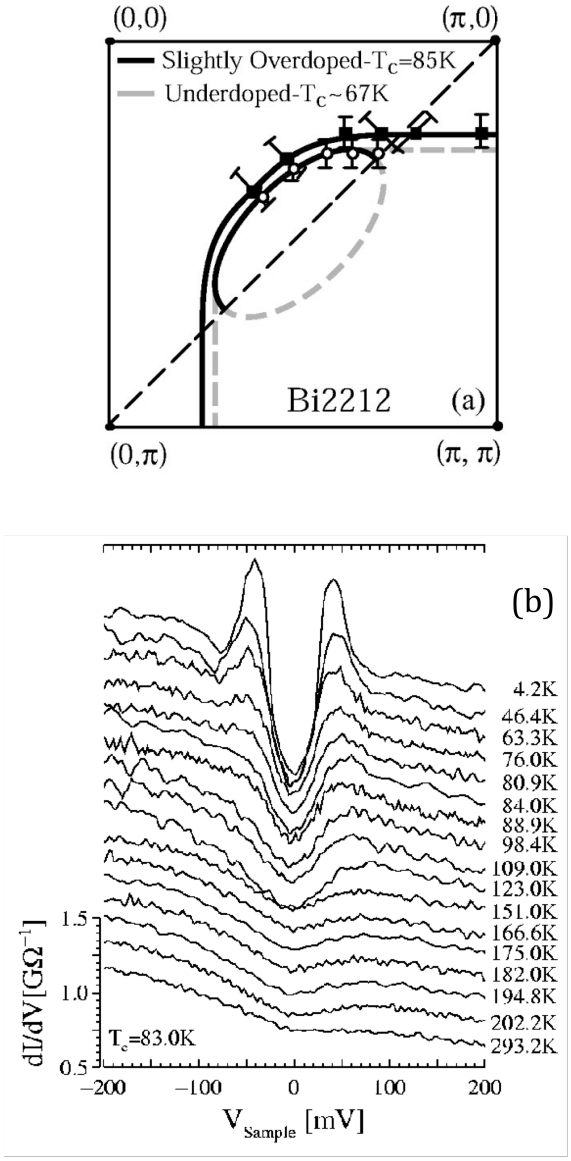

Figure 1.4: (a) Fermi surface for $Bi2212$; both the large FS typical of SM and the small half-pocket FS typical of PG are shown in the second quadrant of the Brillouin zone; from Ref. [36]. (b) Tunnelling density of states at various temperatures in a sample of underdoped $Bi_2Sr_2CaCu_2O_{8+\delta}$ with $T_c = 83K$; approaching the SC state peaks develop at $\pm 45meV$; from Ref. [35].

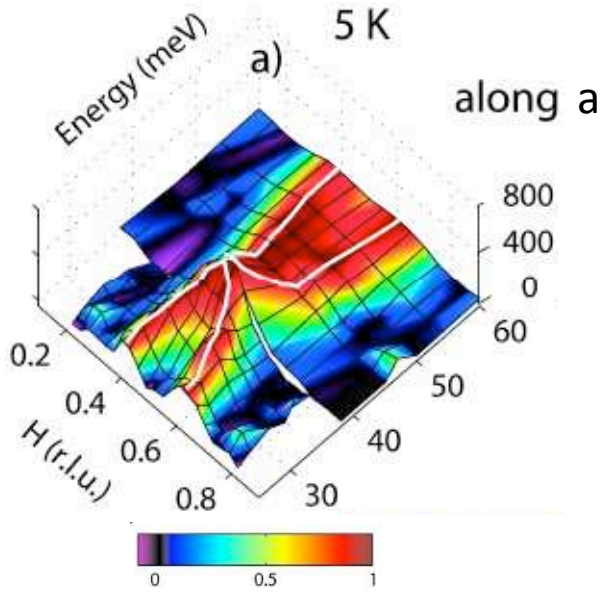

Figure 1.5: Representation of the magnetic intensity in the SC regime ($T_c = 61K$) along the a-axis. The crossing black lines represent measured data points and the white lines connect the fitted peak positions giving rise to the hourglass; from Ref. [37].

Chapter 2

Spin-Charge gauge approach to the t-J model

2.1 $SU(2) \times U(1)$ Chern–Simons bosonization of the t-J model

Explicit prohibition of double occupancy, ensured by the potential in Eq. (1.5), allows (in two dimensions) to formally perform spin-charge decomposition of the fermionic field in Eq. (1.4) by means of Chern-Simons (CS) bosonization. Although every bosonization scheme is an exact identity, mean field approximations (MFA), in different bosonization schemes, yield different results because they may incorporate some different non perturbative features.

Accepting the suggestion from the one-dimensional model, in which the semion statistics of spin and charge degrees of freedom lead to the correct correlation function in the scaling limit [8], we look for a semionic representation of the electron field also in the two-dimensional case.

An improved mean field treatment is obtained by looking for optimal statistical CS fluxes in mean field and considering fluctuation of spin and charge degrees of freedom (d.o.f.). The resulting action describes the low energy physics of the $t - J$ model we assumed for cuprates.

To apply this procedure we recall the main results of the $U(1) \times SU(2)$ CS bosonization for spin $\frac{1}{2}$ fermionic fields with hard-core term [14]. The classical euclidean action of a system of spin $\frac{1}{2}$ non-relativistic hard-core fermion fields, $\Psi_\alpha, \Psi^*_\alpha$, interacting via an instantaneous, spin independent two-body potential and in the presence of an external abelian gauge field A, is denoted by $S(\Psi, \Psi^*|A)$. The $t - J$ model action in Eq. (1.4),

fulfills these conditions if the gauge field A stands for the complex Hubbard-Stratonovich gauge field $X_{<ij>}$. Let $\Phi_\alpha, \Phi^*_\alpha$ be spin $\frac{1}{2}$ non-relativistic bosonic or fermionic fields. We introduce the $U(1)$ CS gauge field B and the $SU(2)$ CS gauge field V (more precisely $V_\mu = V^a_\mu \sigma_a/2,\ a = 1,2,3,\ \mu = 0,1,2$), minimally coupled to the matter fields and gauging the $U(1)$ charge symmetry and the $SU(2)$ spin symmetry of the action respectively. Free CS actions for these fields read

$$S_{c.s.}(B) = \frac{1}{4\pi i}\int d^3x \epsilon_{\mu\nu\rho} B^\mu \partial^\nu B^\rho \tag{2.1}$$

$$S_{c.s.}(V) = \frac{1}{4\pi i}\int d^3x \mathrm{Tr}\epsilon_{\mu\nu\rho}\Big(V^\mu \partial^\nu V^\rho + \frac{2}{3} V^\mu V^\nu V^\rho\Big) \tag{2.2}$$

The two following "bosonization formulas" can be derived.

- The grand-canonical partition function of the fermion system is given by

$$\int \mathcal{D}\Psi \mathcal{D}\Psi^* e^{-S(\Psi,\Psi^*|A)} = \frac{\int \mathcal{D}B\mathcal{D}V \int \mathcal{D}\Phi\mathcal{D}\Phi^* e^{-[S(\Phi,\Phi^*|A+B+V)\pm 2S_{c.s.}(B)+S_{c.s.}(V)]}}{\int \mathcal{D}B\mathcal{D}V e^{-[2S_{c.s.}(B)+S_{c.s.}(V)]}} \tag{2.3}$$

  where the gauge fixings for the gauge symmetries of the actions are understood and the $\Phi_\alpha, \Phi^*_\alpha$ fields are bosonic or fermionic depending on whether the sign in front of the B field action is positive or negative respectively.

- Let $\gamma_x(x = (x^0, \vec{x}))$ denote a string connecting x to infinity in the x^0–euclidean time plane; then the correlation functions of $\Psi_\alpha, \Psi^*_\alpha$ in the fermionic theory and the correlation functions of the non-local fields

$$\Phi_\alpha(\gamma_x|B,V) = e^{i\int_{\gamma_x} B}(Pe^{i\int_{\gamma_x} V})_{\alpha\beta}\Phi_\beta(x), \tag{2.4}$$

$$\Phi^*_\alpha(\gamma_x|B,V) = \Phi^*_\beta(x)e^{-i\int_{\gamma_x} B}(Pe^{-i\int_{\gamma_x} V})_{\beta\alpha} \tag{2.5}$$

  in the "bosonized" theory are identical. $P(\cdot)$ in Eqn. (2.4) denotes path-ordering.

To get an idea of the above statements we notice that integrating the time component of each Chern–Simons gauge field, appearing linearly in the action of Eqn. (2.3), two constraints of the form

$$j_0(x) = \frac{1}{2\pi}\epsilon_{0\nu\rho}W^{\nu\rho}(x), \tag{2.6}$$

are obtained, where $W^{\mu\nu}$ is the field strength of the appropriate CS field. In particular, W^{12} is a magnetic-like field, and j_μ is the current of the matter field. In this way a vortex for each CS field is attached to every matter particle assigning to it a magnetic-like charge. These matter particles also carry an electric-like charge because minimally coupled to each CS gauge field. The presence of both electric-like and magnetic-like charges implies an Aharonov-Bohm effect when the matter particles are exchanged, thus introducing a phase factor for every exchange. The number of exchanges is well defined thanks to hard-core condition.

In Eqn. (2.4) two CS fields contribute to the phase factor under exchange. Integration over CS fields turns the statistics of a bosonic field into fermionic if the total phase change for every exchange is π. In this case a factor factor $(-1)^\sigma$ is associated with each permutation of the matter particles where $\sigma = 0$ if the permutation is even and $\sigma = 1$ if the permutation is odd. But if the phase change is trivial (a factor 1 is associated to every permutation whether it is even or odd), then the statistics is unchanged after CS fields integration.

To analyze the $t - J$ model we choose the latter option so that, integrating both CS gauge fields, the phase factors cancel with each other exactly. As we shall see performing spin-charge separation, this choice allows semionic statistics of spin and charge excitations giving rise to a semionic representation of the electron field.

We apply this CS prescription to the $t - J$ model action in Eqn. (1.4) making the substitutions

$$\Psi^*_{j\alpha}\frac{\partial}{\partial\tau}\Psi_{j\alpha} \longrightarrow \Phi^*_{j\alpha}\Big[\Big(\frac{\partial}{\partial\tau} + iB_0(j)\Big)\mathbf{1} + iV_0(j)\Big]_{\alpha\beta}\Phi_{j\beta}, \tag{2.7}$$

$$\Psi^*_{i\alpha}\Psi_{j\alpha} \longrightarrow \Phi^*_{i\alpha}e^{i\int_{<ij>}B}(Pe^{i\int_{<ij>}V})_{\alpha\beta}\Phi_{j\beta} \tag{2.8}$$

and adding CS actions (2.1) as shown in Eqn. (2.3). CS bosonization formulas lead to the conclusion that the resulting action is equivalent to the starting one but more suitable for a formal spin-charge separation and for the following MFA.

2.2 Spin-Charge separation and $U(1)$ slave particle gauge field

To find the pair of semions making up the electron field, we formally separate the spin and charge degrees of freedom of the fermionic field $\Phi_{j\alpha}$, introduced in the previous section, by a polar decomposition [14]

$$\Phi_{x\alpha} = E_x \Sigma_{x\alpha} \tag{2.9}$$

where Σ_α is a 2-component complex field, called spinon field, and E is a 1-component fermionic field. The Pauli principle for the E field takes naturally into account the no-double occupancy constraint and the condition

$$\Sigma^*_{x\alpha}\Sigma_{x\alpha} = 1 \tag{2.10}$$

at any site x ensures that $\sum_\alpha \Phi^*_{x\alpha}\Phi_{x\alpha} = E^*_x E_x$. The presence of a spinless fermion replaces Gutzwiller projection P_G or, equivalently, the infinite on site repulsion in Eqn. (1.5) can be omitted.

The E field is coupled to the $U(1)$ gauge field B and describes the charge degrees of freedom and the spinon field Σ_α is coupled to the $SU(2)$ gauge field V and describes the spin degrees of freedom of the original fermion field. It follows from CS bosonization that in terms of these new variables the correlation functions of the electron field Ψ_α are given by the correlation functions of the non local field

$$\Psi_\alpha \sim \Phi_\alpha(\gamma_x|B,V) = e^{i\int_{\gamma_x} B} E_x (P e^{i\int_{\gamma_x} V})_{\alpha\beta}\Sigma_{x\beta}. \tag{2.11}$$

In this description the coefficient of the B field action in Eqn. (2.3) has been chosen negative. It follows that the gauge invariant euclidean fields $E_x e^{i\int_{\gamma_x} B}$ and $P(e^{i\int_{\gamma_x} V})_{\alpha\beta}\Sigma_{x\beta}$ give rise to charged field operators and spin $\frac{1}{2}$ field operators which obey semionic statistics [15]. The product of these gauge invariant semionic field operators represents the physical electron field operator.

The theory in terms of spinons Σ_α and E field is not equivalent to that in terms of the electron field Ψ_α or in terms of the field Φ_α because there is a gauge ambiguity involved in the decomposition in Eq. (2.9). We can in fact perform a local $U(1)$ gauge transformation leaving Φ invariant

$$E_j \to E_j e^{i\Lambda_j}, \quad \Sigma_{j\alpha} \to \Sigma_{j\alpha} e^{-i\Lambda_j}, \quad \Lambda_j \in [0, 2\pi[. \tag{2.12}$$

We need a gauge-fixing term not breaking the $U(1) \times SU(2)$ gauge invariance of the Φ-theory to get equivalent theories. It is useful to make manifest this local $U(1)$ gauge symmetry by introducing an emergent $U(1)$ gauge field, called slave particle (or h/s) gauge field, coupling spinon field and E field. Physical quantities, like correlations, are h/s gauge invariant quantities because built up with the gauge invariant Φ field.

Since we are interested in $t-J$ model near half filling (low doping), the last step is to describe charge degrees of freedom in terms of a hole-like Grassmann field H, called holon field, introduced making the substitution $E \to H^*, E^* \to H$.

To summarize, we begin from Eqn. (1.4) and introduce CS gauge fields via CS bosonization, Eqns. (2.3) and (2.7). Then making spin-charge decomposition, our dynamical variables became spinons and holons. Finally performing the integration over the auxiliary gauge fields X, the grand-canonical partition function $\Xi(\beta,\mu)$ can be written as

$$\Xi(\beta,\mu) = \int \mathcal{D}H\mathcal{D}H^*\mathcal{D}\Sigma_\alpha\mathcal{D}\Sigma^*_\alpha\mathcal{D}B\mathcal{D}V e^{-S(H,H^*,\Sigma,\Sigma^*,B,V)}\delta(\Sigma^*\Sigma - 1), \tag{2.13}$$

where the euclidean action in terms of $\{H, H^*, \Sigma, \Sigma^*, B, V\}$ is given by

$$\begin{aligned} S(H,H^*,\Sigma,\Sigma^*,B,V) \;=\; & \int_0^\beta dx^0 \Big\{ \sum_j \Big[H^*_j \Big(\partial_0 - iB_0(j) - (\mu + \frac{J}{2}) \Big) H_j + iB_0(j) \\ & + (1 - H^*_j H_j)\Sigma^*_{j\alpha} \Big(\partial_0 + iV_0(j) \Big)_{\alpha\beta} \Sigma_{j\beta} \Big] \\ & + \sum_{<ij>} \Big[(-tH^*_j e^{i\int_{<ij>} B} H_i \Sigma^*_{i\alpha} (Pe^{i\int_{<ij>} V})_{\alpha\beta} \Sigma_{j\beta} + h.c.) \\ & + \frac{J}{2}(1 - H^*_j H_j)(1 - H^*_i H_i) \Big(|\Sigma^*_{i\alpha} (Pe^{i\int_{<ij>} V})_{\alpha\beta} \Sigma_{j\beta}|^2 - \frac{1}{2} \Big) \Big] \Big\} \\ & - 2S_{c.s.}(B) + S_{c.s.}(V) \end{aligned} \tag{2.14}$$

and $\delta = \mu + J/2$ is the shifted chemical potential, proportional to the doping concentration. Notice that $U(1)$ h/s and $SU(2) \times U(1)$ gauge symmetries have to be gauge-fixed. This t-J model action in terms of holons, spinons and gauge fields (CS and h/s gauge fields) is the starting point for our improved MFA [5].

2.3 Gauge–fixing of the $SU(2) \times U(1)$ symmetry

The h/s symmetry, unlike $SU(2) \times U(1)$ symmetry, is kept exact in our treatment to ensure the validity of the Ioffe-Larkin rule [18] and we postpone its gauge-fixing according to convenience. In the spin-charge gauge approach the hole is a bound states of a spinon

and a holon while the h/s (or slave-particle) gauge field provides the necessary attractive interaction. The Ioffe-Larkin rule follows naturally from this picture stating that the resistivity of the hole ρ is the sum of the resistivity of the spinon ρ_s and the resistivity of the holon ρ_h, $\rho = \rho_s + \rho_h$. This non-standard feature can be intuitively understood as a consequence of the h/s gauge string binding spinon and holon, therefore the velocity of the hole is determined by the slowest (not the fastest!) among spinon and holon.

To proceed, as usual in gauge theories, we need a gauge-fixing of the $SU(2) \times U(1)$ symmetry.

We first gauge–fix the $U(1)$ symmetry imposing a Coulomb condition on B ($\mu = 1, 2$)

$$\partial^\mu B_\mu = 0. \tag{2.15}$$

To retain the bipartite lattice structure induced by the anti-ferromagnetic (AF) interactions, we gauge–fix the $SU(2)$ symmetry by a "Néel gauge" condition ($|j| = j_1 + j_2$)

$$\Sigma_j = \sigma_x^{|j|} \begin{pmatrix} 1 \\ 0 \end{pmatrix}, \quad \Sigma_j^* = (1, 0)\sigma_x^{|j|}, \tag{2.16}$$

Then we split the integration over V into an integration over a field $V^{(c)}$, satisfying the Coulomb condition:

$$\partial^\mu V_\mu^{(c)} = 0, \tag{2.17}$$

and its gauge transformations expressed in terms of an $SU(2)$-valued scalar field g, i.e. $V_a = g^\dagger V_a^{(c)} g + g^\dagger \partial_a g$, ($a = 0, 1, 2$).

Integrating over B_0 we obtain Eqn. (2.6) which, written in inverse form, becomes

$$B_\mu = \bar{B}_\mu + \delta B_\mu, \quad \delta B_\mu(x) = \frac{1}{2} \sum_j H_j^* H_j \partial_\mu \arg\,(x - j), \tag{2.18}$$

where $\bar{B}_\mu$ gives rise to a π-flux phase, i.e. $e^{i \int_{\partial p} \bar{B}} = -1$, for every plaquette p. Similarly integrating over V_0, we find

$$V_\mu^{(c)} = \sum_j (1 - H_j^* H_j)(\sigma_x^{|j|} g_j^\dagger \frac{\sigma_a}{2} g_j \sigma_x^{|j|})_{11} \partial_\mu \arg\,(x - j)\sigma_a. \tag{2.19}$$

After the $U(1) \times SU(2)$ field being gauge-fixed, the action in Eq. (2.14) becomes $S = S_1 + S_2$,

$$S_1(H,H^*,A,U) = \int_0^\beta dx^0 \Big\{ \sum_j \Big[H_j^* \Big(\partial_0 - \delta \Big) H_j + i(1 - H_j^* H_j) A_j \Big] + \sum_{<ij>} (-t H_i^* U_{<ij>} H_j + h.c.) \Big\}, \tag{2.20}$$

$$S_2(H,H^*,U) = \int_0^\beta dx^0 \sum_{<ij>} \frac{J}{2} (1 - H_i^* H_i)(1 - H_j^* H_j) \Big(|U_{<ij>}|^2 - \frac{1}{2} \Big). \tag{2.21}$$

where the lattice gauge fields A_j (real) and $U_{<ij>}$ (complex with $|U_{<ij>}| \leq 1$) depend on spin and charge variables as

$$iA_j = (\sigma_x^{|j|} g_j^\dagger \partial_0 g_j \sigma_x^{|j|})_{11}, \tag{2.22}$$

$$U_{<ij>} = e^{-i \int_{<ij>} (\bar{B} + \delta B)} (\sigma_x^{|i|} g_i^\dagger (P e^{i \int_{<ij>} V^{(c)}}) g_j \sigma_x^{|j|})_{11}. \tag{2.23}$$

S_1 is the action of spinless fermions gas with hopping parameter $t|U_{<ij>}|$, coupled to a gauge field with temporal component A_j and link component $e^{i \arg(U_{<ij>})}$. Action S_2 describes a Heisenberg anti-ferromagnet with spins situated at the non-empty sites and with a link dependent coupling constant [17].

Notice that CS actions do not introduce spurious degrees of freedom. The dynamical variables are the fermionic field H (2 d.o.f.) and the $SU(2)$ field g (3 d.o.f.) describing charge and spin degrees of freedom respectively. Remembering the constraint coming from the h/s gauge fixing (-1 d.o.f.), we reproduce the correct counting of degrees of freedom of the original fermionic field Ψ_α (2+2 d.o.f.).

2.4 Optimizations of the spinon configuration

To find out a low temperature effective action, we look for a holon dependent spinon configuration $g^m(H, H^*)$ minimizing the action. Then we consider spin fluctuations around this minimum configuration as a MFA.

The optimization procedure, presented in detail in Ref. [5], is a kind of Born-Oppenheimer approximation for the spinons in the presence of the holons, justified in the limit $t >> J$. Soft spinon fluctuations, surrounding the moving and massive hole, adjust themselves in a much shorter time scale. The relevant quantity for the optimization procedure is the statistical magnetic flux $\prod_{<ij> \in \partial p} U_{<ij>}$ per plaquette p. Once we found its optimal

value, we look for the spinon configuration g^m fulfilling this condition. We note from its definition in Eqn. (2.23) that choosing a constant spinon configuration when no particle hops we get $A_j = 0$. As a consequence g^m appears in actions of Eqn. (2.21) only through the complex gauge field $U_{<ij>}$. Moreover, for a fixed link $< ij >$, in every holon configuration the term $(\sigma_x^{|i|} g_i^\dagger P e^{i \int_{<ij>} V^{(c)}} g_j \sigma_x^{|j|})_{11}$ appears either in the hopping term of holons or in the Heisenberg term of spinons, but never simultaneously. This is a consequence of the single-occupancy constraint and permits a separate optimization of S_1 and S_2. For holon-empty sites $U_{<ij>} = 0$ in S_2 is the optimal choice. This can be achieved choosing g^m without off-diagonal elements for holon-empty sites. For the optimal configuration Eq. (2.19) becomes

$$V^{(c)}(x) = \sum_j (1 - H_j^* H_j) \frac{(-1)^{|j|}}{2} \partial_\mu \arg\,(x - j)\sigma_z, \tag{2.24}$$

since $V^{(c)}$ depends only on sites where there are no holes. In this way $g_i^\dagger P e^{i \int_{<ij>} V^{(c)}} g_j$ has only diagonal components which means that the RVB order parameter of the Heisenberg term is very small [22].

Regarding the action S_1, aside from the phase factor due to the B gauge field, $U_{<ij>}$ plays the role of the AM order parameter [3], and defines statistical fluxes. We list some results to justify our following optimal choices concerning statistical fluxes:

- Lieb proves [19] that at half-filling ($\delta = 0$) the optimal configuration for a magnetic field on a square lattice in 2D has a flux π per plaquette at arbitrary temperature.
- At low densities and high temperatures the optimal configuration has 0 flux per plaquette.
- At $T = 0$ it has been proven that the ground state energy has a minimum corresponding to one flux quantum per spinless fermion [20].
- Numerical simulations [21] suggest that increasing T gives rise to a competition between these minima and at sufficiently high T only 0 and π flux survive.

We expect that the perturbation introduced by the J term in the $t - J$ model changes the boundary, but not the essence of the phenomenon of the $\pi \longrightarrow 0$ crossover, π-flux corresponds to PG and 0-flux to SM.

From the above results, the optimization conditions we impose for the PG region correspond to

$$|\hat{U}_{<ij>}| = 1, \quad \arg\,(\hat{U}_{\partial p}) = \pi(1-\delta). \tag{2.25}$$

On the other hand, for SM region we choose

$$|\hat{U}_{<ij>}| = 1, \quad \arg\,(\hat{U}_{\partial p}) = 0. \tag{2.26}$$

We note that both in PG and SM Ioffe-Larkin rule holds because AM order parameter, unlike RVB, leaves unbroken the global slave particle symmetry h/s.

Translating these conditions on the spinon configuration g, in a path-integral first-quantized formalism, we obtain

$$g_j = \bar{g}_j R_j \tilde{g}_j = e^{-\frac{i}{2}\sum_{\ell\neq j}(-1)^{\ell}\sigma_z \arg(\ell-j)} R_j \tilde{g}_j \tag{2.27}$$

with the fluctuations R_j being represented in CP^1 form as

$$R_j = \begin{pmatrix} b_{j1} & -b^*_{j2} \\ b_{j2} & b^*_{j1} \end{pmatrix}, \tag{2.28}$$

$$b^*_{j\alpha} b_{j\alpha} = 1. \tag{2.29}$$

where $b_{j\alpha}$ is a two-component complex field. The optimal configuration g^m is given by $R = 1$. The role of $\bar{g}$ is to kill the fast fluctuating term in Eq. (2.24), in fact the relation $\bar{g}_i^{\dagger} e^{i\int_{<ij>} V^{(c)}} \bar{g}_j = e^{i\int_{<ij>}\bar{V}}$ holds and

$$\bar{V} = -\sum_j H^*_j H_j \frac{(-1)^{|j|}}{2} \partial_\mu \arg\,(x-j)\sigma_z \tag{2.30}$$

is the remaining term. The statistical field $\bar{V}$ is the new feature of our treatment of the $t-J$ model. It comes from the $SU(2)$ sector and depend only on holons distribution. Its effect is to attach to the holons a vortex of $SU(2)$-vorticity $\pm\sigma_z\frac{\pi}{2}$ and the sign depends on the Néel sublattice where the holon is located [52].

The difference between PG and SM lies in $\tilde{g}_j$. In PG it provides an additional spin flip for the holon-occupied sites

$$\tilde{g}_j = e^{i\frac{\pi}{2}(-1)^{|j|}\sigma_y H^*_j H_j} \tag{2.31}$$

while in SM it is responsible for cancellation of the statistical flux carried by the charge gauge field B by means of the flux carried by the spin gauge field V and it has the form

$$\phi_j = \begin{cases} \tilde{g}_j = e^{i(\vec{\sigma}\cdot\vec{n}_j)}, \quad n_j = (\cos\phi_j, \sin\phi_j, 0), \quad \frac{\pi}{4}(-1)^{|j|}, & \text{if} \quad H_j^* H_j = 1 \\ \tilde{g}_j = 1, & \text{if} \quad H_j^* H_j = 0. \end{cases} \tag{2.32}$$

Plugging Eq. (2.27) in Eqs. (2.20) and (2.21) we obtain two different, but exactly equivalent, actions describing $t-J$ model. The action obtained using Eq. (2.31), suitable for a MFA of the PG region, is $S = S_h + S_s$

$$\begin{aligned} S_h &= \int_0^\beta dx^0 \left\{ \sum_j H_j^* \left[\partial_0 - (\sigma_x^{|j|} R_j^\dagger \partial_0 R_j \sigma_x^{|j|})_{11} - \delta \right] H_j \right. \\ &\left. + \sum_{<ij>} \left[-t H_j^* e^{-i\int_{<ij>}(\bar{B}+\delta B)} H_i \left(\sigma_x^{|i|} R_i^\dagger P e^{i\int_{<ij>}(\bar{V}+\delta V)} R_j \sigma_x^{|i|} \right)_{11} + h.c. \right] \right\}, \end{aligned} \tag{2.33}$$

$$\begin{aligned} S_s &= \int_0^\beta dx^0 \left\{ \sum_j (\sigma_x^{|j|} R_j^\dagger \partial_0 R_j \sigma_x^{|j|})_{11} \right. \\ &\left. + \sum_{<ij>} \frac{J}{2}(1 - H_i^* H_i)(1 - H_j^* H_j) \left[|(\sigma_x^{|i|} R_i^\dagger P e^{i\int_{<ij>}(\bar{V}+\delta V)} R_j \sigma_x^{|j|})_{11}|^2 - \frac{1}{2} \right] \right\}, \end{aligned} \tag{2.34}$$

where $\delta V = V^{(c)} - \bar{V}$ and the relation $\tilde{g}_j \sigma_x^{|j|} = \sigma_x^{|j|+1}$, holding in the scalar products, was used.

The action obtained via Eq. (2.32) is $S = S_h + S_s$

$$\begin{aligned} S_h &= \int_0^\beta dx^0 \left\{ \sum_j H_j^* \left[\partial_0 - (\sigma_x^{|j|} \tilde{g}_j^\dagger R_j^\dagger \partial_0 R_j \tilde{g}_j \sigma_x^{|j|})_{11} - \delta \right] H_j \right. \\ &\left. + \sum_{<ij>} \left[-t H_j^* e^{-i\int_{<ij>}\delta B} H_i (\sigma_x^{|i|} \tilde{g}_i^\dagger R_i^\dagger P e^{i\int_{<ij>}(\bar{V}+\delta V)} R_j \tilde{g}_j \sigma_x^{|i|})_{11} + h.c. \right] \right\}, \end{aligned} \tag{2.35}$$

$$\begin{aligned} S_s &= \int_0^\beta dx^0 \left\{ \sum_j (\sigma_x^{|j|} \tilde{g}_j^\dagger R_j^\dagger \partial_0 R_j \tilde{g}_j \sigma_x^{|j|})_{11} \right. \\ &\left. + \sum_{<ij>} \frac{J}{2}(1 - H_i^* H_i)(1 - H_j^* H_j) \left[|(\sigma_x^{|i|} \tilde{g}_i^\dagger R_i^\dagger P e^{i\int_{<ij>}(\bar{V}+\delta V)} R_j \tilde{g}_j \sigma_x^{|j|})_{11}|^2 - \frac{1}{2} \right] \right\}, \end{aligned} \tag{2.36}$$

and is appropriate for describing small fluctuations in SM region. We note that in this case the statistical field $\bar{B}$ carrying π-flux has disappeared.

2.5 Approximations, spinons and holons effective actions

To proceed further we need our main approximation. We neglect δB_μ and δV_μ, i.e. the feed–back of charge fluctuations on B and of spin fluctuations on V^c. Presumably the main neglected effect is a statistic transmutation giving rise to semionic statistics for holons and spinons. We argue that the this statistics is not strongly relevant because we expect the formation of bound states, via slave particle gauge field, representing physical quantities, such as electron (spinon plus anti-holon) or magnon (spinon plus anti-spinon).

In this approximation the low-energy continuum effective action for spinons is the same in both PG and SM (except for a correction in the mass term at relatively high temperature). We assume

$$b^*_{j\alpha}\vec{\sigma}_{\alpha\rho}b_{j\beta} \sim \vec{\Omega}_j + (-1)^{|j|}\epsilon\vec{L}_j, \tag{2.37}$$

with $\vec{\Omega}_j^2 = f \sim 1$, $\vec{\Omega}\cdot\vec{L} = 0$, where $\vec{\Omega}$ and $\vec{L}$ are defined on a sublattice to maintain the correct number of degrees of freedom. To make manifest the h/s gauge field A, we integrate ferromagnetic degrees of freedom $\vec{L}$ and rewrite anti-ferromagnetic ones $\vec{\Omega}$ in the CP^1 form

$$\vec{\Omega} = z^*_\alpha\vec{\sigma}_{\alpha\beta}z_\beta, \qquad z^*_\alpha z_\alpha = f, \tag{2.38}$$

with z_α a spin $\frac{1}{2}$ complex hard-core boson field. Sum over repeated (non-spatial) indices is understood. This procedure leads to the non-linear σ-model action with a mass term

$$S_s = \int_{[0,\beta]\times\mathbf{R}^2} d^3x \frac{1}{g}\left[|(\partial_0 - A_0)z_\alpha|^2 + v_s^2|(\partial_\mu - A_\mu)z_\alpha|^2 + m_s^2 z^*_\alpha z_\alpha\right]. \tag{2.39}$$

with $g = 8/J$ and $v_s = \sqrt{2}Ja$ (a lattice constant). The mass term stems from the average over holon configurations with a mean density δ of the term $\vec{\Omega}^2\bar{V}_z^2$ arising from the lowest order interaction between $\vec{\Omega}$ and $\bar{V}$ in the Heisenberg term in the case of unbroken rotational symmetry. An estimation of this average for small δ gives [16],

$$\langle\bar{V}_z^2\rangle = m_s^2 \sim -\delta\ln\delta. \tag{2.40}$$

Hence spinons, scattering against spin vortex attached to holons, gain a mass term increasing with δ. This disordered regime with unbroken symmetry and correlation length $\xi_{AF} \sim 1/m_s$ is fully consistent with neutron scattering data [23]. We see that within this approach spin gap in cuprates is mainly due to short range AF order.

In Eqn. (2.39) the self generated $U(1)$ h/s gauge field

$$A_a = z^*_\beta \partial_a z_\beta \tag{2.41}$$

has been introduced. This is an internal variable over which we integrate after the $U(1)$ symmetry is gauge fixed.

We now turn to the holon sector which is different in PG, Eq. (2.33), and SM, Eq. (2.35), because of the presence in PG of a π flux per plaquette due to the $\bar{B}$ gauge field. The AM order parameter in the hopping term is nearly one in both cases and together with the temporal term will provide the interaction between holons and spinons through a minimal coupling to the h/s gauge field defined in Eq. (2.41).

To define a continuum holons effective action for PG, we fix the gauge of $\bar{B}$ field choosing a phase of $\pm\pi/4$ on every link and, according to the d staggered symmetry typical of cuprates, see Fig. (2.1), we define 4 sublattices ((1) for j_1, j_2 even, (2) for j_1 odd, j_2 even, (3) for j_1 even j_2 odd, (4) for j_1, j_2 odd). They can be grouped into two "Néel" sublattices $A = \{(1),(4)\}$, $B = \{(2),(3)\}$. Setting $\gamma_0 = \sigma_z$, $\gamma_\mu = (\sigma_y, \sigma_x)$ and

$$\Psi_1 = \left(\Psi_1^{(A)}, \Psi_1^{(B)}\right)^t = \left(e^{-i\frac{\pi}{4}} H^{(1)} + e^{i\frac{\pi}{4}} H^{(4)}, e^{-i\frac{\pi}{4}} H^{(3)} + e^{i\frac{\pi}{4}} H^{(2)}\right)^t \tag{2.42}$$

$$\Psi_2 = \left(\Psi_2^{(B)}, \Psi_2^{(A)}\right)^t = \left(e^{-i\frac{\pi}{4}} H^{(2)} + e^{i\frac{\pi}{4}} H^{(3)}, e^{-i\frac{\pi}{4}} H^{(4)} + e^{i\frac{\pi}{4}} H^{(1)}\right)^t \tag{2.43}$$

and assigning charge $e_A = +1, e_B = -1$ to the fields corresponding to A and B sublattices, respectively, the continuum effective action for holons can be rewritten as

$$S_h = \int_{[0,\beta]\times \mathbf{R}^2} d^3x \sum_{r=1}^{2} \bar{\Psi}_r \Big[\gamma_0(\partial_0 - \delta - e_r A_0) + v_F \gamma_\mu (\partial_\mu - e_r A_\mu)\Big] \Psi_r \tag{2.44}$$

This action describes Dirac-like fermions (except for the presence of a chemical potential breaking relativistic invariance) as excitation of the staggered flux phase, with vertices of the double-cone dispersion relations in the reduced Brillouin zone (BZ) centered at $\left(\pm\frac{\pi}{2}, \pm\frac{\pi}{2}\right)$ and chemical potential δ. The upper components of Ψ describe gapless excitations with small FS ($\epsilon_F \simeq O(\delta t)$), whereas the lower components describe massive excitations whose mixing is expected to reduce the spectral weight in the outer part of the reduced BZ.

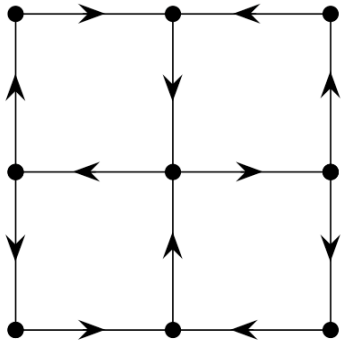

Figure 2.1: Staggered π-flux phase in the PG region respecting the d-wave symmetry of underdoped cuprates; we fix the gauge in such a way that the phase is $+\pi/4$ on every link according to the arrows. Notice the invariance under a translation by a diagonal of the plaquette.

As regards SM, the $\pi \longrightarrow 0$ crossover in the MF treatment of the holon hopping term converts, via Hofstadter phenomenon, the PG spectrum in a more conventional tight binding spectrum defined in the entire BZ. The continuum low energy action is given by

$$S_h = \int_{[0,\beta]\times\mathbf{R}^2} d^3x H^*(x^0,\vec{x}) \left[i\partial_0 - \epsilon_F - A_0 - \frac{1}{2m^*}(\vec{\nabla} - i\vec{A})^2 \right] H(x^0,\vec{x}) \tag{2.45}$$

with effective chemical potential $\epsilon_F \sim 4t(1-\delta)$, $v_F \sim 2t$ is doping independent, $k_F \propto (1-\delta)$ and $m^* = k_F/v_F = (1-\delta)/2t$, where for convenience we rename $H^* \to H$ since the closed FS is for H^*. As above fermionic excitations are gapless but now there is a large Fermi surface (circular as a first approximation) whose bottom is located at the center of the BZ.

2.6 Slave particle gauge field effective action

In the previous section we obtained the effective actions for PG region and for SM region by summing Eqs. (2.39) with Eq. (2.44) or Eq. (2.45) respectively.

Holon and spinon sectors are strongly correlated via the emergent slave particle $U(1)$ gauge field A. It has no proper dynamics but, owing to quantum effects, it gain an effective action via integration of spinon and holon degrees of freedom. Since z_α is gapful,

the spinon contribution is Maxwellian with a thermal mass m_0 for A_0. On the contrary, holons have a finite FS (in both PG and SM) and their contribution to the transverse component exhibits the so-called Reizer singularity [24]. The leading behavior of the transverse A propagator is $(i, j = 1, 2)$ [9], [44]

$$\langle A_i^T A_j^T \rangle(\omega, q) \sim \left(\delta_{ij} - \frac{q_i q_j}{\vec{q}^2}\right) \left(i\kappa \frac{\omega}{|\vec{q}|} - \chi \vec{q}^2\right)^{-1}, \tag{2.46}$$

where $\kappa \sim k_F$ is the Landau damping and $\chi = \chi_s + \chi_h$ with $\chi_s \sim \frac{J}{6\pi m_s}, \chi_h = \frac{t}{6\pi k_F}$, is the total diamagnetic susceptibility, dominated, at least for small δ, by the holon contribution. There is a characteristic scale of gauge fluctuations emerging from the Reizer singularity at finite T. It is a kind of anomalous skin depth, derived by assuming as typical energy $\omega \sim T$, with the consequence that the transverse gauge interaction is peaked at $q = Q_T = \left(\frac{\kappa T}{\chi}\right)^{\frac{1}{3}}$. The Reizer singularity is due to the simultaneous appearance of a finite FS and a mass gap for the bosonic excitations z_α. If bosons were massless they would condense gapping the gauge field via Anderson-Higgs mechanism and destroying Reizer singularity.

In our approach, the competition between the spinon mass and the dissipation due to the h/s gauge field coupling to holons will be responsible for the anomalous behavior of many transport phenomena, in particular for the metal insulator crossover (MIC) in underdoped cuprates.

The scalar component A_0 has a low energy propagator given by

$$\langle A_0 A_0 \rangle(\omega, q) \sim \left[\kappa \left(1 + i\frac{\omega}{|\vec{q}|}\right) \theta\left(|\vec{q}| - |\omega|\right) + m_0^2\right]^{-1} \tag{2.47}$$

where m_0 is a thermal mass due to spinons and θ the step function. In view of the constant term in Eq. (2.47), the interaction mediated by A_0 is short ranged and hence subleading at large distance w.r.t. the interaction mediated by A^T, triggered by the Reizer singularity. Nevertheless, since we are in 2D, the attractive force mediated by the gauge field is expected to produce bound states with the quantum numbers of the spin wave of the electron.

We note the gauge field propagator has the same form in PG and SM, but the modification in the structure of the FS affects the value of the involved parameters. The main change is the value of k_F: it is small and proportional to δ in PG while in SM it is larger by a factor of order 5-10, being proportional to $1 - \delta$. As a consequence the spinon gap effects are less effective in SM.

2.7 Main predictions in the normal state

In this section we outline some prediction in terms of phenomena and experimental physical quantities, useful in the following, in the framework of this approach to the $t-J$ model [9], [11].

A difficulty in considering the gauge fluctuations is the lack of a small parameters for expansions. On the basis of gauge invariance we expect some kind of binding to get bound states (or resonances) with the quantum numbers of the electron (spinon and holon) and of the magnon (spinon and anti-spinon).

Roughly speaking, spinons and holons behave like separate particles and their scattering against gauge fluctuations renormalizes their properties and, at small energy scale, binds spinon and anti-spinon into the magnon resonance and spinon and holon into the electron resonance with non-Fermi-liquid properties. These low-energy excitations are no longer well-defined quasi-particles but rather loosely bound composite particles.

Because a perturbative treatment would be insufficient to implement binding, we obtain the correlation functions of physical (hence gauge invariant) fields applying a kind of eikonal resummation of (transverse) gauge fluctuations [11]. This resummation is obtained by treating first A_μ as an external field and expanding the correlation function in terms of first-quantization Feynman paths. Integrating out A_μ we obtain an interaction between paths which is treated in the eikonal approximation. Finally a Fourier transform is performed to get the retarded correlation function. However further approximations are needed, especially in the treatment of short scales, to get the following results about magnon and electron [12], [43].

2.7.1 Metal-insulator crossover

As a consequence of the slave particle gauge field binding spinon to holon, the velocity of the electron is determined by the slowest among spinon and holon. In this sense Ioffe-Larkin rule (stating that the inverse conductivity of the electron is the sum of the inverse conductivities of the spinon and the holon) make it possible to reconcile the insulating behavior at low temperatures with the presence of a finite FS. Moreover the universality of MIC can be qualitatively explained noting that the leading behavior comes from the spinon (bosonic) sector, without a detailed reference to the FS of the holon (fermionic) sector.

MIC (clearly shown in the two higher curves of the panel (a) in Fig. (1.2)) is an outcome of competition between the AF short range order (SRO) and the dissipative

motion of the charge carriers. We start from the Mott insulating state showing AF long range order (LRO). Upon doping beyond certain threshold, since holes distort the AF background, the AF LRO is destroyed, being replaced by SRO, characterized by the AF correlation length $\xi = \frac{1}{m_s}$, providing the first length scale. As we shall see in the next subsection, a competing factor is the diffusive motion of the charge carriers with characteristic energy Tm_h, where $m_h \sim \frac{\delta}{t}$ is the effective mass of holons in the PG phase. The corresponding length scale is the thermal de Broglie wave length $\lambda_T \sim \sqrt{\frac{t}{T\delta}}$. At low temperatures $\xi \leq \lambda_T$, the AF SRO dominates and the charge carriers become weakly localized (not exponentially) showing insulating behavior (this localization is mainly due to interaction rather than disorder). On the contrary, at high temperatures $\xi \geq \lambda_T$, the diffusive motion of charge carriers prevails, exhibiting metallic conductivity. Therefore the competition of the real part of the spinon self-energy, the mass gap, and the imaginary part, the dissipation, gives rise to MIC.

It turns out that a number of experimental observations in the PG phase can also be explained by the competition of these two factors and the composite nature of low-energy excitations.

2.7.2 $T^*(\delta)$ and magnon correlation

For δ, T small, a parameter region identified with PG, it turns out numerically that the spatial Fourier transform in the eikonal approximation is dominated by a nontrivial complex $|\vec{x}|$-saddle point, $|x|_{s.p.} = Q_T^{-1} e^{i\frac{\pi}{4}}$ due to the effect of gauge fluctuations. The self-consistency requirement for this eikonal approximation yields a region of validity given approximately by $m_s Q_T \leq \frac{T}{\chi} \leq m_s^2$. The upper bound temperature roughly coincides, both as order of magnitude and as $\delta - T$ dependence (for low doping), with the pseudogap temperature T^* (entering the SM region) slowly decreasing with doping δ

$$T^*(\delta) \sim \chi m_s^2 \sim \frac{t}{6\pi\delta} |\delta \ln \delta| \sim \frac{t}{6\pi} |\ln \delta|. \tag{2.48}$$

The main effect of the complex saddle point within the above range is to induce a shift in the mass of spinons

$$m_s \to M = \sqrt{m_s^2 - ic\frac{T}{\chi}} \tag{2.49}$$

where $c \sim 3$ is a constant, thus introducing a dissipation proportional to T. Physically, due to the Ioffe-Larkin rule electron conductivity is dominated by spinons, and the

competition between the mass gap and the dissipation appearing in M is responsible for the MIC, as explained above.

The retarded magnon propagator derived in PG is given by

$$\langle\vec{\Omega}\cdot\vec{\Omega}\rangle^{PG}(\omega,\vec{q}) \sim \frac{Z_\Omega^{PG}}{\omega-2M} J_0\left(\frac{|\vec{q}||x|_{s.p.}}{2}\right) \tag{2.50}$$

where J_0 is the Bessel function and $Z_\Omega^{PG} = \frac{1}{Q_T}\sqrt{k_F M}$.

For sufficiently high δ or T, i.e. in the SM region, the saddle point contribution is negligible w.r.t. the contribution of fluctuations around 0 in the range $|\vec{x}| \leq Q_T^{-1}$. The result of gauge fluctuations can also be summarized in terms of the appearance of a dissipative term

$$m_s \to m_s - i\Gamma_\Omega^{SM} \tag{2.51}$$

with $\Gamma_\Omega^{SM} = c'\frac{T}{\chi m_s^2}Q_T$ and $c' \sim 0.1$. In SM, however, the change of k_F from δ to $1-\delta$ yields a decrease of diamagnetic susceptibility χ, implying that the thermal de Broglie wave length is shorter than in PG. Therefore the spin-gap effects ($\xi_{AF} < \lambda_T$) are less effective, being confined to very low temperatures.

The retarded magnon propagator in SM reads

$$\langle\vec{\Omega}\cdot\vec{\Omega}\rangle^{SM}(\omega,\vec{q}) \sim \frac{Z_\Omega^{SM}}{\omega-2m_s+i\Gamma_\Omega^{SM}} \frac{e^{-\frac{|\vec{q}|^2}{a}}}{a} \tag{2.52}$$

where $a = \frac{T}{\chi m_s}Q_T \propto T^{\frac{4}{3}}$ and $Z_\Omega^{SM} = Q_T^2 \propto T^{\frac{2}{3}}$.

From Eqs.(2.50) and (2.52) we see that the transverse gauge fluctuations couple spinon and anti-spinon into a magnon resonance with mass gap $2m_s$ and inverse life time

$$\Gamma_\Omega^{PG} = \Im M \propto \begin{cases} T & \text{if} \quad m_s^2 >> \frac{cT}{\chi} \\ T^{\frac{1}{2}} & \text{if} \quad m_s^2 \sim \frac{cT}{\chi} \end{cases} \tag{2.53}$$

in PG and

$$\Gamma_\Omega^{SM} \propto T^{\frac{4}{3}} \tag{2.54}$$

in SM.

Moreover Γ_Ω^{-1} turns out to be proportional to to the electron life-time, which thus always increases as T decreases. The point is that above MIC the increase of the electron life-time yields an increase of conductivity, but below MIC the mobility decreases as T lowers because the spinon can move only through thermal diffusion, induced by gauge

fluctuations due to gapless holons, and, because of binding, the electron can move only if the spinon does. The electron retarded propagator at the FS reads

$$G^R(\omega, \vec{k}_F) \sim \frac{Z}{\omega + i\Gamma} \tag{2.55}$$

where $Z \approx \sqrt{Q_T m_s}$ and $\Gamma = \frac{\Gamma_\Omega}{2}$. Therefore the gauge fluctuations are able to bind spinon and holon into a resonance for low energies but with a strongly temperature dependent wave function renormalization. The electron resonance is responsible for the inter-plane transport properties, indeed, because of gauge invariance, spinon and holon must bind before hopping between adjacent CuO_2 planes.

2.7.3 In-plane resistivity

The in-plane resistivity ρ_{ab} is calculated via the Ioffe-Larkin rule, $\rho_{ab} = \rho_s + \rho_h$, where ρ_s is the resistivity of the spinon-gauge subsystem and ρ_h of the holon-gauge subsystem. The last one is subdominant and of standard form (both in PG and SM) for a FL interacting with a gauge field, thus exhibiting Reizer singularity,

$$\rho_h \sim \frac{1}{\tau_{imp}} + \epsilon_F \left(\frac{T}{\epsilon_F}\right)^{\frac{4}{3}} \tag{2.56}$$

where we added the contribution of impurity scattering $\frac{1}{\tau_{imp}}$ via Matthissen rule.

As for spinons in PG, we put $\vec{J} = \vec{j}_s$ (where $\vec{j}^s \sim \partial\vec{\Omega} \sim Q_T\vec{\Omega}$ is the spinon current) in the Kubo formula of Eq. (1.6) and using Eq. (2.50) we obtain

$$\rho \sim \rho_s \sim \frac{|M|^{1/2}}{\sin(\frac{\arg M}{2})} \sim \begin{cases} T^{-1} & m_s^2 >> \frac{cT}{\chi} \\ T^{\frac{1}{4}} & m_s^2 \sim \frac{cT}{\chi}. \end{cases} \tag{2.57}$$

From the above equation MIC is recovered and, due to the square root in M, there is an inflection point $T^* \sim \chi m_s^2$ at higher temperature, found also experimentally [33]; see Fig. (2.2). In our approach the MIC is due to correlation effects, not to a disorder-induced localization, in fact the insulating behavior is power-law like, not exponential. Moreover a universal behavior of the normalized resistivity $\rho_n = [\rho - \rho(T_{MIC})]/[\rho(T^*) - \rho(T_{MIC})]$ results as a function only of the ratio $y = cT/T^*$.

On the other hand, in SM one obtains

$$\rho_s \simeq 2\frac{\lambda}{Q_T}\left(\Gamma_\Omega^{SM} + \frac{m_s^2}{\Gamma_\Omega^{SM}}\right) = \frac{c'T}{\chi m_s^2}\lambda^2 + \frac{4m_s^4\chi}{c'TQ_T^2}, \tag{2.58}$$

where $\lambda \approx 0.7$. In the high temperature limit $Q_T >> m_s$, the damping rate in Eq. (2.58) dominates over the spin gap $2m_s$ and the spinon contribution to resistivity is linear

in T, with a slope $\alpha \simeq \frac{1-\delta}{m_s^2}$, see Fig. (2.3). Lowering the temperature, the second term in gives rise first to a superlinear behavior and then, at the margin of validity of our approach, an unphysical upturn.

The deviation from linearity here is due to the spin gap effects and is cut off in the underdoped samples by the crossover to the PG phase. We will show that actually, because of the formation of incoherent holon pairs in SM region (as a precursor regime of superconductivity), the deviation from linearity begins at higher temperature (as is experimentally observed) and at lower temperatures both contributions sum up.

The celebrated (approximate) T-linearity can also be understood qualitatively as a consequence of Γ and the effectiveness of the gauge fluctuations to form electron resonance predominantly contributing to conductivity in a slab of momenta Q_T around the Fermi surface. In fact the conductivity derived from the Boltzmann transport theory would be $\sigma_0 \sim \Gamma^{-1}$, but due to effectiveness the physical conductivity is $\sigma \sim \sigma_0 Q_T \sim T^{-4/3}T^{1/3} \sim T^{-1}$. Similar considerations apply also to the spin relaxation time $^{63}(TT_1)$ and the Knight shift K_s.

2.7.4 Spin lattice relaxation rate

Assuming Q_T as cutoff for the $|\vec{q}|$ integration and using the smoothness of the hyperfine field at this scale we derive in PG

$$\begin{aligned} {}^{63}(\frac{1}{T_1T}) &\sim (1-\delta)^2|M|^{-\frac{1}{2}}(a\cos(\frac{\arg M}{2}) + b\sin(\frac{\arg M}{2})) \\ &\sim \begin{cases} a+bT & m_s^2 >> \frac{cT}{\chi} \\ T^{-\frac{1}{4}} & m_s^2 \sim \frac{cT}{\chi} \end{cases} , \end{aligned} \tag{2.59}$$

with $a/b \sim 0.1$, and the two terms are due to the real and the imaginary parts of J_0 in Eq. (2.50); se Fig. (2.4). Thus we obtain a broad peak, observed in some cuprates, and, up to a multiplicative constant, a universality curve as a function of $y = cT/T^*$.

In SM one finds

$${}^{63}(\frac{1}{T_1T}) \sim \frac{(1-\delta)^2}{\rho_s}. \tag{2.60}$$

Therefore in the high temperature limit we recover the linear in T behavior for $^{63}(T_1T)$ and at high doping or low temperatures the superlinear deviation, also found experimentally in overdoped samples of LSCO, see Fig. (2.5).

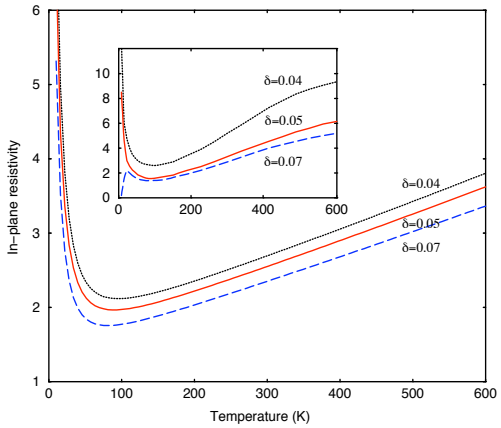

Figure 2.2: The calculated temperature dependence of the in-plane resistivity for various dopings δ in comparison with the corresponding experimental data (inset) on $La_{2-\delta}Sr_{\delta}CuO_4$ in units of $m\Omega cm$, taken from Ref. [33].

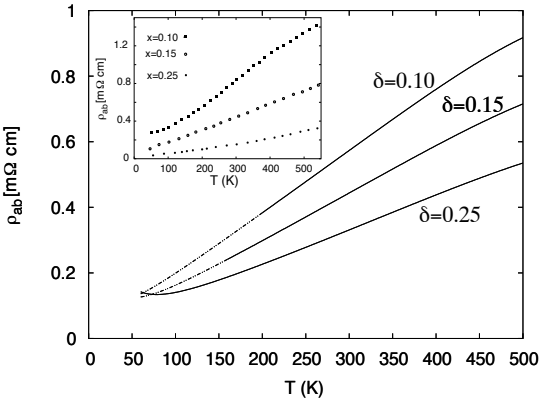

Figure 2.3: The calculated temperature dependence of the in-plane resistivity for various dopings δ. Below the PG temperature T^* the curve is shown in dashed line. Inset: in-plane resistivity versus T measured in $LSCO$ crystals with different Sr content x [53].

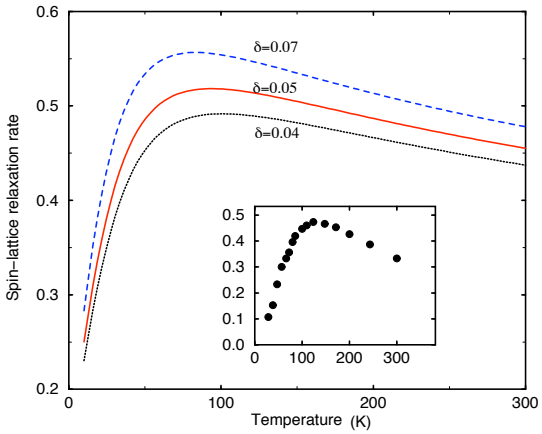

Figure 2.4: The calculated temperature dependence of the spin lattice relaxation rate ${}^{63}(\frac{1}{T_1T})$ for various dopings δ. Inset data of $YBa_2Cu_3O_{6.52}$ single crystal in units of $s^{-1}K^{-1}$, taken from Ref. [54].

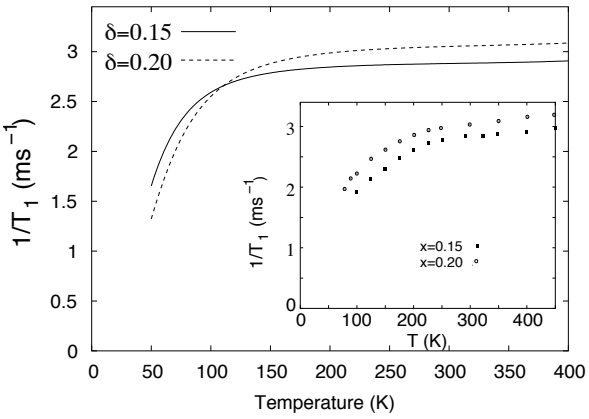

Figure 2.5: Calculated temperature dependence of the spin lattice relaxation rate $\frac{1}{T_1}$ for different doping concentrations δ. Inset data of $LSCO$ samples with different Sr content x, taken from Ref. [55].

Chapter 3

Non-BCS superconductivity from attraction between spin-vortices

3.1 Order parameters

Up to now our theory dealt with the normal (i.e. PG and SM) state of cuprates. In this chapter we discuss superconductivity arising from the PG region. We extend the spin-charge gauge approach to the superconducting dome (SC) following a non-BCS mechanism recently proposed in [10] and we analyze the consequences of this phase transition on the normal state.

This mechanism is based on the composite structure of the hole understood as a bound state of spinon and holon. There are three steps to get superconductivity:

- At a higher crossover temperature T_{ph} a finite density of incoherent holon pairs appears. The necessary holon attractive interaction comes from the attraction between spin-vortices of opposite chirality centered on holon positions in opposite Neel sublattice, Eq. (2.30).

- At a lower crossover temperature T_{ps} a finite density of incoherent RVB (spin singlet) spinon pairs appears, giving rise, together with preformed holon pairs, to incoherent hole pairs and to a gas of magnetic vortices in the plasma phase. It is the gauge attraction between holon and spinon that, using the holon pairs as a source of attraction, induces the formation of short range RVB spinon pairs with a reduction of the spinon gap.

- At an even lower temperature T_c both holon pairs and RVB spinon pairs, i.e. hole pairs, simultaneously became coherent, condense and magnetic vortices becomes

dilute. This is the SC transition. Superconductivity occurs at a finite doping value even at $T = 0$.

This mechanism is not BCS-like since the formation of holon pairs is BCS like (in the sense that the gain is in potential energy) but the formation of spinon RVB pairs is non BCS since it involves a gain in kinetic energy coming from the gauge interactions.

To begin a deeper discussion of the above points we need to define the SC order parameter assumed to be RVB-like

$$\Delta_{ij}^{c} = \langle \epsilon^{\alpha\beta} c_{i\alpha} c_{j\beta} \rangle. \tag{3.1}$$

Neglecting gauge fluctuations we get

$$\Delta_{ij}^{c} = \langle \epsilon^{\alpha\beta} z_{i\alpha} z_{j\beta} \rangle \langle H_i^* H_j^* \rangle. \tag{3.2}$$

Both factors should be non-vanishing to get superconductivity. It can be shown by explicit calculation that in our model a gapless gauge field is inconsistent with coherent holon pairs, i.e. coherent holon pairs (that yield a still gapless gauge fluctuations) cannot coexist with incoherent spinon pairs and in this situation the condensation of both appear simultaneously. It follows that $T_c < T_{ps}$.

The definition of Δ_{ij}^{c} needs some comments. In our PG optimization procedure used to obtain the spinon optimal configuration in a holon background, Eq. (2.31), we considered jumps between nearest neighbor sites and the holon were assumed in the final site of the jump. When strings are inserted to evaluate correlation functions like the order parameter Δ_{ij}^{c} (as explained in the bosonization formula in Eq. (2.4)), we can consider strings as extended jumps from the insertion point to infinity. We have to define what happen to the spinon optimal configuration in these extended jumps. The result of the calculation can be summarized by the rule that if the jump is between different sublattices we have the additional spin flip on holon final position except for strings going to infinity where holon should be considered at the beginning of the jump. This rule agrees with the identity $|AM_{ij}|^2 + |RVB_{ij}|^2 = 1$ if we neglect V in the string γ, see Eq. (2.11). Moreover in MF we can assume that the two strings in the SC order parameter relative to $\langle ij \rangle$ have a common support leaving only a phase factor along the link $\langle ij \rangle$.

Now we analyze in detail the pairing interactions generating nonzero order parameters for holons and spinons. The four fermion interaction in the Heisenberg term, Eq. (2.34), provides a holon-holon repulsive interaction (it has positive coefficient) and can not cause a growth of holon pair density $\langle |H_i H_j|^2 \rangle \simeq \langle |H_i H_j| \rangle^2$. The four fermion interaction we

need can be found in the term coupling holons, spinons and spin-vortices, Eqs. (2.30) and (2.40). When averaged over holons it provides the spinon mass term but when we consider the MF average over spinons we obtain the contribution

$$S_{VA} = \tilde{J}\langle z_\alpha^* z_\alpha\rangle \int_0^\beta dx^0 \int d^2\vec{x}\bar{V}_\mu^{z2}(\vec{x}, x_0) \tag{3.3}$$

$$\int d^2\vec{x}\bar{V}_\mu^{z2}(\vec{x}, x_0) = \sum_{i,j}(-1)^{|i|+|j|}\triangle^{-1}(\vec{i}-\vec{j})H_i^\dagger H_i H_j^\dagger H_j(x_0). \tag{3.4}$$

where $\tilde{J} \equiv J(1-2\delta)$ and $\triangle$ is a 2-D lattice Laplacian. In the static approximation (so that the integrand in Eq. (3.3) is independent of x^0) this contribution becomes the action of a 2D Coulomb gas with charge depending on the sublattice. Incoherent pairing, $\langle|H_i H_j|\rangle \neq 0$, appears as a Kosterlitz-Thouless (KT) transition at $T_{ph} \sim \tilde{J}\langle z^\dagger z\rangle$, which turns out to be inside the SM region. Hence the whole PG region lies below T_{ph}.

Because only a small fraction of holons forms pairs, a finite but slightly lower spinon mass m_s (with the same doping dependence as PG) remains. As a consequence we evaluate the (doping decreasing) expectation value

$$\langle z^* z\rangle \approx \int d^2\vec{q}(\vec{q}^2 + m_s^2)^{-1/2} = \sqrt{\Lambda^2 + m_s^2} - m_s \sim 1 - m_s, \tag{3.5}$$

where the UV cutoff $\Lambda \sim 1$. For the same reason a finite screening effect persists al large scales for the spin-vortices interaction potential. Denoting by ξ the correlation length, in the long wavelength limit the interaction induced by the 2-D Laplacian in Eq. (3.4) is replaced, in Fourier transform, by the effective potential

$$V_{eff}(\vec{q}) = \frac{1}{\vec{q}^2 + \xi^{-2}}, \tag{3.6}$$

where from KT theory $\xi \sim \frac{1}{\sqrt{Jk_F}}$.

We propose to identify the temperature T_{ph} with the observed upper PG temperature, where the in-plane resistivity deviates from the linear behavior. As we shall see, a finite density of incoherent holon pairs induces an angle dependent reduction of holes spectral weight, starting from the antinodal regions and causing the forementioned deviation. The reduction of the spectral weight confirms that holon pairs formation is BCS-like.

To conclude the discussion about holons we note that the origin of holons attraction, Eq.(3.3), comes from the J-term in the $t-J$ model and has therefore a magnetic origin, its scale is related to J but it is not due to exchange of AF spin waves.

Once we have $\langle |H_i H_j| \rangle \neq 0$ via spin-vortices attraction, we can consider spinon RVB pairing. When the density of holon pairs is large enough, the gauge attraction between holons and spinons overcomes the original AF repulsion of spinons (remember that the Heisenberg term is positive in our approach) and at an intermediate crossover temperature T_{ps} (lower than T_{ph} and higher than T_c) a finite density of incoherent RVB spinon pairs emerges, $\langle |\epsilon^{\alpha\beta} z_{i\alpha} z_{j\beta}|^2 \rangle \neq 0$. The gauge attraction in fact favors RVB pairing lowering the spinon kinetic energy from m_s to $\sqrt{m_s^2 - |\Delta^s|^2}$ until Heisenberg repulsion is exceeded. The RVB term, previously discarded, in the leading approximation to continuum provides the contribution

$$S_{RVB} = \frac{J}{2} \int_0^\beta dx^0 \sum_{\langle ij \rangle} |H_i^* H_j^*|^2 |\epsilon^{\alpha\beta} z_{i\alpha} z_{j\beta}|^2 \tag{3.7}$$

It is repulsive and essentially irrelevant in absence of holon pairs but it becomes relevant if pairing occurs. Introducing a complex Hubbard-Stratonovich gauge field Δ_{ij}^s and treating the holon pairs in MF, Eq. (3.7) becomes

$$S_{RVB} = \int_0^\beta dx^0 \sum_{\langle ij \rangle} \left\{ -\frac{2|\Delta_{ij}^s|^2}{J|\langle H_i H_j \rangle|^2} + \Delta_{ij}^{s*} \epsilon^{\alpha\beta} z_{i\alpha} z_{j\beta} + h.c. \right\} \tag{3.8}$$

where the order parameter for spinons is space-independent but direction-dependent and in MF

$$\Delta_{ij}^s = \frac{J}{2} |\langle H_i H_j \rangle|^2 \langle \epsilon^{\alpha\beta} z_{i\alpha} z_{j\beta} \rangle. \tag{3.9}$$

Wee see from Eq. (3.7) that the energy scale related to RVB spinon pairs is again J.

As soon as we have a finite density of spinon pairs together with the preformed holon pairs we can evaluate the modulus of the d-wave pairing amplitude for holes $\Delta_{ij}^c = \Delta_{ij}^s / \langle H_i H_j \rangle$. Δ_{ij}^c non-vanishing corresponds to incoherent hole pairs. The gradient of the phase of Δ_{ij}^c describes mobile magnetic vortices in the plasma phase, in fact incoherence of hole pairs leads to a vanishing expectation value of the exponential of the phase of Δ_{ij}^c.

This region, precursor of superconductivity, shows at a finite doping value even at $T = 0$ and we propose to identify T_{ps} with the experimental crossover corresponding to the diamagnetic Nernst phase.

Finally at temperature T_c we enter in the SC region where hole pairs become coherent. A d-wave condensate $\Delta_{ij}^c = \langle \epsilon^{\alpha\beta} z_{i\alpha} z_{j\beta} \rangle / \langle H_i H_j \rangle \neq 0$ appears, magnetic vortices became

dilute and the gauge field A becomes massive making life time of physical resonances temperature independent (Reizer singularity disappears). This transition is similar to an XY-Stueckelberg transition (as we shall see there is a factor 2 in front of the temporal term) and is driven by kinetic energy but is related again to the energy scale J because dynamic of vortices is triggered by spinon mass and gauge field mass and both are originated by Heisenberg term.

We note that the order parameter Δ^c_{ij} is well defined both in modulus and in phase because the sequence of the pairings is fixed by the explained mechanism (first holons and than spinons) and condensation is simultaneous.

We conclude noting that holon pairing, required in advance to have RVB pairs, enters the game in two ways with opposite effect: the density of holon pairs itself and the strength of the attraction $J(1-m_s)$, in Eq. (3.3). They act in opposite way as doping increases thus yielding a finite range for a non-vanishing value of $|\Delta^s|$, and hence Δ^c_{ij}, starting from a non-zero doping value. Finally this approach preserve finite FS in the region where vortices are not dilute (Nernst region) and nodes on FS appear only below the SC transition when the spectral weight of holes reduces the FS to four points (nodes).

3.2 Holon pairing

In this section we treat in detail holon pairing in the PG phase in MFA. The starting point is the PG π-flux holon action in Eq. (2.33). It is useful to exploit Hamiltonian formalism on two sublattice A (even sites) and B (odd sites). We make the same approximation as above except the continuum limit and neglect the h/s gauge field which can be reinserted later via minimal substitution. Holon π-flux Hamiltonian reads

$$H_0^h = -t \sum_{i\in A, r=1,4} \left[e^{i\frac{\pi}{4}(-1)^{r+1}} A_i^\dagger B_{i+r} + h.c. \right] - \mu \sum_{i\in A} A_i^\dagger A_i - \mu \sum_{i\in B} B_i^\dagger B_i \tag{3.10}$$

where $r = (1,2,3,4) = (\hat{e}_x, \hat{e}_y, -\hat{e}_x, -\hat{e}_y)$ indicates crystal axis, $A_i = H_i$ and $B_i = H_{i+\hat{e}_x}$ if $i \in A$.

Performing Fourier transform, $A_{\vec{k}}$ and $B_{\vec{k}}$ operators are defined in the magnetic Brillouin zone (MBZ) because of the two sublattice separation. We exploit the related additional symmetry making a $\vec{Q}_+$ ($\vec{Q}_-$) translation of 3rd (4th) quadrant modes, as shown in Fig. (3.1), ($\vec{Q}_\pm = (\pm\pi, \pi)$ are reciprocal primitive vectors) followed by a minus sign factor in front of $B_{\vec{k}}$ operators,

$$a_{\vec{k}} = \begin{cases} A_{\vec{k}-\vec{Q}_+}, & \text{if} \quad k_x - \pi < 0, k_y - \pi < 0 \\ A_{\vec{k}-\vec{Q}_-}, & \text{if} \quad k_x + \pi > 0, k_y - \pi < 0 \\ A_{\vec{k}}, & \text{if} \quad k_y \geq 0 \end{cases} \tag{3.11}$$

$$b_{\vec{k}} = \begin{cases} -B_{\vec{k}-\vec{Q}_+}, & \text{if} \quad k_x - \pi < 0, k_y - \pi < 0 \\ -B_{\vec{k}-\vec{Q}_-}, & \text{if} \quad k_x + \pi > 0, k_y - \pi < 0 \\ B_{\vec{k}}, & \text{if} \quad k_y \geq 0. \end{cases} \tag{3.12}$$

The anti-commutation relations remains unchanged and we get a rectangular zone ($k_x \in [-\pi, \pi]$, $k_y \in [0, \pi]$) equivalent to MBZ where the holon dispersions are two Dirac cones centered around $\vec{Q}_R \equiv \frac{1}{2}\vec{Q}_+$ and $\vec{Q}_L \equiv \frac{1}{2}\vec{Q}_-$. Notice that when the arguments of a and b fields belong to the rectangular zone, the arguments of A and B fields belong to the MBZ. We add a flavor index $\alpha = R, L = 1, 2$ to holons with positive and negative k_x, measuring momentum $\vec{k}$ from $\vec{Q}_R$ and $\vec{Q}_L$ respectively, $a_{\vec{Q}_\alpha+\vec{k}} = a_{\alpha,\vec{k}}$ and $b_{\vec{Q}_\alpha+\vec{k}} = b_{\alpha,\vec{k}}$. In the low energy limit we can consider flavors as separate because of PG small Fermi momentum and considering quasi-particles near the FS it is possible to perform a gauge transformation

$$a_{\alpha,\vec{k}} \to a_{\alpha,\vec{k}} e^{i\theta_{\alpha,\vec{k}}/2}, \quad b_{\alpha,\vec{k}} \to b_{\alpha,\vec{k}} e^{-i\theta_{\alpha,\vec{k}}/2} \tag{3.13}$$

where $\theta_{\alpha,\vec{k}} = (-1)^\alpha \left[\frac{\pi}{4} - \arctan\left(\frac{k_y}{k_x}\right)\right]$ is chosen to cancel the phase of the hopping factor. The final hamiltonian reads

$$H_0^h = \sum_{\alpha,\vec{k}\in D} \left[v_F |\vec{k}| (a^\dagger_{\alpha,\vec{k}} b_{\alpha,\vec{k}} + h.c.) - \mu (a^\dagger_{\alpha,\vec{k}} a_{\alpha,\vec{k}} + b^\dagger_{\alpha,\vec{k}} b_{\alpha,\vec{k}}) \right] \tag{3.14}$$

with $v_F = 2t$ and $D = \{\vec{k} : -\frac{\pi}{2} \leq k_x, k_y \leq \frac{\pi}{2}\}$.

Now let's consider holon-holon interaction in the long wavelength limit. Performing Fourier transform of Eq. (3.4) we note that it is invariant under the gauge transformation in Eq. (3.13). The coupling between L and R flavors is neglected since $V_{eff}(\vec{Q}_R - \vec{Q}_L) << V_{eff}(\vec{0})$. Defining

$$\Delta^h_{\alpha,\vec{k}} = \tilde{J} \langle z^\dagger z \rangle \sum_{\vec{q}} V_{eff}(\vec{k} - \vec{q}) \langle b_{\alpha,-\vec{q}} a_{\alpha,\vec{q}} \rangle \tag{3.15}$$

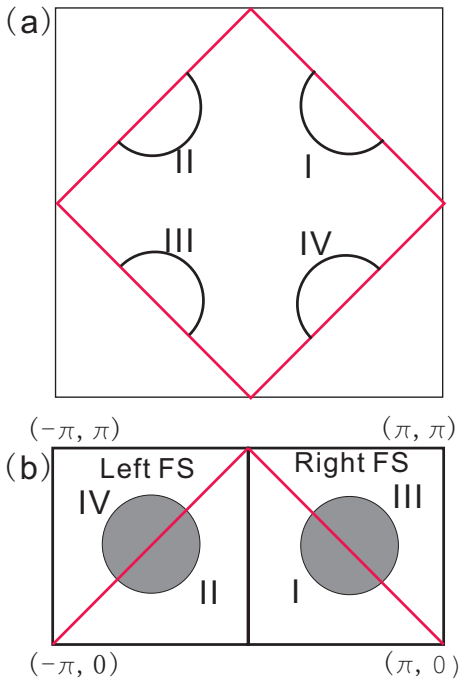

Figure 3.1: (a) the BZ, the MBZ and the FS (defined inside the MBZ) of free holons in the "π-flux phase". The MBZ is equivalent to the rectangular zone shown in (b) obtained translating the 3rd and 4th zones. Holon dispersion consists of two Dirac cones giving rise to two circular Fermi surfaces defined in the rectangular zone.

we perform standard BCS approximation and introduce Nambu fields

$$\Psi_{\alpha,\vec{k}} = (a_{\alpha,\vec{k}}, b_{\alpha,\vec{k}}, a^{\dagger}_{\alpha,-\vec{k}}, b^{\dagger}_{\alpha,-\vec{k}})^t. \tag{3.16}$$

The holon Hamiltonian becomes $H_{h,\alpha} = \sum_{\vec{k}} \Psi^{\dagger}_{\alpha,\vec{k}} \mathcal{H}_{\alpha,\vec{k}} \Psi_{\alpha,\vec{k}}$, where the 4×4 matrix reads

$$\mathcal{H}_{\vec{k}} = \begin{pmatrix} -\mu & v_F k & 0 & \Delta^h_{\vec{k}} \\ v_F k & -\mu & -\Delta^h_{-\vec{k}} & 0 \\ 0 & -\Delta^{h*}_{-\vec{k}} & \mu & -v_F k \\ \Delta^{h*}_{\vec{k}} & 0 & -v_F k & \mu \end{pmatrix}. \tag{3.17}$$

It can be block-diagonalized and for odd parity $\Delta^h_{-\vec{k}} = -\Delta^h_{\vec{k}}$ (notice that because of Eqs. (3.11) and (3.12) the order parameter $\Delta^h_{\alpha,\vec{k}}$ in quadrant 3rd and 4th changes its sign because of translation in the rectangular zone) we obtain four branches for the dispersion relation

$$E_{\alpha,\vec{k}} = \pm\sqrt{(v_F k \pm \mu)^2 + |\Delta_{\alpha,\vec{k}}|^2}. \tag{3.18}$$

The high and the low band are completely decoupled and we can neglect the contribution of high band without FS. The low energy relevant field operators are the combination $\psi_{\vec{k}} = \frac{1}{\sqrt{2}}(a_{\vec{k}} + b_{\vec{k}})$ and its Hermitian conjugate $\psi^{\dagger}_{\vec{k}}$. In terms of these fields the low energy effective Hamiltonian reads

$$H^h_{\text{eff}} = \sum_{\alpha,\vec{k}} (v_F k - \mu) \psi^{\dagger}_{\alpha,\vec{k}} \psi_{\alpha,\vec{k}} - \frac{1}{2}\left(\Delta^h_{\alpha,\vec{k}} \psi^{\dagger}_{\alpha,\vec{k}} \psi^{\dagger}_{\alpha,-\vec{k}} + h.c.\right). \tag{3.19}$$

The gap equation at $T = 0$, obtained by minimum condition self-consistently with the definition in Eq. (4.6), is

$$\Delta^h_{\alpha,\vec{k}} = \tilde{J}\langle z^{\dagger} z\rangle \int \frac{d^2 q}{(2\pi)^2} V_{eff}(\vec{q} - \vec{k}) \frac{\Delta^h_{\alpha,\vec{q}}}{2E_{\alpha,\vec{q}}}. \tag{3.20}$$

A consistent solution of this integral equation near the FS having d-wave symmetry in the full MBZ is obtained gluing two p-wave solutions (odd parity in agreement with the foregoing) in the L and R regions [25],

$$\Delta^h_{R[L]}(|\vec{p_F}|, \theta_p) = \Delta^h(|\vec{p_F}|)[+[-]\cos(\theta_p) - \sin(\theta_p)] \tag{3.21}$$

where solving numerically the gap equation on the FS we obtain

$$\Delta^h = \Delta^h(|\vec{p_F}|) = \tilde{J}\langle z^\dagger z\rangle \xi e^{-\frac{c}{\tilde{J}\langle z^\dagger z\rangle \xi^2 k_F}} \tag{3.22}$$

with a constant c. As common for non-weakly coupled attractive Fermi systems the MF temperature at which Δ^h becomes non-vanishing is T_{ph}. The result of Eq. (3.21) can be extended in momentum space in a range $O(k_F)$ as

$$\Delta^h(\vec{p}) = \Delta^h \frac{\pm p_x - p_y}{k_F}. \tag{3.23}$$

In this way the dispersion relation of the excitations exhibits one node in each of the holon FS arch along the diagonal directions. Nodes indicate gapless excitations.

To proceed we assume $\Delta^h \neq 0$ and perform nodal approximation expanding momenta around the nodes. We can restore the slave particle gauge symmetry introducing the holon pair field phase factor ϕ^h as $\Delta^h \to \Delta^h e^{i\phi^h}$ and making the off-diagonal derivatives covariant w.r.t. $\frac{\phi^h}{2}$, i.e. $i\partial_\mu - \partial_\mu \frac{\phi^h}{2}$ (under a gauge transformation with parameter λ we have $\phi^h \to \phi^h + 2\lambda$). Inserting the slave particle gauge field A in diagonal terms via minimal substitution, performing Anderson trick (to multiply the first nodon field by $e^{-i\frac{\phi^h}{2}}$ and the second one by the complex conjugate factor) and defining $a_\mu = A_\mu - \partial_\mu \frac{\phi^h}{2}$ we obtain the nodal hamiltonian in R region inside the MBZ

$$\mathcal{H}^h_{1st} = \begin{pmatrix} 2t(i\partial_+ + a_+) + a_0 & e^{i\frac{\pi}{4}} v_\Delta \partial_- \\ e^{-i\frac{\pi}{4}} v_\Delta \partial_- & -2t(i\partial_+ - a_+) + a_0 \end{pmatrix} \tag{3.24}$$

where $v_\Delta = \frac{\Delta^h}{k_F}$ and $\partial_\pm = \frac{1}{\sqrt{2}}(\partial_x \pm \partial_x)$ [46], [47]. Successive rotations of $\pi/2$ provide Hamiltonians of the other quadrants.

By suitable redefinition of space and time units it is possible to rewrite the Hamiltonian in Eq. (3.24) as Dirac Hamiltonian of QED_3 with the gauge field $\tilde{a}^{1st}_\mu = \{-ia_+, ia_0, 0\}$. Similarly for the other nodes. We conclude that the low energy effective action for a is a slight variant of QED_3 (see e.g. [26]) but not gauge invariant

$$S^{1st}_{eff}[\tilde{a}^{1st}_\mu] = -\ln\det[\gamma^\mu(\partial_\mu - i\tilde{a}^{1st}_\mu)] \tag{3.25}$$

and it can be shown that the gauge field a does not acquire gap even if the global h/s gauge symmetry in the gauge-holon system is broken from $U(1)$ to $\mathbf{Z}_2$, that is $\langle e^{i\phi^h}\rangle \neq 0$ (due to the charge two of the condensate). We note that if the action of the gauge field a were exactly QED_3, then superconductivity would be possible without spinon sector but the above action is not gauge invariant and this fact prevents superconductivity.

3.3 Spinon pairing and superconductivity

We begin from Eq. (3.8) and consider the continuum limit. We assume $\Delta^s_{ij} \sim \Delta^s_\mu e^{i\phi^s(\vec{x})}$ where $\vec{x} = i$, i.e. it is the product of a direction dependent (but position independent) factor times a space dependent phase $\phi^s(\vec{x})$. μ indicates the direction from i to j and for a gauge transformation of parameter λ we have $\phi^s \to \phi^s + 2\lambda$. Note that no pairing occurs in temporal direction.

To obtain the spinon Lagrangian we add Eq. (2.39) to the continuum limit of Eq. (3.8) obtained using the continuum limit relation $\epsilon^{\alpha\beta} z_{i\alpha} z_{j\beta} \sim \epsilon^{\alpha\beta} z_\alpha \partial_\mu z_\beta$. We note that in this way the slave particle gauge field has been introduced and consistently, because gauge invariance is needed, we make the off diagonal derivatives covariant w.r.t. ϕ^s, i.e. $\partial_\mu - i\partial_\mu \frac{\phi^s}{2}$. Finally we use Anderson trick defining the Nambu doublet $Z = [e^{i\frac{\phi^s}{2}} z_1, e^{-i\frac{\phi^s}{2}} z_2^*]^t$. The final result is

$$L_s = Z^\dagger [(\partial_\mu \mathbf{1} + i Y^a_\mu \sigma^a)^2 + (m_s^2 - |\Delta^s|^2)] Z \tag{3.26}$$

where

$$Y^a_\mu = \begin{pmatrix} 0 & 0 & a_0 + \partial_0 \frac{\Phi}{2} \\ Im(\Delta^s_1) & Re(\Delta^s_1) & a_1 + \partial_1 \frac{\Phi}{2} \\ Im(\Delta^s_2) & Re(\Delta^s_2) & a_2 + \partial_2 \frac{\Phi}{2} \end{pmatrix} \tag{3.27}$$

is a fictitious $SU(2)$ gauge field and $\Phi = \phi^h - \phi^s$ is a slave particle gauge invariant phase field (it is a physical quantity). Φ is by definition the phase of the hole pairs field Δ^c_{ij} and turns out to describe standard magnetic vortices.

Neglecting h/s gauge field and phase fluctuations and assuming rotational invariance in the continuum limit, $\Delta^s_\mu \Delta^{s*}_\nu + \Delta^s_\nu \Delta^{s*}_\nu = 2\delta_{\mu\nu} |\Delta^s|^2$, we may solve the spinon spectrum

$$\omega(\vec{k}) = \pm 2t \sqrt{m_s^2 - |\Delta^s|^2 + (|\vec{k}| \pm |\Delta^s|)^2} \tag{3.28}$$

.

There are two positive branches with the same spin and momentum but different energies for a finite density of spinon pairs. If $|\Delta^s| \neq 0$ the spinon system contains a gas of RVB spinon pairs which become coherent and condense if $\langle \Delta^s \rangle \neq 0$. The minimum at $|\vec{k}| = |\Delta^s|$ in the lower branch has energy lower than m_s and behaves like a roton minimum. A backflow of the gas of spinon pairs dresses bare spinons lowering the spinon

kinetic energy. We will show that if a suitable attraction mechanism between spinon and anti-spinon works, a similar hourglass dispersion holds also for the magnon resonance (spin waves).

As a consequence of rotational invariance $\arg\Delta_1^s - \arg\Delta_2^s = \pm\frac{\pi}{2}$ holds, that is the spinon RVB order parameter has a d-like staggered phase which can be chosen to cancel the phase contribution to the SC order parameter Δ_{ij}^c in MF coming from the B field.

When RVB pairs condense, $\langle e^{i\phi^s}\rangle \neq 0$, the global slave particle symmetry is broken from $U(1)$ to $\mathbf{Z}_2$ also in the gauge-spinon system. The breaking in both sectors (holon and spinon) of the symmetry imply a breaking of the global electromagnetic $U(1)$ symmetry (electromagnetic gauge field is minimally coupled in the same way as h/s gauge field), characterizing the SC phase. Being the RVB order parameter uniform, Anderson-Higgs mechanism implies a gap of order $|\Delta^s|$ (increasing with density of RVB pairs) for the gauge field A. Owing to this gap, Reizer singularity disappears (Reizer singularity was responsible of an anomalous skin effect and of overdamped resonances with anomalous T-dependent life-time in the normal state) making magnon and electron resonances sharper in the SC state.

We can integrate Z field in Eq. (3.26) to get explicitly the spinon contribution to the effective action of the gauge invariant fields a and Φ in the SC phase. Since the Z field is massive, the effective actions is Maxwell-Yang-Mills like up to a UV scale $\Lambda \sim m_s$. Then another contribution non-gauge invariant but rotationally invariant $Y_\mu^1 Y_\mu^1 + Y_\mu^2 Y_\mu^2 \sim |\Delta^s|^2$ should be added because Y^a, $a = 1, 2$, is actually a constant field. The result up to quartic terms for the lagrangian density is

$$\begin{aligned} L_{eff}(a, \partial\Phi) &= \frac{1}{2\sqrt{m_s^2 - |\Delta^s|^2}} \left\{ F_{\mu\nu}^2 + |\Delta^s|^2 [2(2a_0 - \partial_0\Phi)^2 + (2\vec{a} - \vec{\nabla}\Phi)^2] \right\} \\ &\quad + c_1|\Delta^s|^2 + c_2|\Delta^s|^4 \end{aligned} \tag{3.29}$$

where the field strength $F_{\mu\nu} = \partial_\mu a_\nu - \partial_\nu a_\mu$.

The mass term for a in the above equation (strictly speaking this is not properly a mass term because of the factor 2 in front of the zero component) is a XY-Stueckelberg action which means that if the coefficient $|\Delta^s|^2$ is sufficiently small the phase Φ fluctuates strongly and does not produce a mass term for a since $\langle e^{i\Phi}\rangle = 0$. On the other hand, for a sufficiently large coefficient we are in the SC phase, $\langle e^{i\Phi}\rangle \neq 0$, the symmetry is broken and the Φ fluctuation are exponentially suppressed. We conjecture that the situation $|\Delta^s| \neq 0$ but $\langle e^{i\Phi}\rangle = 0$ correspond to the Nernst region (where free physical magnetic vortices proliferate) above the SC dome in the phase diagram. As soon as $e^{i\Phi}$ condenses,

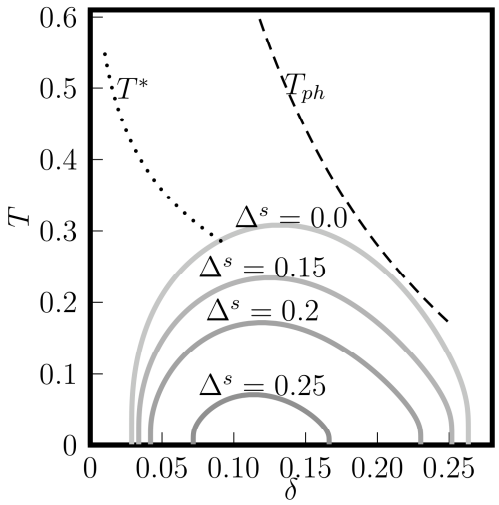

Figure 3.2: The (T, δ) phase diagram of the mean field gap equation of spinons for different values of the spinon pairing $|\Delta^s|$ (gray lines) which could be compared with different levels of Nernst signal; $|\Delta^s| = 0$ is T_{ps} (the curves at high dopings are not quantitatively reliable as they do not take into account the crossover to SM). The dashed line is T_{ph}, the "upper PG crossover temperature". The dotted line is T^*, the crossover temperature between the PG and the SM regions. The temperature and $|\Delta^s|$ are in units of J.

the same occurs to $\langle H_i H_j \rangle$ so that SC emerges and $T_c < T_{ps}$.

Neglecting the phase Φ (which represents fluctuations and can be added later) and the QED_3 contribution to the a field action (coming from holons and subleading than spinon contribution owing to the mass term in Eq. (3.29)) we can derive the gap equation at $T = 0$ for $|\Delta^s|$ computing the free energy in MFA and minimizing with respect to $|\Delta^s|^2$

$$\begin{aligned} \frac{\Lambda^3}{m_s^2} - \frac{4\Lambda^2}{J|\langle H_i H_j \rangle|^2} &= -\frac{1}{4}\int d\omega d^2k \left(\frac{1}{\omega^2 + \vec{k}^2 + \frac{|\Delta^s|^2}{2}} + \frac{1}{\omega^2 + \frac{\vec{k}^2 + |\Delta^s|^2}{2}} \right) \\ &+ \int d\omega d^2k \frac{4\vec{k}^2}{(\omega^2 + \vec{k}^2 + m_s^2)^2 - 4|\Delta^s|^2\vec{k}^2} \end{aligned} \tag{3.30}$$

The l.h.s. terms come from the lowering of the spinon mass $m_s \to \sqrt{m_s^2 - |\Delta^s|^2}$ and the repulsive Heisenberg term in Eq. (3.8) respectively while the first r.h.s. term comes from gauge fluctuation in Eq. (3.29) (it can be neglected as subdominant at low temperatures) and the second one comes from spinon action in Eq. (3.26). A non-vanishing solution is possible only for a sufficiently large MF holon pair density to make positive the l.h.s.. It follows that spinon RVB pairs, and hence the SC state, appears at a finite value of doping δ even at $T = 0$ and that $T_{ps} < T_{ph}$. From the r.h.s. of Eq. (3.30) we see how gauge field favors RVB spinon pairing and that the temperature T_{ps} at which $|\Delta^s|$ becomes non-vanishing turns out to be above the SC transition T_c and below T_{ph}, as shown in Fig.(3.2).

Notice that the crossover T^* is distinct from T_{ph} that fully lies within SM region. The two crossovers T_{ph} and T_{ps} have mainly a magnetic origin being described by the statistical spin flux related to the $SU(2)$ CS field V, see Eq.(2.30), while T^* has a charge origin due to the charge flux related to the $U(1)$ CS field B.

3.4 Spin-spin correlation

In this section we will show that if a suitable attractive interaction for spinon and anti-spinon works in the SC phase, then the magnon resonance (a bound state of spinon and anti-spinon) has an hourglass-shape dispersion near the anti-ferromagnetic vector $\vec{Q}_{AF} = (\pi, \pi)$ similar to that previously found for spinons in Eq. (3.28) [6]. This dispersion is directly comparable with experimental data in Fig. (1.5) (white lines).

There is an ongoing debate about the origin of this resonant peak near Q_{AF} below the particle-hole continuum. RPA calculations yield only the lower branch while acoustical and optical spin waves lead to the growing branches [39]. A recent approach [31] shows

that both RPA and spin wave fluctuations are important to produce the two branches of the hourglass.

We will follow another path. Within the spinon sector, we consider the effect of the RVB spinon pairs on the massive spin waves. Defining $v_\mu = a_\mu + \partial_\mu \Phi$, the action for spinons in Eq. (3.26) reads $S_s = S_s^1 + S_s^2$ where

$$S_s^1 = \int_{[0,\beta]\times \mathbf{R}^2} d^3x \left(|D_\mu Z_1|^2 + |D_\mu^* Z_2|^2 + m_s^2 Z_i^* Z_i \right), \tag{3.31}$$

$$S_s^2 = 2 \int_{[0,\beta]\times \mathbf{R}^2} d^3x \left(\Delta_\mu^{s*} Z_1 \partial_\mu Z_2^* + c.c. \right), \tag{3.32}$$

$D_\mu = \partial_\mu - i v_\mu$ and $\Delta_\mu^s = \frac{|\Delta^s|}{\sqrt{2}} \left\{ 0, e^{-i\frac{\pi}{4}}, e^{i\frac{\pi}{4}} \right\}$.

To evaluate the anti-ferromagnetic spin-spin correlation (or the magnon propagator) [40]

$$\langle \Omega^+(x)\Omega^-(x) \rangle = \langle Z_1^*(x) Z_2^*(x) Z_2(y) Z_1(y) \rangle \tag{3.33}$$

we begin considering the action S_s^1. It is the action of the non-linear σ-model with a mass term written in the CP^1 form, where $\vec{\Omega} = z^\dagger \frac{\vec{\sigma}}{2} z$. This action is equivalent to

$$S_s^1 = \int_{[0,\beta]\times \mathbf{R}^2} d^3x \left[(\partial_\mu \vec{\Omega})^2 + m_s^2 \vec{\Omega}^2 + i\lambda(\vec{\Omega}^2 - f) \right] \tag{3.34}$$

where λ is a x-dependent Lagrange multiplier enforcing the constraint $\vec{\Omega}^2 = f$. In this representation the gauge invariant bound state of spinon and anti-spinon is the field $\vec{\Omega}$. In the unbroken phase Eq. (3.34) leads to the anti-ferromagnetic spin-spin correlation

$$G_b(k) = \int d^3x e^{ikx} \langle \Omega^+(x)\Omega^-(0) \rangle \sim \frac{1}{k^2 + M_b^2} \tag{3.35}$$

where the mass $M_b = M_b(m_s, \langle\lambda\rangle) = 2m_s - E_b$ is the sum of the free-particle masses (spinon and anti-spinon have the same mass m_s) reduced by the binding energy E_b.

In the CP^1 form $G_b(x-y)$ (the Fourier transform of $G_b(k)$) is the four field expectation value $\langle Z_1^*(x) Z_2^*(x) Z_2(y) Z_1(y) \rangle$ and represents the propagator of the bound state of spinon and anti-spinon where the gauge field v_μ provides the necessary attractive interaction.

When the RVB condensate is introduced through the perturbation S_s^2 some changes have to be made. Z_1 and Z_2 have opposite charge but when the perturbation acts on one of them, it changes the relative sign because the RVB condensate has charge two. Thus the attraction between the two propagating particles becomes repulsion and vice versa whenever the perturbation acts. Moreover the gauge field is gapped in the superconducting

phase by Anderson-Higgs mechanism leading to a short-range interaction. We conclude that there have to be another charge-independent attractive interaction binding spinon and anti-spinon into the gauge invariant magnon resonance (spinon and anti-spinon are not gauge invariant fields).

In the superconducting phase the $U(1)$ gauge symmetry is spontaneously broken but, because of the charge two of the condensate, the subgroup $\mathbf{Z}_2$ is unbroken. We propose that the residual $\mathbf{Z}_2$ symmetry, which sees charge modulo 2, provides the needed charge-independent interaction exceeding the charge dependent gauge interaction.

With these clarifications, we can justify the following assumptions which allows us to consider together, in a reasonable manner, a bound state of two particle with an interaction acting only on one of them.

- Because of gauge invariance we expect an overall bound state and we use the bound state propagator of Eq. (3.35) for each pair of propagating particles but with different bound state masses depending on the relative charge. We use the mass M_B when the two propagating particles have opposite charge and the mass $M_A > M_B$ when they have the same charge. In fact in the former case both the $\mathbf{Z}_2$ and gauge interactions are attractive while in the latter case $\mathbf{Z}_2$ is attractive but gauge interaction is repulsive. In both cases we get a bound state but the mass is different because the former attraction is stronger.

- We use the constraint $Z_i^* Z_i = f$ to modify the RVB interaction S_s^2 into an effective action with a four particle local vertex $S_s^2 \to (S_\Delta + c.c.)$, where

$$S_\Delta = \frac{2}{f} \int_{[0,\beta]\times\mathbf{R}^2} d^3x (Z_1 Z_1^* + Z_2 Z_2^*) \Delta_\mu^s Z_1^* \partial_\mu Z_2. \tag{3.36}$$

  This means that we consider only scattering off the RVB condensate if the two propagating particles are close enough and this is the case when they form a bound state. The two close propagating particles realize that one of them is scattered (changing its charge) through the subleading short range gauge field v_μ. In a path integral formalism this means that we neglect paths in which the two particles are too far. Indeed, in the unbroken phase, the local constraint $Z_i^* Z_i = f$ is relaxed, it reasonably holds only for close particles.

Now we are able to evaluate the magnon propagator with the perturbation in Eq. (3.36) due to the RVB condensate. It reads

$$\begin{aligned}\langle\Omega^+(x)\Omega^-(y)\rangle &= \langle e^{-(S_\Delta+c.c.)}\Omega^+(x)\Omega^-(y)\rangle_{S^1_s} \\ &= \sum_{n=0}^{\infty}\langle\frac{(S_\Delta)^n}{n!}\frac{(S^*_\Delta)^n}{n!}\Omega^+(x)\Omega^-(y)\rangle_{S^1_s} \end{aligned} \tag{3.37}$$

where we took into account that the perturbation must act an even number of times and there must be the same number of Δ^s_μ and Δ^{s*}_μ in an alternate way on each particle path to get non-vanishing expectation values.

In what follows we will evaluate the $n = 1$ term of the above series using Wick theorem and complete the series as if it were a geometric Dyson series. The $n = 1$ term reads

$$\langle S_\Delta S^*_\Delta\Omega^+(x)\Omega^-(y)\rangle_{S^1_s} = \frac{4}{f^2}|\Delta^s|^2\int\frac{d^3p}{(2\pi)^3}e^{ip(x-y)}\vec{p}^2G_A(p)G_B(p)^2, \tag{3.38}$$

where, when necessary in the computation, we integrate by parts the integrand of the perturbation in Eq. (3.36), in such a way to exploit our first assumption, i.e. to take the exact four field average of Eq. (3.35) (it represents the bound state propagator in absence of the perturbation).

Performing Fourier transform and summing the geometric series we obtain our estimation for the spin-spin correlation in the superconducting phase

$$\begin{aligned}\langle\Omega^+(k)\Omega^-(k)\rangle &\approx \left[G_B(k)^{-1} - \frac{4}{f^2}|\Delta^s|^2\vec{k}^2G_A(k)\right]^{-1} \\ &= \frac{1}{k^2 + M_B^2 - \frac{4|\Delta^s|^2}{f^2}\frac{\vec{k}^2}{k^2+M_A^2}}. \end{aligned} \tag{3.39}$$

or in real time

$$\langle\Omega^+(\omega,\vec{k})\Omega^-(\omega,\vec{k}))\rangle \approx -\frac{\omega^2 - \vec{k}^2 - M_A^2}{(\omega^2 - \vec{k}^2 - M_B^2)(\omega^2 - \vec{k}^2 - M_A^2) - \frac{4}{f^2}|\Delta^s|^2\vec{k}^2}. \tag{3.40}$$

The two poles of this expression with positive energy give the two branches of the hourglass-shape dispersion of spin waves near the anti-ferromagnetic vector

$$\omega_\pm(\vec{k}) = \sqrt{\vec{k}^2 + S \pm \sqrt{D^2 + d\vec{k}^2}} \tag{3.41}$$

where we defined $S = \frac{M_A^2+M_B^2}{2}$, $D = \frac{M_A^2-M_B^2}{2}$ and $d = \frac{4}{f^2}|\Delta^s|^2$. For $|\vec{k}|$ near zero, up to the second order, we get

$$\omega_+(\vec{k}) \approx M_A + \frac{\vec{k}^2}{2M_A}\left(1+\frac{d}{2D}\right), \tag{3.42}$$

$$\omega_-(\vec{k}) \approx M_B + \frac{\vec{k}^2}{2M_B}\left(1-\frac{d}{2D}\right). \tag{3.43}$$

We see that there is a gap $M_A - M_B$ between the two branches at $|\vec{k}| = 0$ with horizontal tangent. The upper branch starts from M_A at $|\vec{k}| = 0$ and increases monotonically when $|\vec{k}|$ grows. The lower branch starts from M_B at $|\vec{k}| = 0$ and, if $\frac{4}{f^2}|\Delta^s|^2 > M_A^2 - M_B^2$, decreases (starting with a smaller absolute value of the curvature than the upper one) to a minimum $\omega_m = \sqrt{S - \frac{d}{4} - \frac{D^2}{d}}$ located at $|\vec{k}_m| = \sqrt{\frac{d}{4} - \frac{D^2}{d}}$ and then grows.

We remark that this sharp magnetic resonance located around Q_{AF} lies below a threshold energy $\omega_{th}(\vec{q})$ defined by edge of the two particle continuum $\omega_{th}(\vec{q}) \approx \min_{\vec{k}}\{E_{\vec{k}} + E_{\vec{k}+\vec{q}}\}$, above which continuum two particle excitations start. In this case $E_{\vec{k}}$ is the quasi-particle dispersion in the SC state.

Notice that if $|\Delta^s|$ vanishes and $M_A = M_B$ then the two branches coincide and we recover the free bound state dispersion $\omega(\vec{k}) = \sqrt{\vec{k}^2 + M^2}$ of Eq. (3.35).

The imaginary part of the retarded magnon propagator (proportional to the spectral weight) at positive frequencies reads

$$\begin{aligned}\Im\langle\Omega^+(\omega,\vec{k})\Omega^-(\omega,\vec{k}))\rangle^R_{\omega>0} &= -\frac{\pi}{4}\left\{\left[1-\frac{2D}{\omega_+^2(\vec{k})-\omega_-^2(\vec{k})}\right]\frac{\delta[\omega-\omega_+(\vec{k})]}{\omega_+(\vec{k})}\right. \\ &\left. + \left[1+\frac{2D}{\omega_+^2(\vec{k})-\omega_-^2(\vec{k})}\right]\frac{\delta[\omega-\omega_-(\vec{k})]}{\omega_-(\vec{k})}\right\}. \end{aligned} \tag{3.44}$$

The spectral weight is therefore higher on the lower branch than on the higher one. When $|\vec{k}|$ increases the spectral weight first grows on the higher branch and decreases on the lower one, then both decrease slowly.

Introducing in Eq. (3.40) a phenomenological scattering rate γ, $\omega \to \omega + i\gamma$, we plot in Fig. (3.3) the resulting spectral weight. It can be directly compared with the experimental magnetic intensity in Fig. (1.5) that is proportional to the spectral weight. The two plots are in good agreement. Taking the two particle continuum edge into account, we expect an even better agreement because the intensity at high frequencies is reduced.

We note that the holon sector does not appear in the computation and the hourglass-shape dispersion for spin waves in our formalism naturally comes from spinon sector and slave particle gauge field.

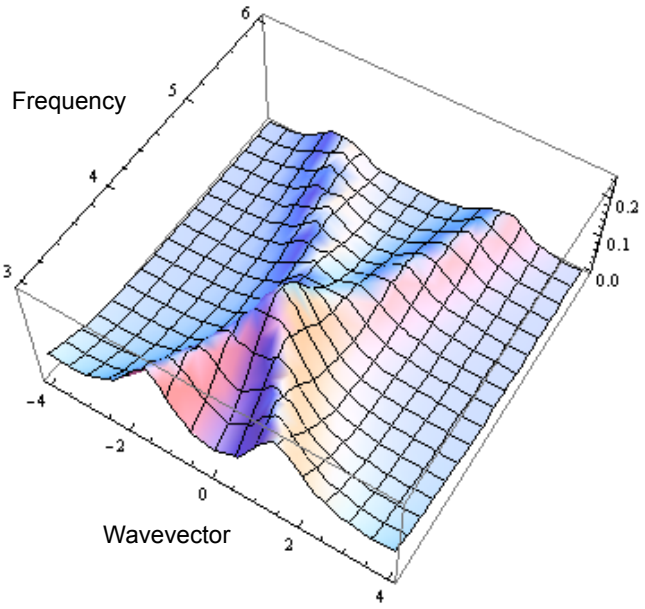

Figure 3.3: Plot (in arbitrary units) of the imaginary part of the magnon retarded propagator along $\vec{k}$-direction. Wavevectors are measured starting from Q_{AF}. A small scattering rate γ has been added. In the plot we chose $\frac{M_B}{M_A} = 0.9$, $\frac{|\Delta^s|}{fM_A} = 0.8$ and $\frac{\gamma}{M_A} = 0.1$.

Chapter 4

Holon pairing and coherence

4.1 Introduction

In this chapter we consider superconductivity arising from the SM region in a framework similar to that of the previous chapter about holon pairing, but now the holon sector is adapted to SM region [7]. Moreover we incorporate in this framework the fluctuations of the phase of the holon pairs order parameter [42].

We add next nearest neighbor hopping for holons to get a FS more appropriate to that of the cuprates and we show that, when incoherent holon pairs are present, an energy scale separating low energy modes with a FL behavior from high energy modes with a d-wave superconducting behavior results naturally and self consistently. This energy scale m_ϕ will be identified with the the inverse correlation length ("mass") of the quanta of the phase of the holon order parameter, i.e. $m_\phi = 1/\xi_\phi$. Its value, which decreases as temperature is reduced, drives the system towards the superconducting phase occurring at $m_\phi = 0$. In this phase, all modes are clearly above m_ϕ and the holon system is a real d-wave superconductor, in particular the holon spectral weight at the FS is reduced to zero except in four nodes. What happens is that decreasing m_ϕ, the well defined FL quasi-particles gradually lose their coherence in favor of SC-like excitations. The latter gain spectral weight and become increasingly well defined excitations.

As a byproduct we obtain some insight on the shape of the FS, which will turn out to be crucial to get a good continuum limit for quasi-particles, to evaluate the Knight shift in the next chapter and to obtain the holon direction dependent spectral weight. Indeed, the formation of holon pairs induces a reduction of the spectral weight of the holon starting from antinodal region. We expect that these results also apply to holes in which case they are directly measurable in $ARPES$ experiments.

Finally we notice that the effects of holon pairing existing in the normal state are much more effective in SM region than in PG region because of the smaller FS, Fermi velocity v_F and Fermi momentum k_F of the latter region than the former.

4.2 Low energy Hamiltonian for holons

In this section we adapt to the SM region the non-BCS mechanism for superconductivity discussed in previous sections in PG. To obtain a FS more similar to that relevant for cuprates, we add to the Hamiltonian of Eq. (2.35) a negative next-nearest-neighbor hopping term t'

$$H_0^h = -t\sum_{\langle ij\rangle}(H_i^\dagger H_j + h.c.) - t'\sum_{\langle\langle ij\rangle\rangle}(H_i^\dagger H_j + h.c.) - \mu\sum_i H_i^\dagger H_i. \tag{4.1}$$

We approach the problem in the two sublattice (even A and odd B) scheme defining $H_i = A_i$ and $H_{i+\hat{e}_1} = B_i$ for $i \in A$. The two fields, defined within the MBZ, which diagonalize H_0^h are

$$\Psi_\pm(\vec{k}) = A_{\vec{k}} \pm e^{ik_1} B_{\vec{k}} \tag{4.2}$$

where $\vec{k} \in MBZ$ and the Fourier transforms $A_{\vec{k}}$ and $B_{\vec{k}}$ are periodic outside the MBZ. The eigenvalues are $\epsilon_\pm(\vec{k}) = -\mu + t'_{\vec{k}} \pm t_{\vec{k}}$, where $t_{\vec{k}} = -2t[\cos(k_1) + \cos(k_2)]$ and $t'_{\vec{k}} = -4t'\cos(k_1)\cos(k_2)$.

Both fields have a FS within the MBZ. Ψ_+ has four hole-like (FS increase as doping increases) large arcs centered at $\vec{K}_1 = \frac{1}{2}(\pi,\pi)$, $\vec{K}_2 = \frac{1}{2}(-\pi,\pi)$, $\vec{K}_3 = \frac{1}{2}(-\pi,-\pi)$ and $\vec{K}_4 = \frac{1}{2}(\pi,-\pi)$ while Ψ_- has small electron-like (FS reduces as doping increases) Fermi surfaces near $\vec{Q}_1 = (\pi,0)$, $\vec{Q}_2 = (0,\pi)$, $\vec{Q}_3 = (-\pi,0)$ and $\vec{Q}_4 = (0,-\pi)$. Notice that the standard FS of the $t-t'$ model, defined in the whole BZ, can be obtained reflecting, in each quadrant, the FS of Ψ_- outside the MBZ and gluing it with the FS of Ψ_+ inside the MBZ.

The holon field, defined in the whole BZ, turns out to be

$$H_{\vec{k}} = \begin{cases} \Psi_+(\vec{k}), & \text{if} \quad \vec{k} \in MBZ, \\ \Psi_-(\vec{k} - 2\vec{K}_v), & \text{if} \quad \vec{k} \notin MBZ, \vec{k} \in BZ. \end{cases} \tag{4.3}$$

with $\vec{K}_v$ ($v = 1,2,3,4$) chosen to keep the argument of Ψ_- inside the MBZ (where it is defined). The FS of $H_{\vec{k}}$ is that of the standard $t-t'$ model. The exceeding FS in the two

sublattice scheme disappears, because of the spectral weight, when $H_{\vec{k}}$ is reconstructed using Eq. (4.3).

Now we define the fields

$$\begin{aligned}\Psi_{+,v}(\vec{k}) &= \Psi_{+}(\vec{k}+\vec{K}_v)\\ \Psi_{-,v}(\vec{k}) &= \Psi_{-}(\vec{k}+\vec{Q}_v)\end{aligned} \tag{4.4}$$

where $\vec{k}+\vec{K}_v$ and $\vec{k}+\vec{Q}_v$ belong to the MBZ. We expect these fields have a good continuum limit because they give rise to closed Fermi surfaces [45]. To see this we exploit the two reciprocal primitive vectors $\vec{Q}_{\pm}=(\pm\pi,\pi)$ to translate the 3rd and 4th quadrants respectively in order to obtain a upper rectangular zone $D=\{k_x\in[-\pi,\pi],\, k_y\in[0,\pi]\}$ equivalent to the MBZ, as done in PG. Both the MBZs of Ψ_+ and Ψ_- fields, in the lower rectangle, are translated. Notice that each translation changes the $\pm$ index of the field because of the minus sign due to the exponential factor in Eq. (4.2) (this is the same minus sign appearing in the field transformation of Eq. (3.12) in the PG case) while $A_{\vec{k}}$ and $B_{\vec{k}}$ do not change when $\vec{k}\to\vec{k}+\vec{Q}_{\pm}$, indeed $\Psi_{\mp}(\vec{k})=\Psi_{\pm}(\vec{k}-\vec{Q}_{\pm})$ where $\vec{k}$ now belongs to D. Moreover the translation exchanges the eigenvalues $\epsilon_{\mp}(\vec{k})=\epsilon_{\pm}(\vec{k}-\vec{Q}_{\pm})$ because $t_{\vec{k}+\vec{Q}_{\pm}}=-t_{\vec{k}}$ therefore D is equivalent to the MBZ and the closed Fermi surfaces are shown in Fig. (4.1).

After these clarifications, in what follows we will introduce spin-vortex attraction and we will consider the translation of $\Psi_{+,3}$ and $\Psi_{+,4}$ applying the transformations of Eqs. (3.11) and (3.12) to $\Psi_{+,v}$ (notice that $b_{\vec{k}}=e^{ik_1}B_{\vec{k}}$). We expect that these fields are more relevant than $\Psi_{-,v}$ because holon pairs suppress quasi-particles starting from antinodal directions. $\Psi_{+,3}$ and $\Psi_{+,4}$, after translation, generate, together with $\Psi_{+,1}$ and $\Psi_{+,3}$ respectively, the large closed hole-like Fermi surfaces centered at $\vec{K}_1$ and $\vec{K}_1$ in the first and second quadrants. Similar considerations also hold for the small closed electron-like Fermi surfaces generated by the fields $\Psi_{-,v}$ around the points $\vec{Q}_v$.

The attractive interaction between different sublattice with opposite vortex charge of Eq. (3.3) is treated in analogy with PG, giving

$$\begin{aligned}H_I^h &= -\sum_{i,j} V(\vec{i}-\vec{j})A_i^{\dagger}B_j^{\dagger}B_jA_i\\ &\approx -\tilde{J}\langle z^{\dagger}z\rangle\sum_{\vec{p},\vec{q}} V_{\text{eff}}(\vec{p}-\vec{q})A_{\vec{p}}^{\dagger}B_{-\vec{p}}^{\dagger}B_{-\vec{q}}A_{\vec{q}}\end{aligned} \tag{4.5}$$

We perform the translation, add right R and left L labels ($\alpha=R,L=1,2$) and

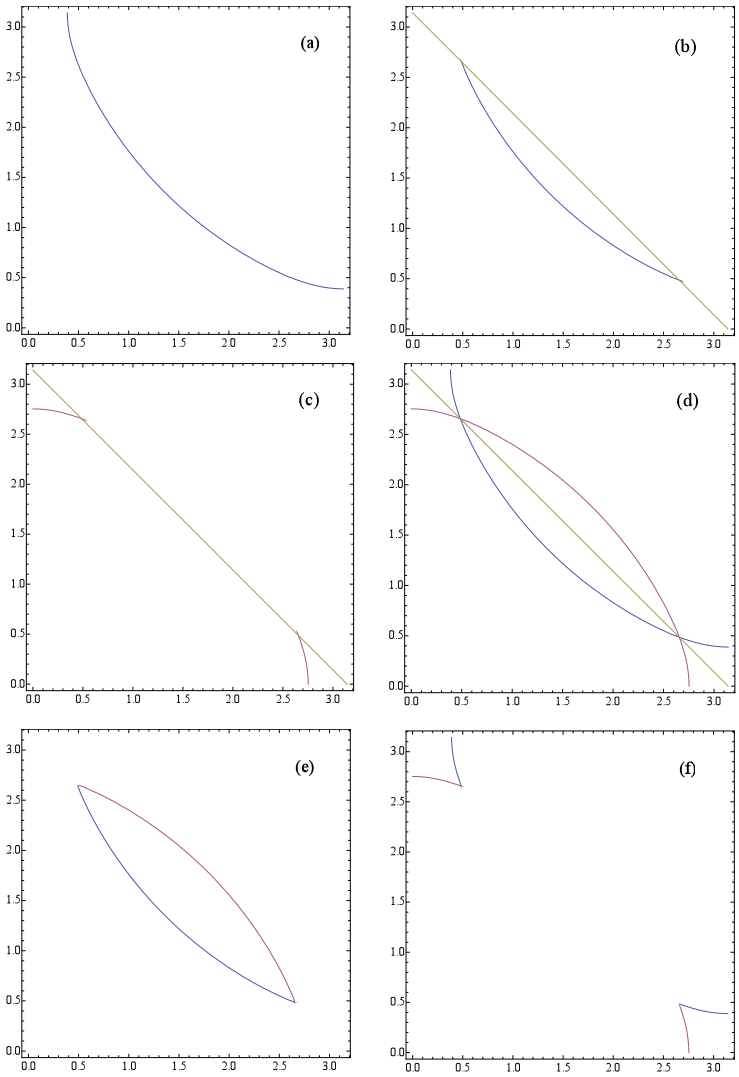

Figure 4.1: Each panel represents the first quadrant of the $t-t'$ model with next nearest neighbor hopping. (a) FS of holons without sublattice separation and defined in the whole BZ; (b) FS of Ψ_+ quasi-particles with sublattice separation and defined in the MBZ, holons fill the closed region near the MBZ boundary; (c) FS of Ψ_- quasi-particles with sublattice separation and defined in the MBZ, holons fill most of the MBZ; the translation of the 3rd quadrant in (d) originates of the two rectangular regions, equivalent to the MBZ, for Ψ_+ in (e) (holons fill the closed region) and for Ψ_- in (f) (holons fill the whole zone except the two small regions near the corners).

measure momenta from $\vec{Q}_R$ and $\vec{Q}_L$ respectively. We neglect the interaction between R and L sectors and perform BCS approximation defining the order parameter

$$\Delta^h_{\alpha,\vec{k}} = \tilde{J}\langle z^\dagger z\rangle \sum_{\vec{q}} V_{eff}(\vec{k}-\vec{q})\langle b_{\alpha,-\vec{q}} a_{\alpha,\vec{q}}\rangle. \tag{4.6}$$

This order parameter has p-wave symmetry as in Eq. (3.23) in such a way to obtain a d-wave symmetry gluing R and L sectors when the RBZ is restored (as we see from its definition, the order parameter changes its sign when the 3rd and 4th quadrants are translated) [41]. Notice that a p-wave symmetry in D, generating a d-wave symmetry in the whole BZ, generates also an s-wave pairing for the small electron-like Fermi surfaces.

Next introducing Nambu fields $\Psi_{\alpha,\vec{k}} = (a_{\alpha,\vec{k}}, b_{\alpha,\vec{k}}, a^\dagger_{\alpha,-\vec{k}}, b^\dagger_{\alpha,-\vec{k}})^t$, we obtain the Hamiltonian $H_{h,\alpha} = \sum_{\vec{k}} \Psi^\dagger_{\alpha,\vec{k}} \mathcal{H}_{\alpha,\vec{k}} \Psi_{\alpha,\vec{k}}$, which can be block-diagonalized using the unitary matrix

$$\mathcal{A} = \frac{1}{\sqrt{2}} \begin{pmatrix} 1 & 1 & 0 & 0 \\ -1 & 1 & 0 & 0 \\ 0 & 0 & 1 & 1 \\ 0 & 0 & 1 & -1 \end{pmatrix} \tag{4.7}$$

with the result $\mathcal{A}^\dagger \mathcal{H}_{\alpha,\vec{k}} \mathcal{A} =$

$$\begin{pmatrix} -\mu - t'_{\alpha,\vec{k}} - t_{\alpha,\vec{k}} & 0 & 0 & -\Delta^h_{\alpha,\vec{k}} \\ 0 & -\mu - t'_{\alpha,\vec{k}} + t_{\alpha,\vec{k}} & \Delta^h_{\alpha,\vec{k}} & 0 \\ 0 & \Delta^{h*}_{\alpha,\vec{k}} & \mu + t'_{\alpha,\vec{k}} - t_{\alpha,\vec{k}} & 0 \\ -\Delta^{h*}_{\alpha,\vec{k}} & 0 & 0 & \mu + t'_{\alpha,\vec{k}} + t_{\alpha,\vec{k}} \end{pmatrix} \tag{4.8}$$

provided that the holon pairing order parameter $\Delta^h_{\alpha,\vec{k}}$ has p-wave symmetry, i.e. $\Delta^h_{\alpha,-\vec{k}} = -\Delta^h_{\alpha,\vec{k}}$. In the above matrix we defined

$$t_{\alpha,\vec{k}} = t_{\vec{k}+\vec{Q_\alpha}} = -2t[\sin k_x - (-1)^\alpha \sin k_y] \tag{4.9}$$

$$t'_{\alpha,\vec{k}} = t'_{\vec{k}+\vec{Q_\alpha}} = -4t'(-1)^\alpha \sin k_x \sin k_y. \tag{4.10}$$

The energy spectrum of the quasi-particles has the BCS form $E_{\alpha,\vec{k}} = \pm\epsilon_{\alpha,\pm,\vec{k}}$ where

$$\epsilon_{\alpha,\pm,\vec{k}} = \sqrt{(\pm t_{\alpha,\vec{k}} - t'_{\alpha,\vec{k}} - \mu)^2 + |\Delta_{\alpha,\vec{k}}|^2}. \tag{4.11}$$

The attractive interaction in Eq. (4.5) is able to distinguish between the two sublattice and so does the resulting BCS interaction. Therefore, when incoherent holon pairs appear, the two descriptions with or without sublattice separation are no more equivalent. The first one turns out to be able to justify the closed Fermi surfaces, the small electron-like one and the two large hole-like ones, observed in experiments.

In the low energy limit only quasi-particle near the closed FS are relevant and, in each sector, we linearize the quasi-particle dispersion about the FS. In this way the continuum low energy effective Hamiltonian for $\psi_{\alpha,+}(\vec{k}) = \psi_{\alpha,\vec{k}}$ can be written as

$$\begin{aligned} H^h_{\text{eff}} &= \sum_{\alpha,\vec{k}} \left\{ \vec{v}_F(\alpha,\theta_k) \cdot \hat{k} \left[|\vec{k}| - k_F(\alpha,\theta_k) \right] \right\} \psi^\dagger_{\alpha,\vec{k}} \psi_{\alpha,\vec{k}} \\ &\quad + \sum_{\alpha,\vec{k}} \frac{1}{2} \left(\Delta^h_{\alpha,\vec{k}} \psi^\dagger_{\alpha,\vec{k}} \psi^\dagger_{\alpha,-\vec{k}} + h.c. \right) \end{aligned} \tag{4.12}$$

where the sum over spatial momenta $\vec{k}$ is made on a strip of thickness 2Λ about the FS. We notice that when $\vec{k}$ lies close to an arc of the FS, then $-\vec{k}$ lies close to the other arc. The above hamiltonian emphasizes that, in the holon sector, the main differences between SM and PG are the shape of the FS and the higher value of the Fermi momentum of the former $k_F \sim 1 - \delta$ w.r.t. the latter $k_F \sim \delta$.

4.3 Integration of high energy modes

In this section we derive the low energy effective action which describe the pairing process in the normal state down to superconductivity.

Starting from the spinon sector, the relevant action is the non-linear σ-model action with a mass term in Eq. (2.39). The mass term allows us to safely integrate out spinon degrees of freedom obtaining an effective action for the slave particle gauge field A. Because of gauge invariance, the second order result is a Maxwell-like action:

$$S^A_{\text{eff}}(A_\mu) = \frac{1}{3\pi m_s} \int_{[0,\beta]\times\mathbf{R}^2} d^3x F^2_{\mu\nu}. \tag{4.13}$$

For the holon sector, we need to consider phase fluctuations of the order parameter. Therefore we generalize the BCS interaction in Eq. (4.12) between holon pairs and FL quasi-particles and for sake of simplicity we neglect the direction dependence of k_F and v_F. The holon hamiltonian reads

$$
\begin{aligned}
H^h_{\text{eff}} &= \sum_{\alpha,\vec{k}} [E(\vec{k}) - \mu] \psi^\dagger_{\alpha,\vec{k}} \psi_{\alpha,\vec{k}} \\
&\quad - \sum_{\alpha,\vec{k},\vec{q}} \frac{1}{2} \left\{ \Delta^h_\alpha(\vec{k}+\vec{p}) [\gamma_\alpha(\vec{k}) - \gamma_\alpha(\vec{p})] \psi^\dagger_{\alpha,\vec{k}} \psi^\dagger_{\alpha,\vec{p}} + h.c. \right\}
\end{aligned} \tag{4.14}
$$

where $\gamma_\alpha(\vec{k}) = \sin(k_x) + (-1)^\alpha \sin(k_y)$ takes the p-wave symmetry of the order parameter consistently with Eq. (3.23) and $E(\vec{k}) - \mu \approx v_F(|\vec{k}| - k_F)$ near the FS. We notice that in the case of constant order parameter $\Delta^h_\alpha(\vec{k}) \to \Delta^h_0 \delta^2(\vec{k})$, Eq. (4.14) reproduces the standard BCS coupling of Eq. (4.12).

The next step is to obtain the dynamics of the order parameter, in particular we are interested in its phase since as usually is argued to be the origin of the leading fluctuations. We write down the holon action, derived from the Hamiltonian in Eq. (4.14), in terms of Matsubara frequencies k_0

$$
\begin{aligned}
S^{h,\Delta}_{\text{eff}}(\psi_\alpha, \Delta^h_\alpha) &= \sum_{\alpha,\vec{k},k_0} [ik_0 - E(\vec{k}) + \mu] \psi^\dagger_{\alpha,k} \psi_{\alpha,k} \\
&\quad - \sum_{\alpha,\vec{k},\vec{p},k_0,p_0} \frac{1}{2} \left\{ \Delta^h_\alpha(k+p) [\gamma_\alpha(\vec{k}) - \gamma_\alpha(\vec{p})] \psi^\dagger_{\alpha,k} \psi^\dagger_{\alpha,p} + c.c. \right\}
\end{aligned} \tag{4.15}
$$

where we put $k = (k_0, \vec{k})$. Then, considering the order parameter Δ^h_α as constant in modulus and fluctuating in phase

$$
\Delta^h_\alpha(\vec{x}, x_0) = \Delta^h_{\alpha,0} e^{i\phi^h(\vec{x},x_0)}, \tag{4.16}
$$

we integrate out holons modes with frequency higher than an IR cut-off Λ_h, retaining gapless quasi-particle in the low energy effective theory. In this way no singular terms due to integration of gapless excitations arise and both dynamics and interactions of the order parameter will be local in space. *We assume that these high frequency integrated modes are d-wave superconducting modes.* This assumption will be proved to be self consistent later with a proper choice of Λ_h. We can guess the result of this integration by symmetry considerations [28], [29]. The gap equation, Eq. (4.6), has a degenerate manifold of solutions for arbitrary phase ϕ^h therefore the energy should depend only on gradients of ϕ^h. Assuming time reversal invariance and making a gradient expansion up to the second order we obtain the action of the phase field in the continuum limit (we take $v_F = 1$)

$$
S^\Delta_{\text{eff}}(\phi^h, A) = \frac{c}{2} \Delta^{h2}_{\alpha,0} \int d^2\vec{x} dt \left(\partial_\mu \phi^h - 2A_\mu + 2\pi n_\mu \right)^2 (\vec{x}, t) \tag{4.17}
$$

where we introduced the slave particle gauge field A_μ by minimal substitution and the vector of integer currents $n_\mu(\vec{x},t)$ allows ϕ^h to be a multi-valued function and takes into account the presence of vortices. Summation on n_μ is understood. This can be made precise with a lattice regularization which is used in the following.

We notice that if we had integrated out gapless quasi-particle in the presence of the slave particle gauge field, in addition to singular long range interactions for the order parameter, we get (for $m_\phi \neq 0$) a Reizer singularity for the transverse component of the gauge field owing to the finite FS. The Reizer singularity, at low energy (or temperature) would be dominant over the Maxwell-like action of Eq. (4.13) generated by massive spinons.

In conclusion, the continuum low energy effective action we are interested in consists of three contributions $S_{\text{eff}} = S^A_{\text{eff}} + S^\Delta_{\text{eff}} + S^{h,\Delta}_{\text{eff}}$ and the last term has UV cut-off Λ_h. The relevant fields are the UV cutoff holon field ψ_α, the phase ϕ^h of the order parameter and the slave particle gauge field A_μ. For the moment we do not consider the interaction between holons and the slave particle gauge field which can be restored at any time in Eq. (4.15) via minimal substitution.

4.4 Order parameter propagator

In this section we will show that the Euclidean correlation function of the holon pairs order parameter $\Delta^h(\vec{x},x_0)$, because of its fluctuating phase, is given by

$$\langle \Delta^h_\alpha(\vec{x},x_0)\Delta^{h*}_\alpha(\vec{0},0)\rangle = \Delta_0^{h2} G_\Delta(\vec{x},x_0), \tag{4.18}$$

$$G_\Delta(\vec{x},x_0) = \langle e^{i[\phi^h(\vec{x},x_0)-\phi^h(\vec{0},0)]}\rangle \simeq e^{-m_\phi\sqrt{v_F^2x_0^2+\vec{x}^2}}. \tag{4.19}$$

This relation defines the holon pairs phase coherence length $\xi_\phi = 1/m_\phi$. m_ϕ can be thought as the mass of the phase ϕ^h of the holon pairs field and ξ_ϕ as the mean distance between phase vortices. The important point of Eq. (4.19) is that it decays exponentially for large $|x|$ but it does not show any singularity for small $|x|$ (in particular it is a constant at $x=0$). A similar correlation, taken as an assumption, can be found in [27].

To prove Eq. (4.19) we evaluate the correlation $G_\Delta(x)$ weighted by the action $S^A_{\text{eff}}+S^\Delta_{\text{eff}}$ in the Coulomb gauge $\Delta_i A_i = 0$ ($i=1,2$ indicates spatial components and $x=(\vec{x},x_0)$). Using Dirac's trick, we introduce the gauge invariant field

$$e^{i\Phi(x)} = e^{i[\phi^h(x)+2\sum_y E^x_\mu(y)A^\mu(y)]} \tag{4.20}$$

where $E^x_\mu(y) = \delta_{x_0,y_0}(E^{\vec{x}}_1(\vec{y}), E^{\vec{x}}_2(\vec{y}), 0)$ and $\Delta_i E^{\vec{x}}_i(\vec{y}) = \delta^2_{\vec{x},\vec{y}}$. Because it reduces to $e^{i\phi^h(x)}$ in the Coulomb gauge, we can evaluate the correlation $G_\Delta(x)$ estimating the expectation value $\langle e^{i[\Phi(x)-\Phi(0)]}\rangle$ without gauge fixing. Notice that the "electric" field $E^x_\mu(y)$ has no temporal component and it is different from zero only in the temporal plane $x_0 = y_0$.

Taking into account the periodicity of the phase (i.e. the presence of vortices) we apply Poisson formula rewriting the action S^Δ_{eff} in the following form

$$S^\Delta_{\text{eff}}(\phi^h, A, J) = -\frac{1}{2}\sum_x \left[\frac{J_\mu J_\mu}{\Delta_0^{h2}} + iJ_\mu(\partial_\mu\phi^h - 2A_\mu)\right] \tag{4.21}$$

where $J_\mu(x)$ are integer currents over which we sum when functional integrals are evaluated.

Then defining $\gamma^\mu_{x,y}(z)$ a current of charge two supported on a path from x to y (i.e. $\Delta_\mu\gamma^\mu_{x,y}(z) = \delta^3_{z,x} - \delta^3_{z,y}$), we can write

$$\phi^h(x) - \phi^h(0) = \sum_z \gamma^\mu_{x,0}(z)\Delta_\mu\phi^h(z) \tag{4.22}$$

and performing the functional integration in ϕ^h, which appears linearly in the action, we obtain the constraint $\Delta_\mu J_\mu(z) = \delta^3_{z,x} - \delta^3_{z,0}$, or equivalently $\Delta_\mu(J_\mu - \gamma^\mu_{x,0}) = 0$. The final step is to integrate out the slave particle gauge field A_μ. The result at zero temperature is $G_\Delta(x) =$

$$\frac{\sum_{\{J_\mu:\partial_\mu J_\mu = \delta^3_x - \delta^3_0\}} e^{-\frac{1}{2}\sum_z \frac{J_\mu J_\mu}{\Delta_0^{h2}}} e^{-\frac{m_s}{4}\sum_z\sum_w [J_\mu(z)+E^x_\mu(z)-E^0_\mu(z)]\Delta_3^{-1}(z-w)[J_\mu(w)+E^x_\mu(w)-E^0_\mu(w)]}}{\sum_{\{J_\mu:\partial_\mu J_\mu=0\}} e^{-\frac{1}{2}\sum_z \frac{J_\mu J_\mu}{\Delta_0^{h2}}}} \tag{4.23}$$

where $\Delta_3^{-1}(z)$ is the 3-dimensional inverse lattice Laplacian. The sum in the numerator is on currents J_μ starting from the point $z = 0$ up to the point $z = x$ and on closed currents while only closed current are considered in the denominator.

In the limit of small Δ_0^h, closed currents are suppressed and only the currents close to the straight line connecting the endpoints 0 and x give a significant contribution proportional to the distance $|x|$, for large $|x|$. Indeed the gauge interactions force the fluctuations of the current to be non-gaussian, lying within a thin tube surrounding the shortest straight path. Therefore we expect that the leading contribution to $G_\Delta(x)$ is an exponential of a linearly decreasing function of the distance $|x|$.

Taking this into account we estimate Eq. (4.23) in the particular case $x = (\vec{0}, x_0)$, retaining only the straight current, in the continuum limit. The important current has therefore only the temporal component, $J_\mu(z) = \delta_{\mu 0}\delta^2(\vec{z})\theta(x_0 - z_0)$, and, because E_μ has no temporal component, we can decouple J_μ from E_μ in the term with the inverse Laplacian in Eq. (4.23) and factorize two contributions in $G_\Delta(x)$. The first one is due to the straight current $J_\mu(z)$ and the second one is due to the "electric" field E^z_μ,

$$G_\Delta(x_0, \vec{0}) \approx e^{-\left[\frac{1}{\Delta_0^{h2}} x_0 + \frac{m_s}{4}\int_0^{x_0} dt \int_0^{x_0} dt' \Delta_3^{-1}(t-t', \vec{0})\right]} e^{-\frac{m_s}{4} D(x_0)} \tag{4.24}$$

where

$$\begin{aligned} D(x_0) &= \int d^3z \int d^3w [E^x_\mu(z) - E^0_\mu(z)]\Delta_3^{-1}(z-w)[E^x_\mu(w) - E^0_\mu(w)] \\ &= 2\int d^2x \int d^2y \frac{1}{|\vec{x}|}\frac{1}{|\vec{y}|}\left[\frac{1}{\sqrt{(\vec{x}-\vec{y})^2 + \varepsilon^2}} - \frac{1}{\sqrt{|\vec{x}-\vec{y}|^2 + x_0^2 + \varepsilon^2}}\right] \\ &\sim cx_0[1 + c' \ln(x_0)]. \end{aligned} \tag{4.25}$$

Eq. (4.25) follows from the continuum limit definitions of $E^x_\mu(z) = \delta(z_0 - x_0)\frac{1}{|\vec{z}-\vec{x}|}(z_1 - x_1, z_2 - x_2, 0)$ and of the inverse 3-D Laplacian $\Delta_3^{-1}(z) = \frac{1}{\sqrt{z_1^2+z_2^2+z_0^2}}$ with ε an UV cutoff. The last step holds in the limit $x_0 >> 1 >> \varepsilon$ and c and c' are constants.

The important point is that the logarithmic contribution in Eq. (4.25) is exactly eliminated from the integral in the first exponential of Eq. (4.24) due to the straight current,

$$\begin{aligned} \int_0^{x_0} dt \int_0^{x_0} dt' \Delta_3^{-1}(t-t', \vec{0}) &= \int_0^{x_0} dt \int_0^{x_0} dt' \frac{1}{\sqrt{(t-t')^2 + \varepsilon^2}} \\ &\sim cx_0[1 - c' \ln(x_0)] \end{aligned} \tag{4.26}$$

In conclusion $G_\Delta(x)$ turns out to be an exponential of a decreasing linear function of the distance $|x|$ and does not develop singularities in the limit of small $|x|$. From the above discussion, our estimate of the inverse coherence length is

$$m_\phi \approx \frac{1}{\Delta_0^{h2}} + m_s - P(\Delta_0^h) \tag{4.27}$$

where $P(\Delta_0^h)$ is a polynomial to take into account the fluctuation of the current $J_\mu(x)$ which ensures the right behavior when the SC phase is approached. Indeed the first two addends, which follow from the above calculations, are relevant in the limit of small Δ_0^h

(in this limit the approximations we made hold) while the polynomial $P(\Delta_0^h)$ becomes relevant when Δ_0^h is no more a small parameter and m_ϕ is approaching zero.

In such a way the form of the phase correlation taken at the beginning in Eq. (4.19) is justified.

4.5 Holon self energy due to order parameter

In this section we extend the discussion of the previous chapter about holon pairing. We exploit the action in Eq. (4.15) and the result of Eq. (4.18) to evaluate, in the continuum limit, the zero temperature quasi-particle self energy $\Sigma(\omega, \vec{k})$ arising from scattering of the phase fluctuations of the order parameter.

What follows holds both in PG region and in SM region, the FS shape is irrelevant. The difference between the two regions lies in the value of the involved parameters, v_F and k_F, that makes the SM results much more effective. The only condition we need is parity invariance which implies the quasi-particle excitation energy verifies $E(\vec{k}) = E(-\vec{k})$.

We consider the right sector, the left sector is similar with $\gamma_R(\vec{k}) \to \gamma_L(\vec{k})$. In the limit $|\Delta_0^h| << \epsilon_F$ the self energy reads

$$\Sigma(\omega, \vec{k}) = \frac{|\Delta_0^h|^2}{4}\gamma_R(\vec{k})^2 \int \frac{d^3q}{(2\pi)^3} \frac{G_\Delta(q_0, \vec{q})}{i(q_0 - \omega) - E(\vec{k} - \vec{q})} \tag{4.28}$$

where the $\vec{q}$ dependence of γ_R has been neglected for $|\vec{q}| << |\vec{k}| \sim k_F >> m_\phi$ and

$$G_\Delta(q_0, \vec{q}) = \frac{8\pi m_\phi}{(p^2 + m_\phi^2)^2} \tag{4.29}$$

is the Fourier transform of $G_\Delta(x)$ obtained by taking the derivative w.r.t. m_ϕ of the relation $\int d^3p \frac{e^{ipx}}{p^2+m^2} = \frac{2\pi^2}{x} e^{-mx}$. This fact allows us to rewrite Eq. (4.28) as

$$\Sigma(\omega, \vec{k}) = \frac{|\Delta_0^h|^2}{4}\gamma_R(\vec{k})^2 2\pi m_\phi \frac{d}{dm_\phi^2} I(k), \tag{4.30}$$

$$I(k) = \int \frac{d^3q}{(2\pi)^3} \frac{1}{q^2 + m_\phi^2} \frac{1}{i(q_0 - k_0) - E(\vec{q} - \vec{k})}. \tag{4.31}$$

Considering quasi-particles on a shell of thickness $2\Lambda << k_F$ about the FS we can linearize the quasi-particle dispersion $E(\vec{q} - \vec{k}) = v_F(|\vec{q} - \vec{k}| - k_F) \approx -\vec{q} \cdot \hat{k} + \delta k$, where $v_F = 1$ and $\delta k \equiv |\vec{k}| - k_F$.

To evaluate $I(k)$ we use cylindrical coordinates $r = \sqrt{q_1^2 + q_0^2}$ and $\theta = \arctan\left(\frac{q_0}{q_1}\right)$ with cylinder axis directed along $\hat{y}$ axis. Moreover we choose the $\hat{x}$-axis directed along the

unit vector $\hat{k}$ in such a way that the $\hat{y}$-axis is a tangent vector to the FS. Then, in the plane orthogonal to the cylinder axis, we define the vector $\vec{r}_0 = (\delta k, k_0) = r_0(\cos\varphi, \sin\varphi)$ where $r_0 = \sqrt{\delta k^2 + k_0^2}$ and $\varphi = \arctan\left(\frac{k_0}{\delta k}\right)$. With these definitions we can write

$$I(k) = \int \frac{dr d\theta dq_2}{(2\pi)^3} \frac{r}{q_2^2 + r^2 + m_\phi^2} \frac{1}{r_0 e^{i\varphi} - r e^{i\theta}} \tag{4.32}$$

which can be exactly evaluated with the result (see appendix)

$$\begin{aligned} I(k) &= \frac{1}{4\pi} \frac{\sqrt{r_0^2 + m_\phi^2} - m_\phi}{r_0 e^{i\varphi}} \\ &= \frac{1}{4\pi} \frac{\sqrt{k_0^2 + \delta k^2 + m_\phi^2} - m_\phi}{i k_0 + \delta k} \end{aligned} \tag{4.33}$$

where in the last equality the relation $2i \arctan(z) = \ln(1 + iz) - \ln(1 - iz)$ has been used.

Inserting Eq. (4.33) into Eq. (4.30) and posing $E(\vec{k}) = \delta k$ we obtain an exact result for the self energy

$$\Sigma(\omega, \vec{k}) = \frac{|\Delta_0^h|^2}{4} \gamma_R(\vec{k})^2 \frac{1}{i\omega + E(\vec{k})} \left[1 - \frac{m_\phi}{\sqrt{\omega^2 + E(\vec{k})^2 + m_\phi^2}} \right] \tag{4.34}$$

where $\gamma_R(\vec{k})^2 = 2k_F^2 \sin^2\theta_{\vec{k}}$ and $\theta_{\vec{k}}$ is the angle between the vector $\vec{k}$ and the nodal direction $\vec{Q}_+$ in the right sector.

The quasi-particle Green's function is given by

$$\begin{aligned} G(\omega, \vec{k}) &= [i\omega - E(\vec{k}) - \Sigma(\omega, \vec{k})]^{-1} \\ &= \frac{1}{\left\{ 1 + \frac{|\Delta_0^h|^2}{4} \gamma_R(\vec{k})^2 \frac{1}{\omega^2 + E(\vec{k})^2} \left[1 - \frac{m_\phi}{\sqrt{\omega^2 + E(\vec{k})^2 + m_\phi^2}} \right] \right\} [i\omega - E(\vec{k})]}. \end{aligned} \tag{4.35}$$

We notice that at zero frequency, $\omega = 0$, the only pole of the Green's function $G(\omega, \vec{k})$ is located at $E(\vec{k}) = 0$, that is at the FS. This means that there is always a FS except exactly at $m_\phi = 0$ which we associate with the transition to the superconducting phase.

To understand the meaning of $G(\omega, \vec{k})$ we analyze the two limits of low and high frequency ω w.r.t. m_ϕ.

- In the first case $\omega << m_\phi$, we expand the self energy in powers of $\frac{\omega}{m_\phi}$ up to the second order and the Green's function becomes

$$G(\omega, \vec{k}) \simeq \frac{Z_\Delta(\vec{k})}{i\omega - E(\vec{k})}, \tag{4.36}$$

$$Z_\Delta(\vec{k}) = \frac{1}{1 + \frac{|\Delta_0^h|^2}{8m_\phi^2}\gamma_R(\vec{k})^2}. \tag{4.37}$$

  Thus for low frequencies the effect of holon pairing appears through wave function renormalization factor (or weight) $Z_\Delta(\vec{k})$. The system behaves like a FL with unchanged FS and Fermi velocity v_F but with a strongly direction dependent weight $Z_\Delta(\vec{k})$ that heavily suppress (if $|\Delta_0^h| >> m_\phi$) quasi-particles in antinodal directions reducing the effective FS. The spectral weight is one in the nodal direction and only nearby modes are important.

- In the second case $\omega >> m_\phi$, we expand the self energy in powers $\frac{m_\phi}{\omega}$ and we get the Green's function

$$G(\omega, \vec{k}) \simeq -\frac{i\omega + E(\vec{k})}{\omega^2 + E(\vec{k})^2 + \frac{|\Delta_0^h|^2}{4}\gamma_R(\vec{k})^2} \tag{4.38}$$

  which is the quasi-particle Green's function of a p-wave superconductor. Thus for high frequencies the system behaves like a d-wave superconductor obtained gluing γ_R and γ_L having p-wave symmetry in each sector.

We notice that if $m_\phi = 0$ the condition $\omega >> m_\phi$ is always fulfilled and the system is in the superconducting phase as expected. As soon as $m_\phi > 0$ the FS and the FL quasi-particle peak of weight $Z_\Delta(\vec{k})$ appear for low frequencies and the system behave like a metal because of them. When $|\omega| \geq m_\phi$, quasi-particles begin to scatter significantly with the quanta of the phase of the order parameter changing significantly both quasi-particle dispersion and coherence. FL quasi-particles modes are suppressed in favor of d-wave SC modes that become much more coherent and relevant. This means that the value of m_ϕ, decreasing, drives the system behavior from metallic towards superconducting.

This behavior strongly dependent on m_ϕ value, can be made smoother introducing an additional scattering rate η modeling quasi-particle coherence. It originates mainly from the scattering against gauge fluctuations and broadens peaks in spectral weight functions.

Performing the analytic continuation $i\omega \to \omega + i\eta$ in Eq. (4.35) we obtain the retarded Green's function

$$G^R(\omega,\vec{k}) = \frac{\omega + i\eta + E(\vec{k})}{(\omega+i\eta)^2 - E(\vec{k})^2 - \frac{|\Delta_0^h|^2}{4}\gamma_R(\vec{k})^2\left[1 - \frac{m_\phi}{\sqrt{E(\vec{k})^2+m_\phi^2-(\omega+i\eta)^2}}\right]} \tag{4.39}$$

and its imaginary part is proportional to the spectral weight $A(\omega,\vec{k}) = -\frac{1}{\pi}\Im G^R(\omega,\vec{k})$. The spectral weight at the FS, i.e. $A(\omega,|\vec{k}|=0)$, shows clearly the separation of the regimes of system varying the parameters, in particular m_ϕ, $|\Delta_0^h|$ and η. It is symmetric in frequencies, and exhibits three maxima, the FL-like peak at $\omega = 0$ and two symmetric SC-like peaks roughly at $\omega_{scp} \sim \pm\sqrt{\frac{|\Delta_0^h|^2}{4}\gamma_R(\vec{k})^2 + m_\phi^2}$. Approximately (al least for small η) as long as $\frac{\eta}{m_\phi} < \frac{m_\phi}{\frac{|\Delta_0^h|}{2}\gamma_R(\vec{k})}$, the FL peak is higher than the SC peaks which became negligible for $\omega_{scp} >> \frac{|\Delta_0^h|}{2}\gamma_R(\vec{k})$, while approximately for $\frac{\eta}{m_\phi} > \frac{m_\phi}{\frac{|\Delta_0^h|}{2}\gamma_R(\vec{k})}$, the SC peaks are higher than the FL one. The size of the area under the peaks determines the main behavior of the system and the more strongly the above inequalities are verified, the greater is the difference of peak heights.

Again we notice that, even if small, the FL peak is always present unless m_ϕ strictly vanishes and in this case the spectral weight at the FS does not vanish because of η. A key point is the direction dependence of the condition on the maxima, due to $\gamma_R(\vec{k})$, which determines the effectiveness of the FS

$$\eta\frac{|\Delta_0^h|}{2}\gamma_R(\vec{k}) < [>] m_\phi^2, \qquad \text{if} \quad FL\,[SC]. \tag{4.40}$$

Indeed near the nodal region the behavior is always FL-like with an effective FS while near the antinodal directions most of the spectral weight is concentrated on SC-like modes and even if there is a FS, it has negligible effects.

4.6 Density of states and self consistency

The density of states of holons $\rho_h(\omega)$ can be obtained by numerical integration of the spectral weight $A(\omega,\vec{k})$ in momentum space. Fig. (4.2) shows the result of this calculation for different values of m_ϕ, using the imaginary part of the retarded Green's function in Eq. (4.39). In the plot, instead of γ_R with p-wave symmetry, we used $\cos(2\theta_{\vec{k}})$ with d-wave symmetry to recover the main features of the holon sector in the whole BZ. Moreover we claim that this result roughly holds also for holes because we expect that the main

relevant effect of the spinon sector, near the FS, is a renormalization of the scattering rate η.

We see how decreasing the value of m_ϕ the flat FL density of states in the panel (a) gradually reduces for small frequencies and develops a peak at $\omega \approx \omega_{scp}$. It is a precursor of the SC peak. Higher frequencies are not affected and preserve a flat d.o.s.. As expected, for small m_ϕ, panels (e) and (f), the d.o.s. resembles that of a d-wave superconductor with a well defined and high peak. Notice in panels (d) and (e) the additional small peak at $\omega = 0$ due to the FL quasi-particles which preserve a FS, even if not very effective, unless m_ϕ vanishes.

In Fig. (4.2) we keep fixed $\sqrt{\eta \frac{|\Delta_0^h|}{2}} \approx 0.007$. This value can be compared to the value of m_ϕ to obtain a condition similar to that shown in Eq. (4.40), but "averaged" over the angular dependence due to γ_R.

Taking into account the temperature dependence of m_ϕ via Δ_0^h (Eq. (4.27) holds at least for small Δ_0^h and the temperature dependence of Δ_0^h will be given in the next chapter in Eq. (5.5)), we see that m_ϕ decreases as temperature is reduced, until vanishing at $T = T_c$. Therefore Fig. (4.2) is in qualitative agreement with experimental data of Fig. (1.4,(b)).

The plots of the density of states and the discussion of the previous section show that, above the superconducting transition, there is an energy scale m_ϕ below which the fermionic excitations behaves like well defined FL quasi-particles with a reduced effective FS. The FS has not disappeared but a part of it has a strongly reduced weight. Above this energy scale the fermionic excitations are essentially d-wave gapped. In other words the energy scale m_ϕ separates FL modes from SC modes, therefore *we can consistently match m_ϕ with the cutoff Λ_h*. Fermionic modes higher than Λ_h were previously assumed to be SC-like and had been integrated out to give dynamics to the order parameter, see Eq. (4.17). In this way our earlier assumption on high energy modes is justified because the obtained self energy is consistent with it.

This calculation reflects a new interpretation of m_ϕ. When the order parameter does not fluctuate (standard BCS approximation) the scattering process occurs between particles on opposite sides of the FS with exactly opposite momentum which bind to form the Cooper pair. As we can see from the Feynman diagram for the self energy, when fluctuations of the order parameter are considered a particle with momentum $\vec{k}$ can interact, not only with the opposite one, but with all particles in a region centered at $-\vec{k}$ and allowed by momentum conservation. The range of the fluctuations, that is m_ϕ, determines the size of this region or in other words determines how much of the FS contributes

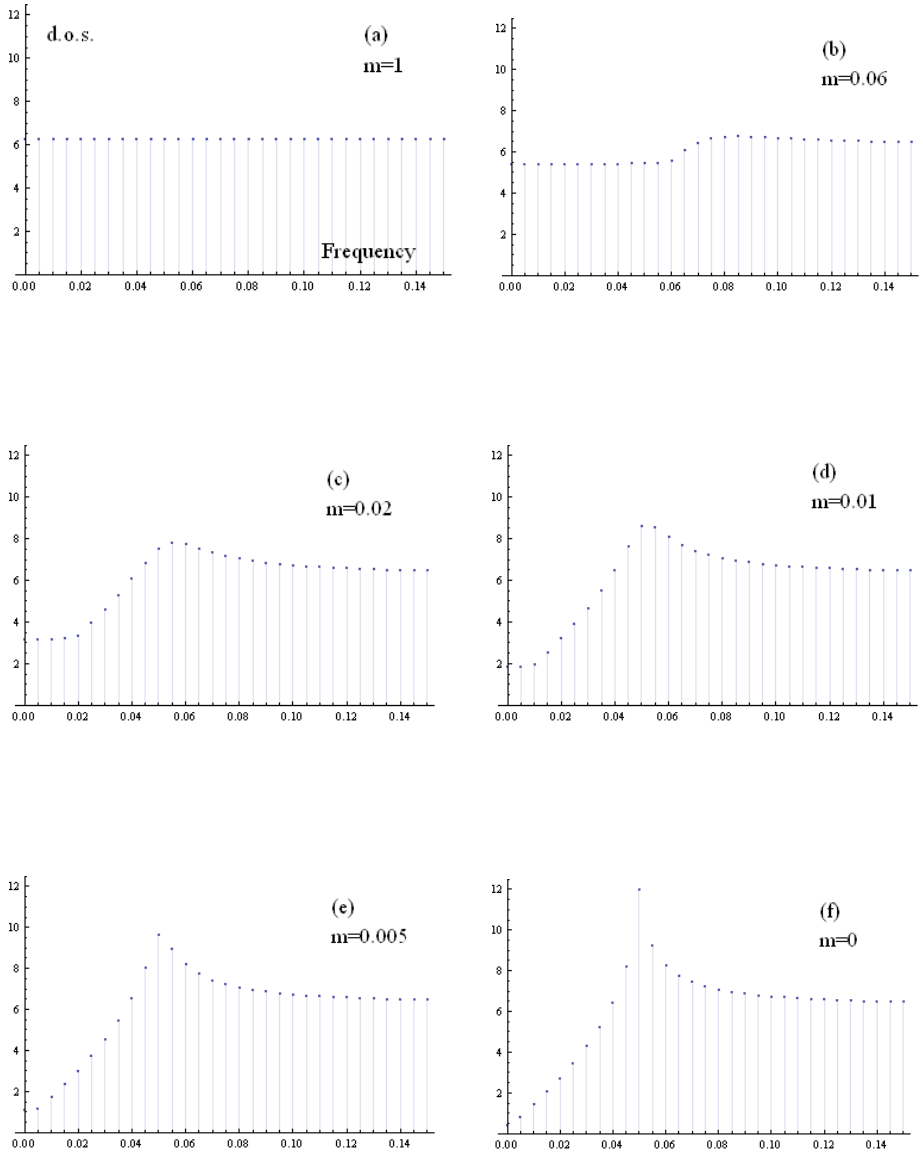

Figure 4.2: Density of states (d.o.s.) obtained from Eq. (4.39) and evaluated for different values of m_ϕ; we posed $v_F = 1$ and we took $k_F = 1$ (accordingly to SM regime) so that $E(\vec{k}) = \frac{1}{2}(\vec{k}^2 - 1)$ and the energy, in the horizontal axis, is measured in units of $2\epsilon_F$. Finally we fixed $\frac{|\Delta_0^h|}{2} = 0.05$ and $\eta = 0.001$. The vertical axis is in arbitrary units.

to the scattering process. Clearly when $m_\phi \to 0$ the contributing region reduces to the opposite point recovering the BCS approximation. This interpretation allows us to give meaningful upper limit to m_ϕ of order k_F which means that most of the FS contributes to the scattering process. This will help us in the next chapter when the temperature dependence of parameters will be treated.

Finally, a treatment similar to that just made for the holon pairs can not be done for spinon pairs because spinons are massive particles.

Chapter 5

Holon pairing effects in the normal state

5.1 Introduction

Besides the "mass" m_ϕ, which vanishes at $T = T_c$, there is another energy scale associated to holon pairs, represented by the order parameter $|\Delta_0^h|$ that, as explained in previous chapters, appears at T_{ph} when a finite density of incoherent holon pairs forms.

In this chapter we analyze the effects of the presence of incoherent holon pairs in the normal phase of underdoped cuprates. We concentrate on SM region, where these effects are much more effective, and analyze how they modify the low energy actions and the observables [7].

We will show that it is possible to ascribe to holon pairs formation the unusual temperature dependence of some experimental data usually associated to PG regime (i.e. to a spin gap) but actually occurring, at least for some doping values, at higher temperature typical of SM. Indeed the appearance of holon pairs generates a holon reduced spectral weight $\bar{Z}_\Delta$ and a wave factor Z_A which reduces the effectiveness of the Reizer-like action of the gauge field until it vanishes at the superconducting transition.

The observable effects we will consider as signatures of the high pseudo-gap crossover are the downturn of resistivity from linear behavior and the downturn of Knight shift (static spin susceptibility) from constant Pauli-like value at low temperatures. Other quantities, like specific heat and entropy, get some modifications but we will not deal with them in this thesis. However Knight shift and resistivity are enough to justify the identification of T_{ph} with the observed upper PG temperature.

When at $T \leq T_{ph}$ the holon reduced spectral weight $\bar{Z}_\Delta$ and the wave factor Z_A begin

to be significantly less than one and all quantities in which they appear feel the effect of their reduction. In this way we are able to explain the proportionality of the temperature derivative of resistivity and the Knight shift and why their deviation from a constant value is simultaneous in terms of temperature dependence.

We finally notice that while the temperature T^* depends mainly on the spinon sector and is therefore nearly material independent, the temperature T_{ph} depends mainly on holon sector and it is strongly material-dependent since pairing phenomenon is strongly connected to the FS features.

5.2 Effective actions of gapless excitations

In this section we will put the action of the system in the standard form, i.e. a sum of three contribution: the spinon term, the holon term and the slave particle gauge field term. In the holon contribution, the holon pairs are considered and the slave particle gauge field is minimally coupled to spinons and holons and receives dynamics from them. This is the starting form for all calculations and predictions performed with our model in the low temperature regime.

In the last chapter we showed that the formation of holon pairs changes holon Green's function via the self energy in Eq. (4.34). We can use the self energy $\Sigma(\omega, \vec{k})$ to take holon pairs into account making the substitution $E(\vec{k}) \to E(\vec{k}) - \Sigma(\omega, \vec{k})$ into the action of holons in Eq. (4.15), and neglecting the interaction with the order parameter. In this way the action of the system in the normal state consist of two contributions, the unchanged spinon contribution of Eq. (2.39) and the modified holon contribution of the previous chapter. Holon Green's function changes by an angle dependent wave function renormalization $Z_\Delta(\vec{k})$ if $\omega < m_\phi$ and looks like a d-wave SC one if $\omega > m_\phi$.

As a first approximation, to simply analyze the modified holon term in the low energy (or temperature) limit, we neglect the angular dependence of $Z_\Delta(\vec{k})$ replacing $\gamma_R(\vec{k})^2$ by its average on the FS. So $Z_\Delta(\vec{k})$ is replaced by

$$\bar{Z}_\Delta = \frac{1}{1 + \frac{|\Delta_0^h|^2 \pi}{4 m_\phi^2} k_F^2 a^2}. \tag{5.1}$$

Its value is essentially one in the PG region because $k_F \sim \delta << 1$ and the FS is located near the nodal directions, but in SM region, with a large FS, its value can be much less than one, leading to relevant effects. For $\omega < m_\phi$ the holon action of Eq. (2.45), in coordinates representation, becomes

$$S_h = \frac{1}{\bar{Z}_\Delta} \int_{[0,\beta]\times\mathbf{R}^2} d^3x H^*(x^0,\vec{x}) \left[i\partial_0 - \mu - A_0 - \frac{(\vec{\nabla} - i\vec{A})^2}{2m^*} \right] H(x^0,\vec{x}), \qquad (5.2)$$

where the slave particle gauge field has been introduced by minimal substitution taking gauge invariance into account. High energy modes $\omega > m_\phi$ are gapped and we do not consider them because they can be safely integrated out giving rise to a Maxwell-like action for the slave particle gauge field, as shown in the previous chapter. A similar argument holds for massive spinons.

In the low energy limit, the relevant dynamics of the slave particle gauge field stems from integrating out low energy modes of holons with a FS. This leads to the Reizer singularity for the transverse component of gauge field as in Eq. (2.46) and to a plasma frequency gap for the scalar component as in Eq. (2.47). At low temperature Maxwell-like action is clearly sub-leading w.r.t Reizer singularity and can be safely neglected for $m_\phi \neq 0$.

In this case, starting from Eq. (5.2), we notice that, because of a Ward identity, the wave function renormalization of holons $\bar{Z}_\Delta$ has no effect on the propagator of the gauge field. Indeed vertex correction exactly cancels the wave function renormalization in the vacuum polarization Feynman diagram. The fact of the matter is that the action for holons in Eq. (5.2) holds only for low frequencies $\omega < m_\phi$. This means that frequencies lower than m_ϕ contribute to Reizer singularity while higher frequencies (being d-wave SC like modes) contribute to the irrelevant Maxwell-like action. In this sense holon pairing, through the energy scale m_ϕ, affects the slave particle gauge field. We model this effect introducing a weight factor Z_A in front of the slave particle gauge field action with the Reizer singularity, having the following properties,

- Z_A vanishes at $T = T_c$ because $m_\phi(T_c) = 0$. Indeed at $T < T_c$ the system is a d-wave superconductor and the generated dynamics is no more Reizer-like;
- Z_A approaches one at $T = T_{ph}$. This is because in this case (and at higher temperature $T > T_{ph}$) the system has a metallic behavior, in fact essentially all the FS contribute to the Reizer singularity and there are not holon pairs.

Hereafter we show explicitly the temperature dependence of parameters when necessary. One can show that for $m_\phi >> k_F$, $Z_A \sim 1$ and for $m_\phi << k_F$, $Z_A \sim \frac{m_\phi}{k_F}$; our choice for Z_A is of the simple interpolating form

$$Z_A = \frac{1}{1 + \frac{k_F}{m_\phi(T)}}, \qquad (5.3)$$

thus the Reyzer-like action of the gapless transverse component reads

$$S_{A^T} = \frac{Z_A}{2\beta} \sum_{\omega_n} \int \frac{d^2k}{(2\pi)^2} \left(i\kappa \frac{\omega_n}{|\vec{k}|} - \chi \vec{k}^2 \right) |A^T|^2. \tag{5.4}$$

We conclude from Eqs. (5.2) and (5.4) that, above the superconducting transition, it is possible to take the presence of incoherent holon pairs into account by means of the two weights $\bar{Z}_\Delta$ and Z_A. From the above actions we see that they renormalize the following quantities:

- the density of states at the FS of holons $N_h(\epsilon_F) \to \bar{Z}_\Delta N_h(\epsilon_F)$;
- the Landau dumping $\kappa \to Z_A \kappa$;
- the diamagnetic susceptibility, $\chi \to Z_A \chi$;
- the plasma frequency $\omega_p \to Z_A \omega_p$.

The last point stems from the scalar component of the gauge field, applying similar considerations to that just made for the transverse component. Thus updating these parameters in formulas we can include the effects of holon pairing. Later in this chapter we will give two examples dealing with resistivity and Knight shift.

Finally we consider the explicit temperature dependence of the two new parameters $|\Delta_0^h|$ and m_ϕ. By a numerical fitting of the solutions of the gap equation for holons in Eq. (3.21) we get

$$|\Delta_0^h|(T) \propto 1 - e^{3\left(1 - \frac{T_{ph}}{T}\right)} \tag{5.5}$$

for $T < T_{ph}$ and $|\Delta_0^h|(T) = 0$ for $T > T_{ph}$.

As for m_ϕ, we know that it must vanish at the superconducting transition temperature T_c (and at lower temperature $T < T_c$) because at the phase transition holon pairs become coherent. Moreover it must be of the form given by Eq. (4.27) for temperatures slightly below T_{ph} when incoherent holon pairs begin to appear, so that the condition of small Δ_0^h is fulfilled.

Finally we point out the relevance in our discussion of the negative next-nearest-neighbor hopping term t' which bends the FS of holons and allows BCS pairing of fields having a good continuum limit in SM region. In the simple $t - J$ model (where $t' = 0$), the FS in SM does not cross the boundaries of the MBZ and our approach to the phase fluctuations of the holon pair order parameter presumably is possible only in the PG

region where closed FS centered at $\frac{1}{2}(\pm\pi, \pm\pi)$ may arise (see Fig. (3.1)) (but in PG the effects of phase fluctuations are not very effective). For this reason in the simple $t-J$ model T^* and T_{ph} may coincide.

5.3 Resistivity in the strange metal region

With the above prescriptions, below Eq. (5.4), we can easily modify the resistivity formula in the SM region, i.e. the sum of Eqs. (2.58) and (2.56). While the spinon contribution, responsible for the T-linearity, does not change significantly, the impurity scattering in holon sector, added by Matthiesen rule and affecting resistivity by an upward shift, is multiplied by $\bar{Z}_\Delta(T)$ because the real time scattering rate is proportional to the density of states at the FS [38]. This introduces an additional temperature dependence that causes an increasingly downward deviation of resistivity when temperature is reduced. The deviation becomes relevant below T_{ph}.

The blue line plotted in Fig. (5.1) shows the resistivity predicted by our model when holon pairs formation is neglected. The red line instead shows the effect of holon pairs on the resistivity. It has a negative second derivative below T_{ph} and smoothly joins to the blue line nearly at T_{ph}, when holon pairs disappear. Both curves show a linear growth at temperature higher than T_{ph} and are not reliable below T_c when they should abruptly drop, because of the superconducting transition.

The red line is in agreement with experimental data [30]; the downward deviation below T_{ph} is evident in panel (b) of Fig. (1.2), while the sign of second derivative can be read moving along a vertical line in panel (c).

We conclude that formation of holon pairs and the increasing coherence length of their phase can explain both the temperature scale of this deviation, set by T_{ph} (not by T^*), and its temperature dependence, at least up to temperatures not too low.

5.4 Knight shift in the strange metal region

In this section we evaluate spin-spin correlation $\langle \vec{S}(x) \cdot \vec{S}(y) \rangle$ in the SM regime and determine the Knight shift K_s using the real part of the retarded correlation

$$\begin{aligned} K_s &\propto \int \frac{d^2p}{(2\pi)^2} F(\vec{p}) \lim_{\omega \to 0} \Re \langle \vec{S}(p) \cdot \vec{S}(-p) \rangle^R \\ &\sim \lim_{\omega \to 0} \Re \langle \vec{S}(\vec{0}, \omega) \cdot \vec{S}(\vec{0}, -\omega) \rangle^R, \end{aligned} \tag{5.6}$$

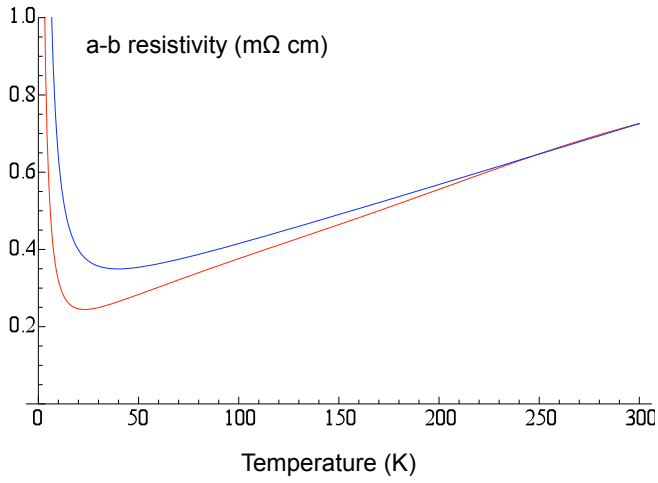

Figure 5.1: Predicted resistivity in SM region (doping $\delta \approx 0.18$) as a function of temperature. The red line shows the downward deviation from linearity below $T_{ph} \approx 250K$. The blue line is the resistivity when holon pairs are neglected. They coincide above T_{ph} and are not reliable below T_c.

where in the last step we assumed the nuclear structure factor $F(\vec{p})$ peaked around $\vec{p}=0$ [48], [49].

In the framework of this spin-charge separation approach, the spin field at the point $x=(\vec{x},x_0)$ reads

$$S_i(x)\sim[1-H^*(x)H(x)]e^{i\vec{Q}_{AF}\cdot\vec{x}}\Omega_i \tag{5.7}$$

where $\vec{\Omega}$ is defined in Eq. (2.37) and represents slowly varying anti-ferromagnetic modes. It follows that the spin-spin correlation reads

$$\langle\vec{S}(x)\cdot\vec{S}(y)\rangle\sim[(1-\delta)^2+\langle n(x)n(y)\rangle_c]e^{i\vec{Q}_{AF}\cdot(\vec{x}-\vec{y})}\langle\vec{\Omega}(x)\cdot\vec{\Omega}(y)\rangle \tag{5.8}$$

where $n(n)=H^*(x)H(x)$ and the subscript c means connected correlation beyond the mean value $(1-\delta)^2$. This mean value gives a contribution to the spin-spin correlation near the anti-ferromagnetic vector because of the exponential factor (remember $\langle\vec{\Omega}(x)\cdot\vec{\Omega}(y)\rangle$ is slowly varying) and determines the spin-lattice relaxation rate $\frac{1}{T_1}$.

In what follows we will consider the first and the third quadrants of the BZ but a similar discussion, with the same results, holds also for the second and the fourth quadrants performing the substitution $\vec{Q}_{AF}\to(-\pi,\pi)$.

To obtain the contribution $D(p)$ to the spin-spin correlation near spatial momentum $\vec{p}=0$, as required by Eq. (5.6), we need the Fourier transform of the connected correlation $\langle n(x)n(y)\rangle_c$ to be non-vanishing near the anti-ferromagnetic vector $\vec{Q}_{AF}$. Indeed performing Fourier transform of the connected contribution in Eq. (5.8) we obtain

$$D(p)=\int\frac{d^3q}{(2\pi)^3}\langle\vec{\Omega}(p+q)\cdot\vec{\Omega}(-p-q)\rangle\langle n(\vec{q}+\vec{Q}_{AF},q_0)n(-\vec{q}-\vec{Q}_{AF},-q_0)\rangle_c \tag{5.9}$$

where $\vec{\Omega}(p)$ and $n(p)$ are the Fourier transform of $\vec{\Omega}(x)$ and $n(x)$ respectively.

Then applying Wick theorem at zero temperature we get

$$\langle n(\vec{q}+\vec{Q}_{AF},q_0)n(-\vec{q}-\vec{Q}_{AF},-q_0)\rangle_c\approx-\int\frac{d^3p}{(2\pi)^3}G(\vec{p},p_0)G(\vec{p}-\vec{q}-\vec{Q}_{AF},p_0-q_0) \tag{5.10}$$

where

$$\begin{aligned}G(p)&=\langle H(p)H^*(p)\rangle\\&=\frac{\bar{Z}_\Delta}{ip_0-E(\vec{p})}\end{aligned} \tag{5.11}$$

is the low energy Green's function of holons in the presence of incoherent holon pairs, see Eq. (5.2).

In the low energy limit the relevant momenta are inside a strip of thickness $2\Lambda << k_F$ about the FS. To get a contribution near the anti-ferromagnetic vector $\vec{Q}_{AF}$ it is necessary that the FS crosses the boundary of the RBZ in such a way that the modes near the crosses on opposite sides of the FS give a contribution to the integral in Eq. (5.10) as follows by momentum conservation.

Linearizing the dispersion of holons and considering the four crossing regions (two lie in the 1st quadrant and two in the 3rd quadrant), where only particle-hole excitations contribute, we obtain the anti-ferromagnetic density-density correlation (see appendix)

$$\langle n(\vec{q}+\vec{Q}_{AF},q_0)n(-\vec{q}-\vec{Q}_{AF},-q_0)\rangle_c \approx \bar{Z}_\Delta^2 \frac{2\Lambda}{\pi^2}\left[1-\frac{q_0}{\Lambda}\arctan\left(\frac{\Lambda}{q_0}\right)\right]+O(\vec{q}^2) \qquad (5.12)$$

which is nearly $\vec{q}$-independent as can be seen noticing that slightly changing $\vec{q}$ the crossing regions slightly changes their position but the size of the overlapping regions does not change.

In this sense the shape of the FS is important evaluating the Knight shift and other quantities in which is necessary a contribution near the anti-ferromagnetic vector $\vec{Q}_{AF}$ in the holon sector and only excitations near the FS are considered. In particular, in this case, the negative next nearest neighbor hopping t' is crucial because it modifies the FS of the simple tight binding model (with only nearest neighbor hopping t) causing the required crosses as shown in the previous chapter.

We can now complete the computation of Eq. (5.9) using Eq. (5.10) and the relation

$$\langle\vec{\Omega}(\vec{q},q_0)\cdot\vec{\Omega}(-\vec{q},-q_0)\rangle = -\frac{1}{\pi}\int dy \frac{\Im\langle\vec{\Omega}(\vec{q},y)\cdot\vec{\Omega}(-\vec{q},-y)\rangle^R}{iq_0-y} \qquad (5.13)$$

to obtain the dynamic propagator once is known the retarded one (see Eq. (2.52)). The connected contribution to the spin-spin correlation reads

$$D(p) = \bar{Z}_\Delta^2 \frac{Z_\Omega^{SM}\sqrt{a}}{2\pi^4}\int_0^\infty dy \frac{\Gamma}{(y-2m_s)^2+\Gamma^2}\left[1-\frac{p_0+iy}{\sqrt{a}}\arctan\left(\frac{\sqrt{a}}{p_0+iy}\right)\right] \qquad (5.14)$$

where we put $\Lambda=\sqrt{a}$ to consistently neglect the $\vec{q}$-dependence in the density-density anti-ferromagnetic correlation of Eq. (5.10).

Performing the analytic continuation $ip_0 \to p_0+i\varepsilon$ in Eq.(5.14) and using the relation $\arctan(iz) = i\tanh^{-1}(z)$ we obtain the retarded function

$$D^R(p) = \bar{Z}_\Delta^2 \frac{Z_\Omega^{SM}\sqrt{a}}{2\pi^4}\int_0^\infty dy \frac{1}{1+\left(y-\frac{2m_s}{\Gamma}\right)^2} \left[1-\frac{\Gamma}{\sqrt{a}}\left(y-\frac{p_0+i\varepsilon}{\Gamma}\right)\tanh^{-1}\left(\frac{\sqrt{a}}{\Gamma}\frac{1}{y-\frac{p_0+i\varepsilon}{\Gamma}}\right)\right]. \quad (5.15)$$

This integral can be evaluated exactly for $p_0 = 0$ in the limit $m_s << \Gamma$ which holds in the SM region at high temperature. The result is (see appendix)

$$\begin{aligned} D^R_{m_s=0}(\vec{p}, p_0 = 0) &= \bar{Z}_\Delta^2 \frac{Z_\Omega^{SM}\Gamma}{4\pi^3}\left[\frac{\sqrt{a}}{\Gamma} + i\tanh^{-1}\left(i\frac{\sqrt{a}}{\Gamma}\right) - \frac{i}{2}\ln\left(1+\frac{a}{\Gamma^2}\right)\right] \\ &\approx \bar{Z}_\Delta^2 \frac{Z_\Omega^{SM}}{12\pi^3}\left(\frac{a^{\frac{3}{2}}}{\Gamma^2} - i\frac{3}{2}\frac{a}{\Gamma}\right) \end{aligned} \quad (5.16)$$

where in the last step we take the limit $\sqrt{a} << \Gamma$ that again holds for sufficiently high temperature.

To proceed we assume that the relevant temperature dependence comes from the parameters, in such a way to extend the above zero temperature calculation to finite temperature. Parameters with the highest power temperature dependence are the most important (remember we are in SM regime). Using Eqs. (5.6) and (5.16), Knight shift, in the high temperature (or large Γ) limit, turns out to be

$$\begin{aligned} K_s &\approx \lim_{p_0\to 0} \Re D^R(\vec{p}=0, p_0) \\ &\approx \bar{Z}_\Delta^2 \frac{Z_\Omega^{SM}}{12\pi^3}\frac{a^{\frac{3}{2}}}{\Gamma^2}. \end{aligned} \quad (5.17)$$

We notice that the temperature dependence of the second and third factors cancels and the remaining temperature dependence comes from $\bar{Z}_\Delta^2$. We conclude that when a finite density of incoherent holon pairs appears at the temperature scale T_{ph}, the weight $\bar{Z}_\Delta^2$ causes a downward deviation of the Knight shift w.r.t. its constant value at high temperature. The second panel in Fig. (1.3) shows that, decreasing temperature, the downward deviation of K_s occurs at a temperature of order T_{ph}, higher than T^* and consistent with the above calculation.

Finally the doping dependence arises mainly from the second and third factors and, accordingly to experimental data, Knight shift grows with doping

$$K_s = \bar{Z}_\Delta^2 \frac{\sqrt{\kappa}}{12\pi^3 c'^2}|\delta\ln\delta|^{\frac{5}{4}} \propto \delta^{\frac{5}{4}}, \quad (5.18)$$

where in the last step we assumed small δ w.r.t. one. Using Eq. (5.18) we plot in Fig. (5.2) the Knight shift as a function of temperature for two different over-doping values. These curves can be compared with the experimental data for optimally doped $YBCO$, represented by the squares in the second panel of Fig. (1.3).

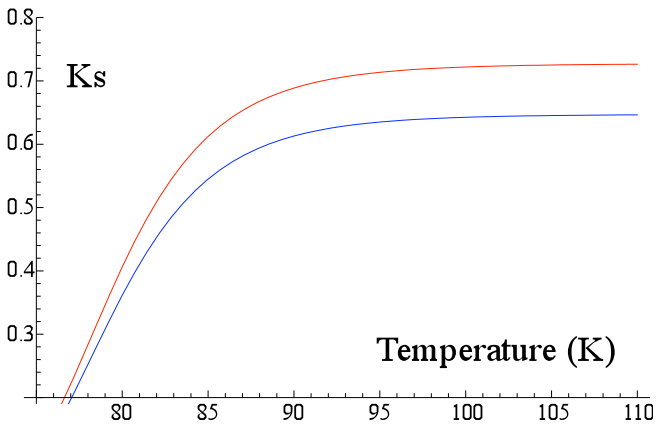

Figure 5.2: Temperature dependence of the Knight shift K_s calculated at two different doping values $\delta = 0.2$ (red curve) and $\delta = 0.16$ (blue curve). In both cases we chose $T_{ph} \approx 130K$.

Chapter 6

Conclusions

We briefly review the main new results achieved in this thesis. We studied the normal to superconducting phase transition in cuprates compounds within the spin charge separation scenario. Our approach exhibits 3 distinct crossover lines: T_{ph} where holons begin to pair reducing the spectral weight of the hole, starting from antinodal directions; T_{ps} where incoherent RVB hole pairs are formed, mainly affecting the magnetic properties since a finite FS still persists; and T^*, intersecting T_{ps}, where one crosses from a large to a small holon FS, half-pocket shaped and located near the nodal direction.

Although many details of our approach are admittedly conjectural, the mechanism of SC proposed is rather complete and has the following appealing features: it is not of simple BCS structure; SC appears only at finite doping above the long range AF order; it allows vortices in the normal state, as in the preformed pair scenario, supporting Nernst signal; the appearance of two positive branches in the spinon dispersion relation that for a suitable spinon-antispinon attraction induce a similar structure for the magnon dispersion around the AF vector, reminiscent of the hourglass found in neutron experiments; in the SC state the gauge gap destroys the Reizer singularity (responsible for the anomalous T-dependence of life-time of magnon and electron resonances in the normal state), therefore the magnon and the electron resonances become sharper.

For the holon pairing in the normal state as a precursor of superconductivity, we generalized the BCS interaction introducing the fluctuations of the phase of the order parameter in a self consistent way. Then we considered the scattering of quasi-particle against the incoherent condensate finding an explicit expression for the Green's function of quasi-particles that exactly interpolates between a FL-like behavior, with a reduced and direction dependent spectral weight, when pairs are incoherent, and a d-wave SC-like behavior, when pairs become coherent at the SC transition. The relevant parameter

that smoothly drives this process is the coherence length. For larger length scales the system behaves like a FL, for shorter scales the system behaves like a superconductor. We obtained also a condition determining which of the two behavior dominates. Notice that the FS becomes less effective but does not disappear until the SC transition and the related density of states is directly comparable with experimental data.

The shape of the FS turned out to be crucial to get a good continuum limit for quasi-particles and to properly evaluate the Knight shift. In particular the next-nearest-neighbor hopping term, bending the FS up to cross the boundaries of the MBZ, both allows a suitable FS for the BCS pairing of holons and provides a constant contribution to the real part of the static spin susceptibility (i.e. to the Knight shift) near $\vec{q} = 0$.

Moreover the interaction through vortices with chirality depending on the sublattice, being able to distinguish the sublattice where they sit, can explain the presence, observed in experiments, of large hole-like Fermi surfaces and small electron-like ones.

The temperature T_{ph}, unlike the temperature T^*, mainly depends on the holon sector and is therefore strongly material dependent. In the SM regime of the simple $t-J$ model, these FS-related effects are absent and the temperatures T_{ph} and T^* probably coincide.

Then we studied how the low energy actions of spinons, holons and slave particle gauge field modifies in the presence of holon pairs. We showed that it is possible to take holon pairs into account introducing a direction and temperature dependent reduced spectral weight for holons and a temperature dependent wave function renormalization for the slave particle gauge field. These factors renormalized the parameters of the actions and using them we sow how holon pairing affects physical observables. We considered in particular resistivity and Knight shift. According to experiments, these quantities showed a simultaneous downward deviation, when temperature is reduced below T_{ph}. These deviations are a confirmation of the existence of a high pseudo-gap temperature T_{ph}, above T^*. Indeed they are due to holon pairing and not to pseudo-gap effects which show up at temperatures lower than T^*.

Let us finally spend few words for future directions of work. There are several aspects to be studied in detail. In the SC phase the slave particle gauge field is gapped and there have to be another attractive interaction to get gauge invariant, i.e. physical, fields. We proposed the residual $\mathbf{Z}_2$ subgroup as a source of attraction, which range needs a deeper understanding.

In the normal state the Nernst effect, the phase vortices and the presence of a magnetic field have to be considered. Also the quantum critical point problem, which we believe to be QED_3, and the controversial issue if the density of states of holes is preserving or

not-preserving when the SC transition is approached have to be studied.

Finally we note that our theory of superconductivity seems to be consistent with a double nature of the SC transition experimentally observed. It is of the XY type for underdoped samples, i.e. the mass of the phase Φ smoothly vanishes at the transition point, and of the BCS type, i.e. the phase mass has a jump at the transition, for overdoped samples.

Appendix A
Calculation of the integral $I(k)$ (chapter 4)

We evaluate the integral $I(k)$ of Eq. (4.31) to obtain the expression in Eq. (4.33). We get

$$\begin{aligned} I(k) &= \int \frac{d^3q}{(2\pi)^3}\frac{1}{q^2+m_\phi^2}\frac{1}{i(q_0-k_0)-E(\vec{q}-\vec{k})} \\ &= \int \frac{d^3q}{(2\pi)^3}\frac{1}{q^2+m_\phi^2}\frac{1}{i(q_0-k_0)+\vec{q}\cdot\hat{k}-\delta k} \\ &= \int \frac{d^3q}{(2\pi)^3}\frac{1}{q^2+m_\phi^2}\frac{1}{i(q_0-k_0)+q_1-\delta k} \\ &= \int \frac{drd\theta dq_2}{(2\pi)^3}\frac{r}{q_2^2+r^2+m_\phi^2}\frac{1}{r_0e^{i\varphi}-re^{i\theta}}. \end{aligned} \tag{0.1}$$

It is the expression shown in Eq. (4.32) and in the in the last step we used the cylindrical coordinates defined in chapter 4 above Eq. (4.32). We proceed integrating in succession q_2, θ and r. We obtain

$$\begin{aligned} I(k) &= -\pi\int \frac{drd\theta}{(2\pi)^3}\frac{1}{\sqrt{r^2+m_\phi^2}}\frac{1}{e^{i\theta}-\frac{r_0}{r}e^{i\varphi}} \\ &= \frac{\pi}{r_0e^{i\varphi}}\int \frac{dr}{(2\pi)^2}\theta(r_0-r)\frac{r}{\sqrt{r^2+m_\phi^2}} \\ &= \frac{\pi}{r_0e^{i\varphi}}\frac{\sqrt{r_0^2+m_\phi^2}-m_\phi}{(2\pi)^2}. \end{aligned} \tag{0.2}$$

The last expression is the desired result, i.e. Eq. (4.33). The θ-integration has been performed applying the residue theorem to the complex contour integral around the unit circle of the complex variable $e^{i\theta}$.

Appendix B
Calculation of the density-density correlation near the anti-ferromagnetic vector (chapter 5)

We evaluate the anti-ferromagnetic density-density correlation in Eq. (5.10) considering the 1st and 3rd quadrants,

$$\begin{aligned}
\langle nn\rangle_c(\vec{q}+\vec{Q}_{AF},q_0) &\equiv \langle n(\vec{q}+\vec{Q}_{AF},q_0)n(-\vec{q}-\vec{Q}_{AF},-q_0)\rangle_c \\
&\approx -\int \frac{d^3p}{(2\pi)^3}\frac{\bar{Z}_\Delta}{ip_0-E(\vec{p})}\frac{\bar{Z}_\Delta}{i(p_0-q_0)-E(\vec{p}-\vec{q}-\vec{Q}_{AF})} \\
&= i\bar{Z}_\Delta^2\int\frac{d^2p}{(2\pi)^2}\frac{\theta[E(\vec{p})]-\theta[E(\vec{p}-\vec{q}-\vec{Q}_{AF})]}{q_0-i[E(\vec{p}-\vec{q}-\vec{Q}_{AF})-E(\vec{p})]}
\end{aligned} \tag{0.3}$$

where the p_0-integration has been performed using residue theorem and θ is the step function.

We proceed reducing the momentum integration within a strip of thickness $2\Lambda << k_F$ about the FS, linearizing the dispersion $E(\vec{k})$ and taking $v_F = 1$. We call Λ_1 (Λ_3) the set of modes around the FS of the 1st (3rd) quadrant. Then translating Λ_1 by the vector $-\vec{q}-\vec{Q}_{AF}$ we get two overlapping regions with Λ_3 in the 3rd quadrant. The particle-hole excitations (as shown by the difference of the step functions in the numerator) within these overlapping regions contribute to the integral in Eq.(5.10) at the value $\vec{q}$ of the momentum. Moreover for small $\vec{q}$ the overlapping regions are nearly squares of side 2Λ and two FS inside them are nearly orthogonal, therefore, considering the contribution of one of these regions to the above integral, we get

$$
\begin{aligned}
\frac{1}{4}\langle nn\rangle_c(\vec{q}+\vec{Q}_{AF},q_0) &\approx i\frac{\bar{Z}_\Delta^2}{(2\pi)^2}\int_{-\Lambda}^{\Lambda}dp_1\int_{-\Lambda}^{\Lambda}dp_2\frac{\theta(-p_1)-\theta(-p_2)}{q_0-i(p_1+p_2)} \\
&= \frac{\bar{Z}_\Delta^2}{(2\pi)^2}\int_{0}^{\Lambda}dp_1\int_{0}^{\Lambda}dp_2\left[\frac{i}{q_0+i(p_1+p_2)}-\frac{i}{q_0-i(p_1+p_2)}\right] \\
&= \frac{\bar{Z}_\Delta^2}{2\pi^2}\int_{0}^{\Lambda}dp_1\int_{0}^{\Lambda}dp_2\frac{p_1+p_2}{q_0^2+(p_1+p_2)^2} \\
&\approx \frac{\bar{Z}_\Delta^2}{\sqrt{2}\pi^2}\int_{0}^{\Lambda}dp_+\frac{p_+}{q_0^2+2p_+^2}\int_{-p_+}^{p_+}dp_- \\
&= \frac{\bar{Z}_\Delta^2}{2\pi^2}|q_0|\int_{0}^{\frac{\sqrt{2}\Lambda}{|q_0|}}dy\frac{y^2}{1+y^2} \\
&= \bar{Z}_\Delta^2\frac{\Lambda}{\sqrt{2}\pi^2}\left[1+\frac{q_0}{\sqrt{2}\Lambda}\arctan\left(\frac{\sqrt{2}\Lambda}{q_0}\right)\right] \qquad (0.4)
\end{aligned}
$$

which is the result in Eq. (5.12) after a trivial redefinition of the cutoff $\sqrt{2}\Lambda \to \Lambda$. The factor 4 is due to summing the contribution of the four overlapping regions. Notice that for $\vec{q}=0$ the contributing regions lie near the intersection points of the FS and the boundary of the MBZ.

Appendix C
Calculation of the static spin-spin correlation near the anti-ferromagnetic vector (chapter 5)

We evaluate the integral in Eq. (5.15) at $p_0 = 0$ in the limit $\frac{m_s}{\Gamma} \to 0$. It reads

$$D^R_{m_s=0}(\vec{p}, p_0 = 0) = \bar{Z}^2_\Delta \frac{Z^{SM}_\Omega \Gamma}{2\pi^4} \int_A dz f(z) \tag{0.5}$$

$$f(z) = \frac{1}{\frac{\Gamma^2}{a} + z^2} \left[1 - z \tanh^{-1}\left(\frac{1}{z}\right) \right] \tag{0.6}$$

where z is a complex variable and A is a ray on the complex z-plane starting at $z = -i\frac{\varepsilon}{\sqrt{a}}$ and reaching $z = +\infty - i\frac{\varepsilon}{\sqrt{a}}$ remaining parallel to the positive real axis.

The function $f(z)$ shows a branch cut between $z = -1$ and $z = 1$ (because of the factor $\tanh^{-1}\left(\frac{1}{z}\right)$) and two poles at $z = \pm i\frac{\Gamma}{\sqrt{a}}$ due to the first factor. Moreover it is an even function, $f(z) = f(-z)$.

The closed integration path we choose consists of four pieces: 1) the ray A; 2) the ray B starting at $z = -\infty + i\frac{\varepsilon}{\sqrt{a}}$ up to $z = +i\frac{\varepsilon}{\sqrt{a}}$ remaining parallel to the negative real axis (it is the reflection of A w.r.t. the origin and, because the integrand is even, it gives the same contribution as A); 3) a path C turning around the positive part of the branch cut (from 0 to 1) and joining the end of B with the beginning of A; 4) the semicircle at infinity in the upper plane that closes the path (it gives a vanishing contribution because of Jordan's lemma).

This path encloses the upper pole $z = i\frac{\Gamma}{\sqrt{a}}$ and does not cross the cut, therefore summing the contributions of the four paths we get $2\pi i$ times the residue of the pole,

$$2\frac{2\pi^4}{\bar{Z}_\Delta^2 Z_\Omega^{SM}\Gamma}D^R_{m_s=0}(\vec{p},p_0=0)+\int_C dzf(z)=\pi\frac{\sqrt{a}}{\Gamma}+i\pi\tanh^{-1}\left(i\frac{\sqrt{a}}{\Gamma}\right). \tag{0.7}$$

The integral around the positive part of the cut reads

$$\begin{aligned}
\int_C dzf(z) &= \int_0^1 dz\left[f(z+i\varepsilon)-f(z-i\varepsilon)\right] \\
&= -\int_0^1 dz\frac{z}{\frac{\Gamma^2}{a}+z^2}\left[\tanh^{-1}\left(\frac{1}{z+i\varepsilon}\right)-\tanh^{-1}\left(\frac{1}{z-i\varepsilon}\right)\right] \\
&= -\int_0^1 dz\frac{z}{\frac{\Gamma^2}{a}+z^2}\frac{1}{2}\left[\ln\left(\frac{1}{z-i\varepsilon}\right)-\ln\left(\frac{1}{z+i\varepsilon}\right)\right] \\
&= i\pi\int_0^1 dz\frac{z}{\frac{\Gamma^2}{a}+z^2} \\
&= i\frac{\pi}{2}\ln\left(1+\frac{a}{\Gamma^2}\right),
\end{aligned} \tag{0.8}$$

notice that ε and $\frac{\varepsilon}{\sqrt{a}}$ are equivalent when the limit $\varepsilon\to 0$ is performed.
We conclude from Eq. (0.7) that

$$D^R_{m_s=0}(\vec{p},p_0=0)=\bar{Z}_\Delta^2\frac{Z_\Omega^{SM}\Gamma}{4\pi^3}\left[\frac{\sqrt{a}}{\Gamma}+i\tanh^{-1}\left(i\frac{\sqrt{a}}{\Gamma}\right)-\frac{i}{2}\ln\left(1+\frac{a}{\Gamma^2}\right)\right] \tag{0.9}$$

which is the result in Eq. (5.16).

List of Figures

Bibliography

[1] A. J. Leggett, *Quantum Liquids* (Oxford University Press 2006).

[2] F. C. Zhang, T. M. Rice, Phys. Rev. **B37**, 5594, (1998).

[3] J. Affleck and J. B. Marston, Phys. Rev. B **37**, 3774 (1988).

[4] J. W. Negele and H. Orland, *Quantum Many Particle Systems* (Addison–Wesley, New York 1988).

[5] P. A. Marchetti, Z.B. Su, L. Yu, Mod. Phys. Lett. **B12**, 173 (1998); Phys. Rev. **B58**, 5808 (1998).

[6] P. A. Marchetti and M. Gambaccini in preparation.

[7] P. A. Marchetti and M. Gambaccini in preparation.

[8] P. A. Marchetti, Zhao-Bin Su, and Lu Yu, Nucl. Phys. B **482** [FS], 731 (1996).

[9] P. A. Marchetti, Z.B. Su, L. Yu, J.Phys.Condens.Matter 19 (2007) 125212.

[10] P. A. Marchetti, F. Ye, Z. B. Su, L. Yu (2009).

[11] P. A. Marchetti, L. De Leo, G. Orso, Z.B. Su and L. Yu, *Phys. Rev.* B **69** 024527 (2004).

[12] P. A. Marchetti, G. Orso, Z.B. Su and L. Yu, *Phys. Rev.* B **71** 134510 (2005).

[13] P. A. Marchetti and A. Ambrosetti, Phys. Rev. B **78**, 085119 (2008).

[14] J. Fröhlich and P. A. Marchetti, Phys. Rev. B **46**, 6535 (1992).

[15] J. Fröhlich, T. Kerler, and P. A. Marchetti, Nucl. Phys. B **374**, 511 (1992).

[16] J. Frohlich, Commun. Math. Phys. **47**, 233 (1976).

[17] G. Orso, Phd Thesis, SISSA Trieste (2003).

[18] L. Ioffe and A. Larkin 1989 *Phys. Rev.* B **39** 8988.

[19] E. H. Lieb, Phys. Rev. Lett. **73**, 2158, (1994).

[20] J. Bellisard and R. Rammel *Europhys. Lett.* **13**, 205 (1990)

[21] G. Qin (2000) unpublished

[22] G. Kotliar, Phys. Rev. B **37**, 3664 (1988).

[23] R. T. Birgenau et al., Phys. Rev. B **38**, 6614 (1988).

[24] M. Reizer, Phys. Rev. B **39**, 1602 (1989).

[25] M. Y. Kuchiev and O. P. Sushkov, Physica C **218** 197 (1993).

[26] D. H. Kim, P.A. Lee and X. G. Wen, Phys. Rev. Lett. **79** 2109 (1997).

[27] T. Senthil, P.A. Lee, Phys. Rev. B **79**, 245116 (2009).

[28] M.P.A. Fisher, cond-mat/9806164 (1998).

[29] S.G. Sharapov, H Beck, V.M. Loktev, Phys. Rev. B **64**, 134519 (2001).

[30] Y. Ando *et al.*, Phys. Rev. Lett. **93**, 267001 (2004).

[31] R. Zeyher, EPL **90** (2010) 17006.

[32] E. Fradkin, *Field theories of condensed matter systems* (Addison-Wesley 1991).

[33] H. Takagi *et al.*, Phys. Rev. Lett. **69**, 2975 (1992).

[34] T. Timusk and B. Statt, Rep. Prog. Phys., **62**, 61-122 (1999).

[35] C. Renner *et al.*, Phys. Rev. Lett. **80**, 149-152, (1998).

[36] D. S. Marshall *et al.*, Phys. Rev. Lett. **76**, 4841 (1998).

[37] V. Hinkov *et al.*, Nature Physics **3**, 780 (2007).

[38] J. L. Tallon and J. W. Loram, Physica C **349**, 53 (2001).

[39] M. R. Norman and C. Pepin, Rep. Prog. Phys. **66**, 1547-1610 (2003).

[40] N. Nagaosa, *Quantum field theory in strongly correlated electronic systems* (Springer 1999).

[41] V.galitski and S. Sachdev, arXiv:0901.0005 (2009).

[42] Z. Tešanović, Nature Physics **4**, 408 (2008).

[43] Y. Chen, D. Föster and A. Larkin, Phys. Rev. B **46**, 5370 (1991).

[44] Y. Chen and D. Föster, Phys. Rev. B **45**, 938 (1991).

[45] R. K. Kaul *et al.*, Phys. Rev. B **75**, 235122 (2007).

[46] O. Vafek *et al.*, Phys. Rev. B **63**, 134509 (2001).

[47] P. W. Anderson, arXiv:cond-mat/981206 (1998).

[48] G. V. M. Williams *et al.*, Phys. Rev. B **58**, 15053 (1998).

[49] A. J. Millis, H. Monien and D. Pines, Phys. Rev. B **42**, 167 (1990).

[50] P. A. Lee, M. Nagaosa and X.-G. Wen, Rev. Mod. Phys **78** 17 (2006).

[51] N. D. Basov anf T. Timusk, Rev. Mod. Phys **77** 721 (2005).

[52] B. Shraiman and E. D. Siggia, Phys. Rev. Lett. **61**, 467 (1988).

[53] K. Takenaka *et al.*, Phys. Rev. B **68**, 134501 (2003).

[54] C. Berthier *et al.*, Physica C **235**, 67 (1994).

[55] S. Fujiyama *et al.*, I. Phys. Soc. Jpn. **66**, 2864 (1997).

Acknowledgements

I would like to especially thank my ingenious supervisor, Prof. Pieralberto Marchetti, for useful daily discussions. He taught and advised me during these three years. I am also indebted to Dr. Ye Fei for his worthwhile notes and to Giuliano Orso for his PhD thesis. I do not know them in person. Finally I am grateful to Prof. Flavio Toigo and Dr. Luca Salasnich for illuminating conversations.